The Dissertation Committee for Lucas Benjamin Henderson certifies that this is the approved version of the following dissertation:

Deposition and Properties of Co- and Ru-based Ultra-thin Films

Committee

_____
John G. Ekerdt, Supervisor

_____
Gyeong S. Hwang

_____
Richard A. Jones

_____
Brian A. Korgel

_____
Charles B. Mullins

Deposition and Properties of Co- and Ru-based Ultra-thin Films

by

Lucas Benjamin Henderson, B.S.; Ch.E.

Dissertation

Presented to the Faculty of the Graduate School of

The University of Texas at Austin

in Partial Fulfillment

of the Requirements

for the Degree of

Doctor of Philosophy

The University of Texas at Austin
December, 2009

Dedication

For my girls

Acknowledgments

There are many people who have helped me in a variety of ways in my five and a half years of studies. My adviser, Prof. John Ekerdt, has been an ever-present source of inspiration and knowledge. His approach and disposition has turned many a frown upside down for this student. I think it is no small compliment to say that if I had to do it all over again, I would eagerly and happily join Prof. Ekerdt's research group. Dr. Yang-Ming Sun, who answered a few years' worth of my innumerable questions on all aspects of vacuum systems and equipment, is another faculty member to whom I remain deeply indebted.

I owe a great deal of thanks to my fellow group members. Jinhong Shin was my unofficial mentor for a few years, and discussions with him were among the most helpful and informative discussions I have had. Jin helped me get to the point where I could take the system as my own, which was no small task. I can't fail to mention the exceptional technical and scientific help I have received from Wes Ahearn, Ryan Fitzpatrick, Tuo Wang, and Kelly Thom. It has also been my privilege to work closely with Dan Bost over the last years, and I can only hope I have paid back all the help I received from my mentors by playing that role for him. Others who have made many and varied contributions to this work, and without whom I could not have succeeded, include Dr. Richard Jones, Dr. Sanjay Banerjee, Dr. Brian Korgel, Dr. Buddie Mullins, Dr. Gyeong Hwang, Hyun-Woo Kim, Joe Rivers, Davood Sharjerdi, April Schricker, Sachin Joshi, Joe Donnelly, Vince Lynch, Hugo Celio, Wyatt Winkenwerder, Navneet Salivati, Ben Spivey, Joe McCrate, Blair Cox, Songyan Jia, Thomas O'Neill, Han-Jong Chia, Mark Monti, Dwight Romanowicz, Jim Smitherman, Butch Cunningham, Johnny Johnson,

Mike Ronalter, T Stockman, Eddie Ibarra, Randy Rife, Kay Swift, Kevin Haynes, Tammy McDade, Charles Thonig, and Terry Watts. This list is far from exhaustive, and surely there are people I am still forgetting who deserve no less thanks.

My time in Austin has been wonderful. The friends I have made, some of whom have been already mentioned, are friends I hope to keep for a very long time, and they, too, deserve thanks. Most importantly, I thank my wife Ariane. She has supported me in every aspect every day tirelessly. She has kept my spirits up, and taught me more than she'll ever realize. She has made me a better person, and for that I am grateful. I only hope I can give her and Lenny Grace as much as they have given me.

Deposition and Properties of Co- and Ru-based Ultra-thin Films

Publication No. _____

Lucas Benjamin Henderson, Ph.D.
The University of Texas at Austin, 2009

Supervisor: John G. Ekerdt

Future copper interconnect systems will require replacement of the materials that currently comprise both the liner layer(s) and the capping layer. Ruthenium has previously been considered as a material that could function as a single material liner, however its poor ability to prevent copper diffusion makes it incompatible with liner requirements. A recently described chemical vapor deposition route to amorphous ruthenium-phosphorus alloy films could correct this problem by eliminating the grain boundaries found in pure ruthenium films. Bias-temperature stressing of capacitor structures using 5 nm ruthenium-phosphorus film as a barrier to copper diffusion and analysis of the times-to-failure at accelerated temperature and field conditions implies

that ruthenium-phosphorus performs acceptably as a diffusion barrier for temperatures above 165 °C.

The future problems associated with the copper capping layer are primarily due to the poor adhesion between copper and the current Si-based capping layers. Cobalt, which adheres well to copper, has been widely proposed to replace the Si-based materials, but its ability to prevent copper diffusion must be improved if it is to be successfully implemented in the interconnect. Using a dual-source chemistry of dicobaltoctacarbonyl and trimethylphosphine at temperatures from 250-350 °C, amorphous cobalt-phosphorus can be deposited by chemical vapor deposition. The films contain elemental cobalt and phosphorus, plus some carbon impurity, which is incorporated in the film as both graphitic and carbidic (bonded to cobalt) carbon. When deposited on copper, the adhesion between the two materials remains strong despite the presence of phosphorus and carbon at the interface, but the selectivity for growth on copper compared to silicon dioxide is poor and must be improved prior to consideration for application in interconnect systems. A single molecule precursor containing both cobalt and phosphorus atoms, tetrakis(trimethylphosphine)cobalt(0), yields cobalt-phosphorus films without any co-reactant. However, the molecule does not contain sufficient amounts of amorphizing agents to fully eliminate grain boundaries, and the resulting film is nanocrystalline.

Table of Contents

List of Tables

List of Figures

List of Illustrations

Chapter 1: Introduction

1.1. OVERVIEW

The cost reduction associated with device scaling has driven the semiconductor industry to produce smaller and smaller features for decades, roughly following Moore's Law. As dimensions have continually shrunk, innovative approaches have been designed and implemented to overcome the problems associated with further scaling. Among the innovations have been improvements in architecture, manufacturing processes, and materials to improve the functionality and density of the integrated circuits. Included among these are significant innovations in the interconnect (IC), which connects transistors and delivers electrical signal and power. Many layers of conductive wires and insulating dielectrics comprise the full IC system, and this has become one of the major focuses for further scaling, due to issues with resistance-capacitance (RC) delay, crosstalk, and power dissipation.

RC delay has become the limiting factor in operating speed, and several generations ago Al, which had traditionally been the metal in IC wires, was replaced by the more conductive Cu; SiO_2, which had been the IC insulating material, began to be replaced with low-k materials. Within the IC, assuming the minimum metal pitch is twice the metal width (W) and the dielectric thickness between metal lines is the same as the metal height (T) as shown in Illustration 1.1 [1], the following equation can be used to calculate the RC. L and P denote total line length and pitch, respectively.

$$RC = 2\rho\varepsilon\varepsilon_0(4L^2/P^2 + L^2/T^2) \tag{1.1}$$

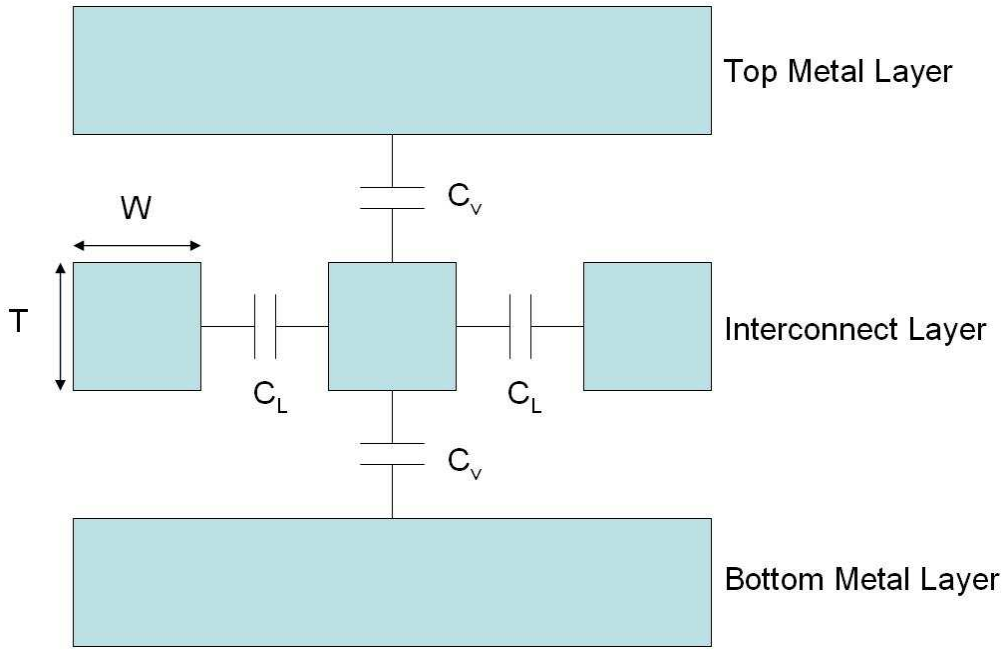

Illustration 1.1. Interconnect system cross-section with parasitic capacitances [1].

Because Cu has a lower resistivity (r) than Al (ρ_{Cu} = 1.7 μΩ·cm and ρ_{Al} = 2.8 μΩ·cm) and low-k materials by definition have lower permittivities than SiO_2, these material changes were effective if reducing the scaling-induced increase in RC delay. Reducing the k value of the dielectrics also provides the added benefit of reducing power dissipation and crosstalk. The method of building a Cu-based IC system is referred to as the dual-damascene process. In this process, the dielectric, such as an etch-stop layer or the inter-metal dielectric (IMD) is deposited first, then etched to form the desired pattern. The newly formed vias and trenches are filled with electroplated Cu, which is then planed down via chemical mechanical polishing, and then capped with a dielectric Cu capping layer. A schematic of a typical IC system is shown in Illustration 1.2 [2].

1.2. BACKGROUND

1.2.1. Current Cu IC Technology

The introduction of Cu created a new set of serious problems. Foremost, Cu readily diffuses into Si [3] and SiO_2 [4-6] or other Si-based low-k materials, especially under an applied electric field, and a barrier liner layer must be added to prevent device reliability degradation. This requires a thin layer to be inserted between the Cu and the IMD to prevent Cu diffusion. The current solution is a multi-step process. First, physical vapor deposited (PVD) TaN is sputtered into trenches to provide barrier capabilities and good adhesion to the IMD. Then PVD Ta is sputtered onto the TaN to improve the adhesion to Cu. Because Ta oxidizes in Cu electroplating bath conditions, a thin layer of PVD Cu is grown on the Ta to act as a seed for Cu electroplating. In order to keep the resistance of the wire as low as possible, the predicted thickness of the Cu liner is

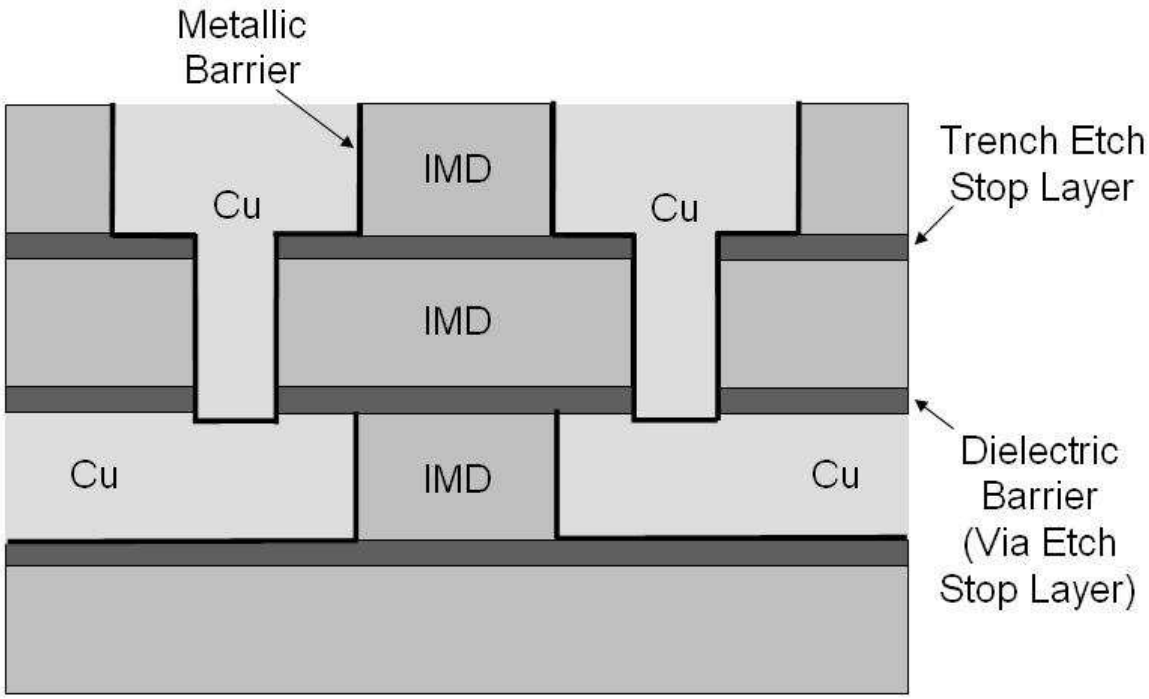

Illustration 1.2. The cross-section of Cu implemented dual damascene structure.

expected to shrink to 3.3 nm by 2010 [7], and it is unclear how much longer the PVD Ta-based bilayer will be extendable. Removal of the TaN layer is a possibility to get the liner thickness below the forecast requirement, however Ta deposited on dielectric surfaces grows in the high ρ β-Ta (ρ ~ 180 μΩ·cm) phase as opposed to the much lower ρ α-Ta phase (ρ ~ 20 – 30 μΩ·cm) that grows on TaN, and any gains in ρ, if any, could be minimal. More likely, the Ta-based bilayer will have to be replaced with an alternative material that provides similar barrier capabilities and adhesion while exhibiting lower ρ.

On the top surface of the Cu, metallic barriers are not used. The Cu wires are capped by dielectric diffusion barriers. Previously, Si_3N_4 that was used as the dielectric diffusion barrier, as it blocks Cu penetration effectively. However, in an effort to reduce the total capacitance of the IC, it has mostly been substituted with SiC_xN_y or SiC_x films ($k_{Si3N4} \sim 7$, $k_{SiCxNy} \sim 5$, and $k_{SiCx} < 5$) [8,9], but these dielectric constants are still high compared to other materials used in the IC. Use of low-k materials in place of these capping layers is not possible due to the poor Cu diffusion capabilities of low-k materials. Another problem concerning the capping materials is that they adhere weakly to Cu, especially compared to the adhesion between Cu and Ta. Cu has higher resistance to electromigration (EM) than Al alloys, meaning the predominant location of EM failure has shifted to the interfaces Cu shares with surrounding materials [10-12]. Interfaces exhibiting weak adhesion experience failure more rapidly than those exhibiting stronger adhesion [13]. In coming generations, failures due to electromigration (EM) within the Cu wires are also expected to become a problem because the predicted J_{max} is expected to

exceed the acceptable limits for dielectric capping layers as soon as 2013, when it is predicted to increase to 2.11×10^{6} A cm^{-2} for intermediate wiring [7].

1.2.2. Potential Solutions

Any potential replacements for the current liner layer and capping layer materials must meet a set of strict requirements. Liner layers must:

- effectively block Cu diffusion
- be minimally soluble in Cu
- not form a compound either with Cu or a dielectric film
- exhibit low electrical resistivity
- adhere well to Cu and dielectric films
- not damage to low-k materials during the deposition process
- be thin when continuous, very smooth, and have good step coverage

An additional trait, although not necessary, is that the liner permits direct Cu electroplating without the need for a Cu seed layer. If a material can be designed that meets all these criteria, it can function as a single-material liner. By eliminating two steps from the dual-damascene process, a single-material liner could cut costs, increase yield, and ease further scaling.

One material that has drawn significant attention as a possible single-material liner replacement for the Ta/TaN bilayer is Ru. Ru has a bulk resistivity less than half that of α-Ta, adheres better to Cu than Ta, is immiscible in Cu at relevant conditions, and

can be directly electroplated upon [14,15]. Unfortunately, Ru is a poor barrier to Cu diffusion [16,17]. The typically columnar grain growth Ru exhibits on dielectric surfaces creates fast diffusion paths for easy Cu diffusion. While the potential exists to improve the current technology by substituting Ru for the PVD Cu/Ta combination, leaving TaN as a diffusion barrier, a promising possibility is the implementation of Ru that lacks grain boundaries. As depicted in Illustration 1.3 [18], films with either a single-crystal or amorphous microstructure have no grain boundaries, while polycrystalline and nanocrystalline films have grain boundaries less conducive to Cu diffusion into the surrounding material than columnar films. Single crystal Ru films would be ideal candidates as diffusion barriers because they would exhibit the lowest ρ among the several possible microstructures. However, the processing difficulties associated with growing single-crystal films make their implementation unlikely. Amorphous Ru lacks the grain boundaries that are the main issue preventing implementation of Ru in Cu ICs and are a much more realistic solution to implementing Ru as a single material liner, although the ρ of amorphous Ru will be somewhat higher than single-crystal Ru.

A series of publications by Shin, *et al.*, reported chemical vapor deposition of amorphous Ru(P) alloy by two different methods, either from a single molecule precursor, *cis*-dihydridotetrakis(trimethylphosphine)ruthenium(II) [*cis*-$RuH_2(PMe_3)_4$] (Me = CH_3) [19,20], or as a dual-source chemistry of triruthenium dodecacarbonyl [$Ru_3(CO)_{12}$] and either triphenylphosphine [PPh_3] (Ph = C_6H_5) or trimethylphosphine [PMe_3] [21,22]. These films are amorphous and remain so at annealing conditions typical of back-end processing [19]. Dual-source films using PMe_3 contain less C than

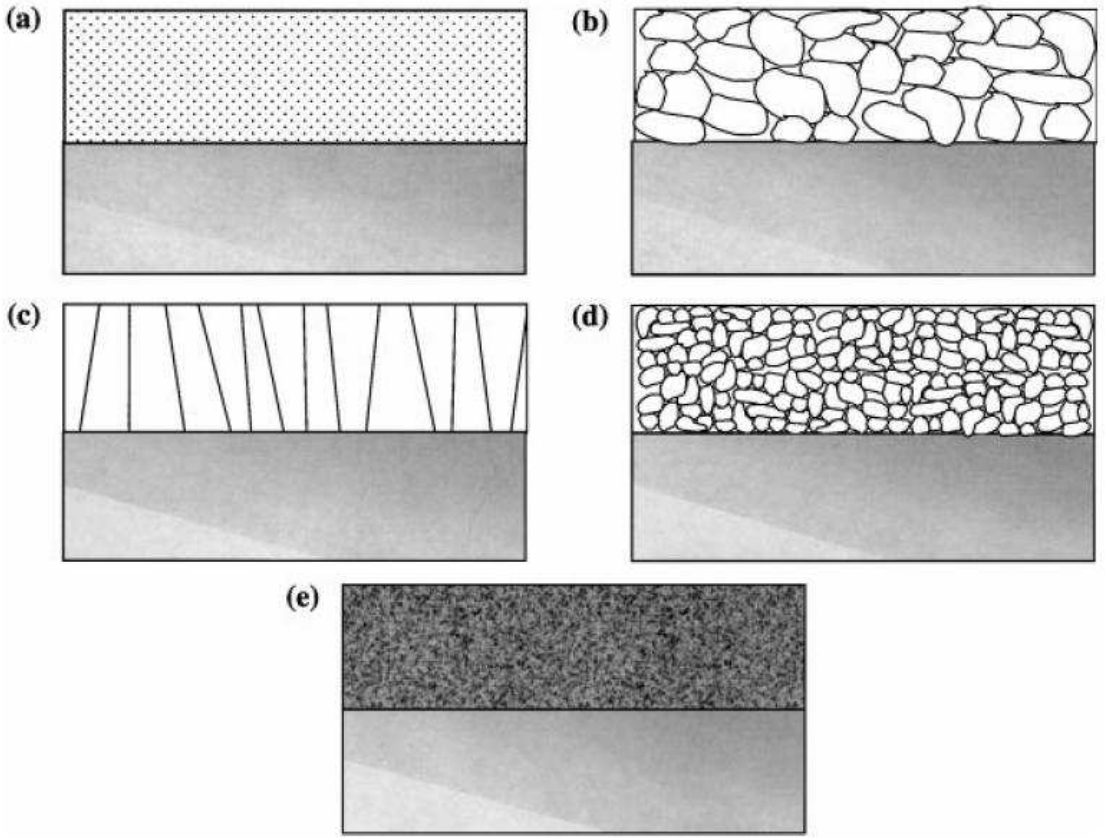

Illustration 1.3. Thin film microstructures, (a) single crystal, (b) polycrystalline, (c) columnar, (d) nano-crystalline, and (e) amorphous [9].

films grown with PPh_3, and have lower ρ [21]. The step coverage of Ru(P) grown via the two source chemistry is significantly improved over the step coverage of CVD Ru from, and the step coverage of Ru(P) grown from the single molecule is better still [22]. Amorphous Ru(P) was demonstrated to be a better barrier to Cu diffusion than PVD Ru, and the adhesion of Cu to Ru(P) is better than the adhesion of Cu to Ta, despite the presence of P at the Ru(P)-Cu interface [22]. However, Shin and co-workers did not determine whether Ru(P) could function as a barrier when ultra-thin and/or in the presence of an applied electric field.

The requirements for capping layers are similar in many respects to the requirements for liner layers. The primary difference is that capping layers may be either metallic or dielectric. Because a major concern at the Cu-cap interface is EM failure caused by poor adhesion, most research into advanced Cu capping layers has focused on metallic caps. As such, potential metal caps must meet the following requirements:

- adhere well to Cu and dielectric films
- grow with excellent selectivity on Cu; no growth on IMD
- be minimally soluble in Cu
- not diffuse into dielectric materials
- not form a compound either with Cu or a dielectric film
- exhibit low electrical resistivity
- not damage exposed materials during the deposition process
- be thin when continuous and very smooth

Furthermore, because metallic capping layers are being investigated as *de facto* replacements for the dielectric capping layer, properly selected capping materials could allow removal of the relatively high-k dielectric capping materials (and therefore further extend the use of low-k materials, lowering the RC delay) if they can serve as an excellent barrier to Cu diffusion and be robust enough to not significantly degrade during dielectric deposition, etching, and resist stripping.

Because of its highly desirable properties, Co has become the primary metal investigated as a potential metallic capping layer. However, like Ru, Co is a poor barrier to Cu diffusion [23,24]. For this reason, a significant amount of research has been conducted on Co alloy films, significantly those with some amount of P added. The addition of just a few atomic percent (at. %) P to Co thin films greatly increases the barrier capability [24-26], and incorporation of P above a certain level should result in the formation the amorphous phase [27,28]. Co-based films are typically deposited by aqueous chemistries, either electro- or electroless deposition [27,29-31]. Some of the chemistries have been reported to show excellent selectivity for growth on Cu, but the ITRS states there is still general concern about line-to-line leakage or shorts between wires following aqueous depositions, and as such the problem of replacing the capping layer is not considered yet to be "solved." It is possible that a non-aqueous deposition chemistry, such as CVD, that shows good selectivity for growth on Cu could resolve this problem and serve as the next generation of Cu capping layers.

1.3. OBJECTIVE AND OVERVIEW OF CHAPTERS

The objective of the work described herein is to determine whether Ru(P) functions as a barrier and additionally to develop methods to deposit amorphous or nanocrystalline Co(P) films via CVD and characterize those films. The motivation is primarily for applications in Cu IC systems, although amorphous or nanocrystalline Co(P) films may find applications in other technologies. Initially, the intent was to further refine deposition chemistries for Ru(P) using PH_3 and/or other Ru precursors to minimize C incorporation in the films, however a lab move undertaken in early 2008 delayed installation of PH_3 gas until late 2009 and forced investigation of alternative amorphous film deposition using PMe_3. Each individual chapter from 2-6 is a single article that has been peer-reviewed and published or accepted for publication in the near future. The chapters are ordered chronologically by the date the corresponding article was submitted for review and publication. Electrical testing using time-to-failure measurements during bias-temperature-stressing indicate that 5 nm CVD Ru(P) is comparable to or better than 5 nm PVD TaN as a Cu diffusion barrier (Chapter 2, published in *Thin Solid Films*). Using a deposition chemistry analogous to that used for Ru(P) deposition, deposition of amorphous Co(P) by CVD with dicobaltoctacarbonyl [$Co_2(CO)_8$] and PMe_3 is described (Chapter 3, published in *Electrochemical and Solid-State Letters*). P and C incorporation in Co films impact film microstructure, forcing an amorphous phase above a certain limit, while increasing the resistivity and thermal stability (Chapter 4, published in the *Journal of the Electrochemical Society*). The adhesion and composition of Co(P) deposited on Cu is favorable for Cu IC implementation, however the selectivity toward growth on Cu is poor (Chapter 5, published in *Microelectronic Engineering*). Tetrakis(trimethylphosphine)cobalt(0), a

single molecule precursor containing Co, P, and C atoms, used for CVD with no additional co-reactant gases forms nanocrystalline Co(P) films containing C impurities (Chapter 6, published in the *Journal of Vacuum Science and Technology A*). A summary of the work and suggestions for future research are discussed in Chapter 7.

Chapter 2 presents the results of Cu diffusion barrier capability testing of both CVD Ru(P) and PVD TaN. PVD TaN represents the industry standard as a diffusion barrier and serves as a control reference film. Stressing metal-oxide-semiconductor (MOS) capacitor structures at accelerated conditions (electric fields and temperatures above those expected during operation of future IC structures) permits extrapolation to conditions more likely to exist in future generations. The data are fit to two models, the *E*-model and the $\sqrt{E}$-model, which are considered to be the most conservative models for estimating operating lifetimes. At every directly compared condition, Ru(P) outperforms TaN as a barrier, and the $\sqrt{E}$-model predicts that 5 nm CVD Ru(P) will act as an acceptable barrier in excess of 200 °C, although the *E*-model predicts neither Ru(P) nor TaN will function as barriers at this temperature when only 5 nm thick. However, for a variety of reasons, 200 °C is likely to be greater than the actual operating temperature within future IC architectures. Evaluation of the activation energy of failure for the MOS capacitor stack and evaluation of the *E*-model as a function of temperature indicates that 5 nm amorphous CVD Ru(P) is a functional barrier up to ~ 165 °C.

The method of depositing amorphous Co(P) films by CVD is presented in Chapter 3. Films grown from a dual-source chemistry of $Co_2(CO)_8$ and PMe_3 at 350 °C are amorphous when the amount of P incorporated is in excess of 8 at. %, and all films, regardless of microstructure, incorporate some C impurity. The bonding states of the

three elements present in the films are investigated by high-resolution X-ray photoelectron spectroscopy (XPS). As described in detail in the chapter, films are primarily composed of metallic Co and the P incorporated is only elemental (*i.e.* zero-valent), but C exists in one of two chemical states, either graphitic (elemental) or carbidic (bonded to Co). P is not homogeneously distributed throughout the film, and XPS depth profiling shows a steady drop in P concentration as sputtering proceeds. Films show exceptional thermal stability, remaining X-ray amorphous after 3 h annealing at 500 °C.

Chapter 4 provides an in-depth study of the effects of composition and substrate temperature on amorphous Co(P) film growth. In addition to the microstructural effects of adding P, C is shown to also contribute to the amorphization of the Co films, although its effect is less pronounced than that of P. Deposition at 250 °C minimizes C incorporation, and deposition at 300 °C minimizes resistivity. Annealing is shown to reduce the resistivity of the amorphous films, and XPS analysis indicates that a breakdown of Co carbides within the film and subsequent increases in metallic Co concentration is partially responsible.

Investigations into the growth of amorphous Co(P) on Cu, the surface on which Co(P) would be deposited upon in advanced IC structures, are presented in Chapter 5. Similar to Co(P) grown on SiO_2, CVD on CVD results in Co(P) that is relatively rich in P and C at the growth interface, and relatively poor in the same at the Cu interface. Because the Co(P)-Cu interface is relatively rich in Co, the adhesion between the two materials could remain sufficiently strong despite the incorporation of C and P at the interface. A scotch tape peeling test verified that the adhesion between the two remains strong. The minimum thickness for film continuity on Cu is found to be only 1.4 nm, but

the selectivity of deposition is poor compared to growth on SiO_2. Since Co(P) must grow selectively on Cu and not at all on SiO_2, explanation of the reasons for the poor selectivity are discussed in terms of the dual-source molecules used in this particular study, and potential methods to improve the selectivity of growth are presented.

The results of Co(P) CVD from a single molecule precursor are in Chapter 6. Tetrakis(trimethylphosphine)cobalt(0) is a non-commercially available molecule that contains 4 PMe_3 ligands around a central Co atom. Films could be deposited at temperatures $\geq$ 225 °C, but not $\leq$ 175 °C, and contained P and C. Unlike films grown from a dual source, the levels of P and C in the films could not be independently controlled, and the amount of P and C incorporated into the films is insufficient to force the amorphous microstructure. Rather, films deposited from this molecule are nanocrystalline (nc), as measured by XRD peak broadening. Like the amorphous Co(P) films, the C atoms incorporated existed in a mixture of elemental and (mostly) carbidic states, but the presence of grain boundaries provided a location for P to saturate, and the P incorporated was a mixture of phosphidic and (mostly) elemental. As-deposited films were only comprised of hcp Co nanocrystallites. Upon annealing to 400 °C remained primarily hcp with minimal allotropic transformation to fcc, although the hcp grains exhibited some extent of growth, but some Co_2P nanocrystallites precipitated.

1.4. REFERENCES

1. M. T. Bohr, IEEE IEDM Tech. Dig., 241 (1995).

2. J. Shin, Ph.D. Dissertation, "Growth and Characterization of CVD Ru and Amorphous Ru-P Alloy Films for Liner Application in Cu Interconnect," p. 8 (2007)

3. A. A. Istratov, C. Flink, H. Hieslmair, and E. R. Weber, Phys. Rev. Lett., 81, 1243 (1998).

4. J. D. McBrayer, R. M. Swanson, and T. W. Sigmon, J. Electrochem. Soc., 133, 1242 (1986).

5. Y. Shacham-Diamand, A. Dedhia, D. Hoffstetter, and W. G. Oldham, J. Electrochem. Soc., 140, 2427 (1993).

6. F. Lanckmans and K. Maex, Microelectron. Eng., 60, 125 (2002).

7. International Technology Roadmap for Semiconductors, 2008 Update, http://public.itrs.net

8. P. Xu, K. Huang, A. Patel, S. Rathi, B. Tang, J. Ferguson, J. Huang, C. Ngai, and M. Laboda, Proceedings of the IEEE International Interconnect Technology Conference, p. 109 (1999).

9. Y. H. Wang, M. R. Moitreyee, R. Kumar, L. Shen, K. Y. Zeng, J. W. Chai, and J. S. Pan, Thin Solid Films, 460, 211 (2004).

10. C.-K. Hu, L. Gignac, and R. Rosenberg, Microelectron. Reliab., 46, 213 (2006).

11. B. Li, T. D. Sullivan, T. C. Lee, and D. Badami, Microelectron. Reliab., 44, 365 (2004).

12. J. R. Lloyd and J. J. Clement, Thin Solid Films, 262, 135 (1995).

13. M. W. Lane, E. G. Liniger, and J. R. Lloyd, J. Appl. Phys., 93, 1417 (2003).

14. D. Josell, D. Wheeler, C. Witt, and T. P. Moffat, Electrochem. Solid-State Lett., 6, C143 (2003).

15. O. Chyan, T. N. Arunagiri, and T. Ponnuswamy, J. Electrochem. Soc., 150, C347 (2003).

16. T. N. Arunagiri, Y. Zhang, O. Chyan, M. J. Kim, and T. Q. Hurd, J. Electrochem. Soc., 152, G808 (2005).

17. M. Damayanti, T. Sritharan, Z. H. Gan, S. G. Mhaisalkar, N. Jiang, and L. Chan, J. Electrochem. Soc., 153, J41 (2006).

18. A. E. Kaloyeros and E. Eisenbraun, Annu. Rev. Mater. Sci., 30, 363 (2000).

19. J.-H. Shin, A. Waheed, K. Agapiou, W. A. Winkenwerder, H.-W. Kim, R. A. Jones, G. S. Hwang, and J. G. Ekerdt, J. Am. Chem. Soc., 128, 16510 (2006).

20. J.-H. Shin, A. Waheed, W. A. Winkenwerder, H.-W. Kim, K. Agapiou, R. A. Jones, G. S. Hwang, and J. G. Ekerdt, Thin Solid Films, 515, 5298 (2007).

21. J. Shin, H.-W. Kim, G. S. Hwang, and J. G. Ekerdt, Surf. Coat. Technol., 201, 9526 (2007).

22. J. Shin, H.-W. Kim, K. Agapiou, R. A. Jones, G. S. Hwang, and J. G. Ekerdt, J. Vac. Sci. Technol. A, 26, 974 (2008).

23. K. M. Chow, W. Y. Ng, and L. K. Yeung, Surf. Coat. Technol., 99, 161 (1998).

24. Paunovic, P. J. Bailey, and R. G. Schad, J. Electrochem. Soc., 141, 1843 (1994).

25. E. J. O'Sullivan, A. G. Schrott, M. Paunovic, C. J. Sambucetti, J. R. Marino. P. J. Bailey, S. Kaja, and K. W. Semkow, IBM J. Res. Dev., 42, 607 (1998).

26. A. Kohn, M. Eizenberg, and Y. Shacham-Diamand, J. Appl. Phys., 94, 3015 (2003).

27. M.A. Sheikholeslam, M.H. Enayati, and K. Raeissi, Mater. Lett., 62, 3629 (2008).

28. F. Cebollada, J. M. González, and P. Adeva, J. Mater. Res., 8, 105 (1993).

29. S. M. S. I. Dulal, H. J. Yun, C. B. Shin, and C.-K. Kim, J. Electrochem. Soc., 154, D494 (2007).

30. R. Tarozaitė, M. Kurtinaitienė, A. Džiūvė, and Z. Jusys, Surf. Coat. Technol., 115, 57 (1999).

31. J. Gambino, J. Wynne, J. Gill, S. Mongeon, D. Meatyard, B. Lee, H. Bamnolker, L. Hall, N. Li, M. Hernandez, P. Little, M. Hamed, I. Ivanov, and C. L. Gan, Microelectron. Eng., 83, 2059 (2006).

Chapter 2: Time-to-failure analysis of 5 nm amorphous ruthenium-phosphorus as a copper diffusion barrier

2.1. INTRODUCTION

As device dimensions have continued to scale, delivering the economic benefits promised by sustaining Moore's Law, alternative materials with more favorable properties have been introduced to improve chip functionality. Within the last several technology generations, Cu has been established as the interconnect (IC) metal. However, Cu readily diffuses into Si [1] and SiO_2 or other Si-based low-dielectric constant (κ) materials [2-4], and a Cu liner layer must be added to prevent device reliability degradation. The current solution is a physical vapor deposited (PVD) Ta/TaN bilayer stack acting as the barrier and adhesion promoter followed by a thin PVD Cu seed layer for subsequent Cu electroplating. The predicted thickness of the Cu liner is expected to shrink to 3.3 nm by 2010 [5], and it is unclear how much longer the PVD Ta-based bilayer will be extendable. This has led to research into alternate materials as Cu liners, especially W, Ta, and Ti, and their nitrides, carbides, ternary metal-N-C and metal-Si-N compounds [6].

Ideally, one material that could function as both the diffusion barrier and permit direct electroplating might enable scaling below the 3.3 nm liner layer thickness target. Previously Ru was considered as a single-layer diffusion barrier candidate because of a bulk resistivity ($\rho \sim 7\ \mu\Omega\cdot$cm) lower than α-Ta (~15-30 $\mu\Omega\cdot$cm) as well as its ability to permit direct Cu electroplating [7,8]. However, Cu diffuses through thin Ru films at unacceptably low temperatures [9,10] due to the fast diffusion paths created by the

columnar grain growth exhibited by Ru. Single-crystal films lack grain boundaries and have superior electrical properties, and would provide an ideal solution as Cu diffusion barriers, but process and materials restrictions make the use of single-crystal barriers unlikely. Amorphous films also lack grain boundaries, but with lower conductivity, should provide better Cu diffusion barrier properties than polycrystalline films, and are a more realistic solution than single-crystal barriers [6].

Recently, amorphous Ru-based films grown by chemical vapor deposition (CVD) were reported when sufficient levels of P were incorporated in the films. Films containing approximately a 17:1 ratio of Ru:P were grown using either a single precursor, $RuH_2(PMe_3)_4$ (Me=CH_3) [11,12], or separate Ru and P sources, $Ru_3(CO)_{12}$ and $P(Me)_3$ or $P(Ph)_3$ (Ph=C_6H_5) [13], and the resulting Ru(P) films remain amorphous after a 3 h anneal at 400 ºC. Density functional theory calculations indicate that amorphous Ru(P) is energetically favored over crystalline Ru(P) when P incorporation is >20% [13]. These growth chemistries result in films containing some level of C contamination. The amount of C does not have a significant impact on film microstructure, but increasing levels of C strongly and negatively impact resistivity. Amorphous Ru(P) film has been shown to be superior to physical vapor deposition (PVD) Ru of a similar thickness at preventing Cu diffusion in an annealing test [14], however to be useful as an IC diffusion barrier Ru(P) must prevent Cu diffusion at elevated temperatures while in the presence of an applied voltage creating an electric field across an adjacent dielectric layer.

The method of barrier testing at high temperatures and fields is referred to as bias-temperature stressing (BTS), and barrier effectiveness can be evaluated using several different methods, such as time-to-failure (TTF), capacitance-voltage measurement,

leakage current, and triangular voltage sweep [15]. Time-to-failure analysis is a particularly useful measure of metallic barrier effectiveness [16,17], and has been used to estimate the functional lifetime of Cu barriers [18,19]. In TTF analysis, metal-insulator-semiconductor (MIS) capacitors are heated and stressed in an electric field to accelerate copper diffusion across the barrier layer. This is essentially the same as time-dependent dielectric breakdown (TDDB) tests, which are used to assess the robustness of low-κ materials. However, in the case of Cu contamination, the lifetime of a dielectric will be greatly diminished and failure occurs before pure TDDB occurs.

Because the necessary lifetime of a gate oxide (and therefore any other chip component, *e.g.*, diffusion barrier) is generally required to be at least 10 years, reasonable TTF or TDDB (from here equivalently referred to as TDDB) studies must be conducted on time scales several orders of magnitude less than the functional lifetime of a dielectric or barrier. A TDDB model must then be used to predict the lifetime of a dielectric or a Cu diffusion barrier based on the failure times at the accelerated conditions. There have been several models for TDDB proposed, and choosing the proper model has been an area of debate, with the main candidates being the thermochemical model, also referred to as the *E* model, and the *1/E* model. The *E* model (Eq. 2.1) states that failure time (τ) is proportional to the exponential of the electric field (*E*) and is physically based on bond breakage within the dielectric as the cause of TDDB [20], while the *1/E* model (Eq. 2.2) proposes that failure time is proportional to the exponential of the inverse of the electric field (1/*E*) and is based on the contention that dielectric breakdown is due to Fowler-Nordheim current conduction [21,22].

$$\ln(\tau) \propto \frac{E_{a1}}{k_B T} - \gamma \cdot E \tag{2.1}$$

$$\ln(\tau) \propto \frac{E_{a2}}{k_B T} + \frac{G}{E} \tag{2.2}$$

In the models, γ and G are field acceleration parameters and E_{a1} and E_{a2} are activation energies of failure, subscripted 1 and 2 due to the difference in the proposed cause of failure. Although TDDB achieved over a small range of fields may match either model well, lifetimes estimated by the *1/E* model can easily be orders of magnitude greater than the *E* model when extrapolated to low electric fields. Whereas the *1/E* model predicts an infinite lifetime in the absence of an electric field, the *E* model may result in an overly pessimistic prediction. Recently, several authors have proposed models derived specifically for Cu diffusion-based failure of dielectrics [23-25]. While the precise mechanisms and forms of the models differ, all include proportionality between TDDB and the exponential of the $\sqrt{E}$. Of the $\sqrt{E}$ models, the Schottky-type models proposed by Suzumura, *et al.*, and Chen, *et al.*, are the most conservative at low fields, as they lack the *1/E* exponential prefactor included in the "impact-damage" and Poole-Frenkel failure mechanism models. In this study the results of Cu diffusion barrier analysis of 5nm CVD Ru(P) and 5 nm PVD TaN films on thermal SiO_2 by TDDB measurements are reported. It is beyond the scope of this paper to evaluate the various models for dielectric failure due to Cu diffusion across a barrier, and lifetime predictions herein will use the thermochemical *E* and Schottky-type $\sqrt{E}$ models to produce conservative, low field scenario estimates.

2.2. EXPERIMENTAL DETAILS

Films were grown in a combined deposition and analysis vacuum system consisting of a load lock, cold-wall CVD chamber, PVD system equipped with direct current magnetron sputtering capability, transfer chamber, and analysis chamber equipped with an X-ray photoelectron spectroscopy (XPS) system (Physical Electronics 3057; Mg K_α). Films 5 nm thick were grown on 20 mm × 20 mm pieces of 100 nm thermal SiO_2 on p-Si(100) 200 mm wafers obtained from Freescale Semiconductor. Film thickness was measured *in situ* by XPS Si 2p electron peak attenuation using electron attenuation lengths calculated from a NIST database and confirmed by TEM images (JEOL 2010F operated at 200 kV). Amorphous Ru(P) was grown using a dual-source chemistry of $Ru_3(CO)_{12}$ and $P(CH_3)_3$. The Ru precursor was carried by H_2 gas. This method is described in greater detail elsewhere [13]. *Ex situ* high resolution XPS analysis was conducted using a Kratos AXIS Ultra DLD equipped with a monochromatic Al K_α source. The *ex situ* spectra indicate that the atomic percentages in Ru(P) used herein were 83% Ru and 17% P, excluding C impurity. Because of the overlap of the Ru $3d_{3/2}$ peak and the C 1s peak and the large difference in XPS sensitivity to these photoelectrons, calculation of C within the film is better reported as a range of possible concentrations rather than a discrete value, and a reasonable estimate is between 10% and 30%. The effect of composition and microstructure of Ru(P) on resistivity for Cu liner applications is discussed in greater detail elsewhere [13, 14]. TaN was deposited by DC magnetron sputtering using 20 sccm Ar at 20 W. The pressure in the PVD chamber was maintained at 1.33 Pa during sputter depositions. The Ta to N ratio was ~5:4, and there was <10% O impurity combined in and on the film; it is important to note that this amount of O impurity makes the TaN used in this study below commercial

manufacturing quality TaN. After Ru(P) or TaN film deposition, ~150 nm PVD Cu was deposited by sputtering. Grazing angle (1º) X-ray diffraction (Bruker-Nonius D8) of both Cu-capped and uncapped barrier films exhibited an absence of diffraction peaks (not shown) associated with Ru, Ta, or TaN_x, indicating the barrier films were amorphous.

MIS capacitors were created in a multi-step lithography process using wet and dry etching. Cu was etched in dilute (~7%) HNO_3, TaN in 1:1:1 $HF:HNO_3:H_2O$. Ru(P) was dry etched in ~10:1 O_2:Ar plasma. After the first lithography step, any remaining photoresist was stripped by sonicating samples in acetone and CuO_x was removed with acetic acid and the sample was blown dry with N_2. The diameter of the capacitors was 1 mm. A second lithography step reduced the size of the Cu cap to 0.33 mm diameter, centered on the 1 mm diameter barrier, in order to eliminate the possibility of Cu diffusion down the barrier sidewall during BTS testing. Again, the MIS structures were cleaned in acetone and acetic acid. To improve electrical contact, the thin native oxide on the wafer backside was scratched through with a diamond-tipped scribe and ~200 nm Al was deposited by electron beam evaporation. A schematic of a completed MIS capacitor is depicted in Illustration 2.1. All structures were annealed in N_2 for 30 min at 300 ºC to remove any sputter damage. Shin, *et al.*, found that Cu does not dewet from the surface of Ru(P) after annealing for 1 h at 400 ºC [14]. XPS and scanning electron microscope (SEM) imaging were used to compare samples of PVD Cu on TaN prior to and after annealing at 300 ºC for 30 min in flowing N_2. Images collected by SEM (not shown) revealed grain growth of Cu, but no obvious signs of Cu agglomeration or dewetting. No Ta peak was observed in XPS, indicating that the ~ 150 nm-thick Cu grown on TaN remained continuous.

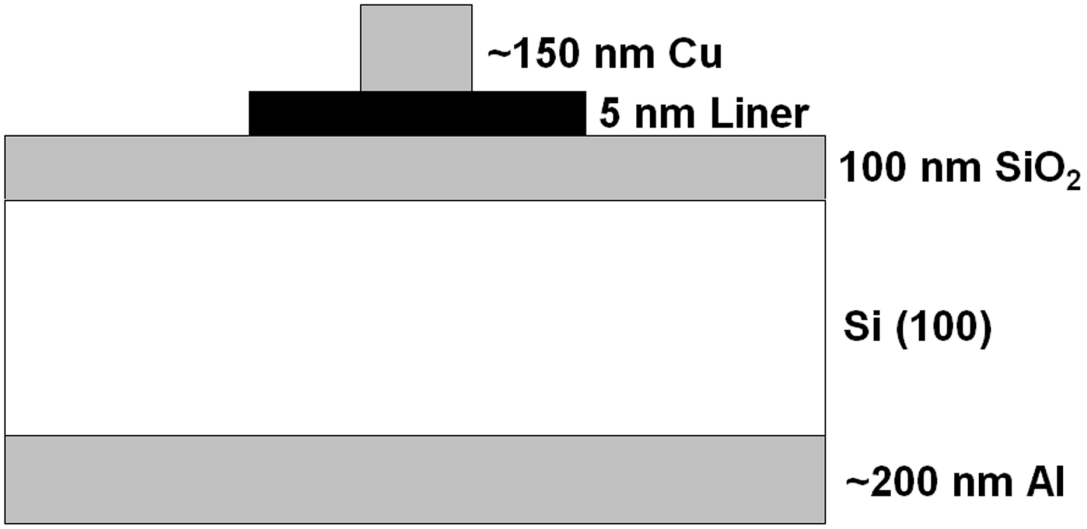

Illustration 2.1. Cross-sectional schematic of a completed MIS capacitor. The metallic gate is circular. The 1 mm diameter liner is either CVD Ru(P) or PVD TaN, and the diameter of the PVD Cu cap is 0.33 mm.

BTS was conducted in a N_2-purged, light-tight Plexiglas glove box, and samples were heated resistively by a grounded gold-coated chuck. Capacitors were heated to the testing temperature, and then a voltage was applied to the Cu gate for periods up to 48 h. An Agilent 4156C Semiconductor Parameter Analyzer applied a constant voltage bias to the gate and collected current measurements, which were sampled from every 0.1 s to every 48 s, depending on the total stressing time. Samples were subjected to temperatures from 200 ºC to 300 ºC and applied fields from 2.0 MV/cm to 4.0 MV/cm. Failure was defined as a sharp, rapid increase in current, typically of several orders of magnitude to the compliance limit of the analyzer. At least six capacitors were stressed at every BTS condition, and the median failure time (τ_{50}) was used for all extrapolations of lifetime and structure failure activation energy. Failure is defined as a rapid increase in leakage current across the device, typically of several orders of magnitude to the analyzer limit.

2.3. RESULTS AND DISCUSSION

Fig. 2.1 features a typical current-time (I-t) curve for a capacitor stressed at elevated conditions, which clearly illustrates the current increase defined as structure failure. Occasionally, small, short-lived current spikes such as those seen in Fig. 2.1 were observed prior to complete failure. This "self-healing" phenomenon has been previously observed, and is believed to be due to local heating caused by non-uniform diffusion of Cu across the dielectric [26,27]. The current initially drops as charges are trapped within the oxide before slowly increasing. Within SiO_2, Cu ions replace O atoms forming non-bridging O (NBO) atoms. The NBO atoms act as carriers, and conductivity

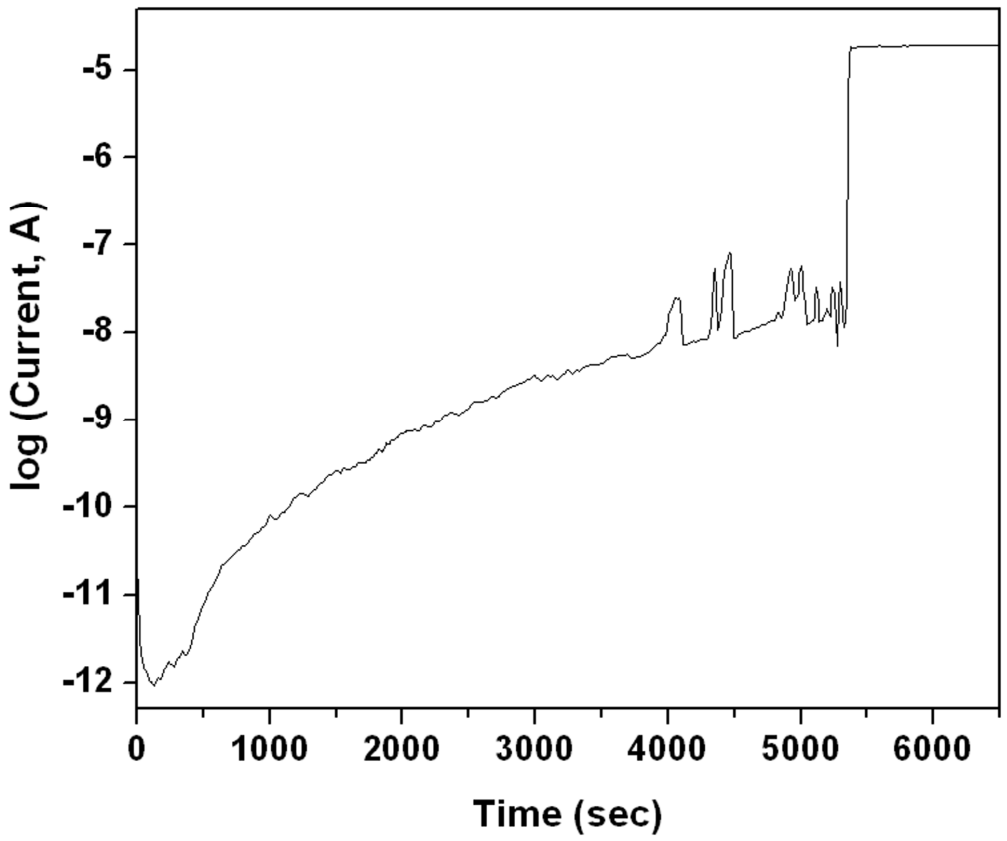

Figure 2.1. Typical leakage current plot for MIS capacitors during BTS. The failure time is defined as the time where the current sustained a large, abrupt increase.

is increased [28]. At about 5400 s the concentration of Cu ions at the SiO_2/Si interface reaches a critical level creating a conductive path between the cathode and anode, and the leakage current through the dielectric spikes at which time the structure is considered to have failed. The natural logarithm of the median failure times of Ru(P) barrier stacks and TaN barrier stacks at 200 °C and different applied fields are shown in Fig. 2.2. At each field, the median failure time was greater for the stacks with a Ru(P) barrier. A linear fit of the data is equivalent to using the *E* model to describe τ_{50} for each barrier. The slopes of the lines are the *E* model field acceleration parameters γ, and are 3.1 cm/MV and 3.9 cm/MV for Ru(P)- and TaN-liner structures, respectively. An extrapolation to low fields indicates that 5 nm Ru(P) is better than 5 nm TaN as a barrier for all fields less than 4 MV/cm. Predictions from various models are presented in Table 2.1. Considering the small number of capacitors tested at each condition, a conservative claim is that Ru(P) is comparable to TaN as a Cu diffusion barrier at low fields. The *E* model predicts a lifetime of <1 year (0.96 year) for the structure using a Ru(P) liner and 0.23 year for the TaN structure at a typical operating condition of 0.2 MV/cm. However, as shown in Fig. 2.3 the Schottky-type $\sqrt{E}$ model shows significant deviation from the *E* model at this field, and the lifetime of Ru(P) structures is >100 years (126.8 years), a difference of less than five powers of *e*. For comparison, the *1/E* model predicts lifetimes of 3.0×10^{46} years and 2.6×10^{48} years for Ru(P) and TaN, respectively, illustrating the extremely long lifetimes predicted when using this model at low fields.

The *E* model and the $\sqrt{E}$ model applied at 200 °C result in conflicting verdicts on the ability of Ru(P) to meet the ten year requirement as a diffusion barrier, but it is important to note that 200 °C could be hotter than the actual temperature at which an IC

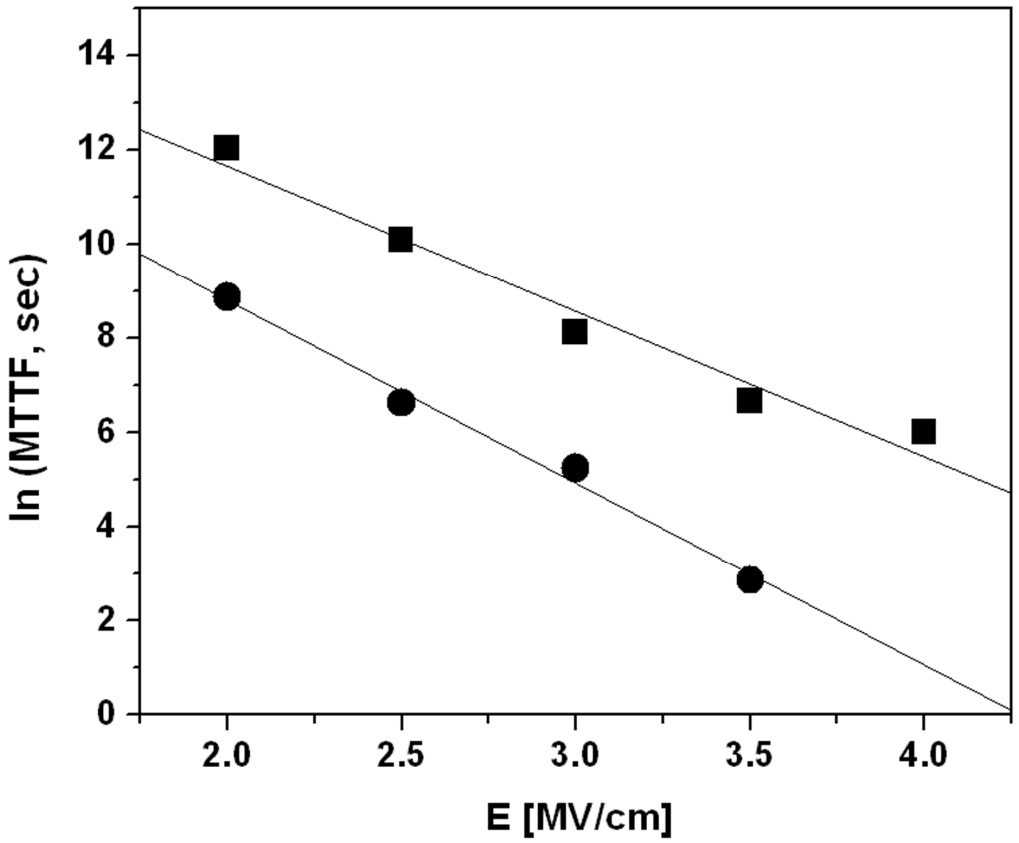

Figure 2.2. Median time-to-failure for Ru(P) (■) and TaN (●) liner structures for BTS performed at 200 ºC between 2 MV/cm and 4 MV/cm. The data are fit to the *E* model, which predicts Ru(P) outperforms TaN at all fields below 4 MV/cm.

Table 2.1. Functional lifetimes of TaN or Ru(P) at 200ºC and 0.2 MV/cm as predicted by multiple TDDB models.

	Functional lifetime (years)		
Liner Material	*E* - Model	*1/E* - Model	Schottky-type $\sqrt{E}$ - Model
5 nm PVD TaN	0.23	2.6×10^{48}	1,252.2
5 nm CVD Ru(P)	0.96	3.0×10^{46}	126.8

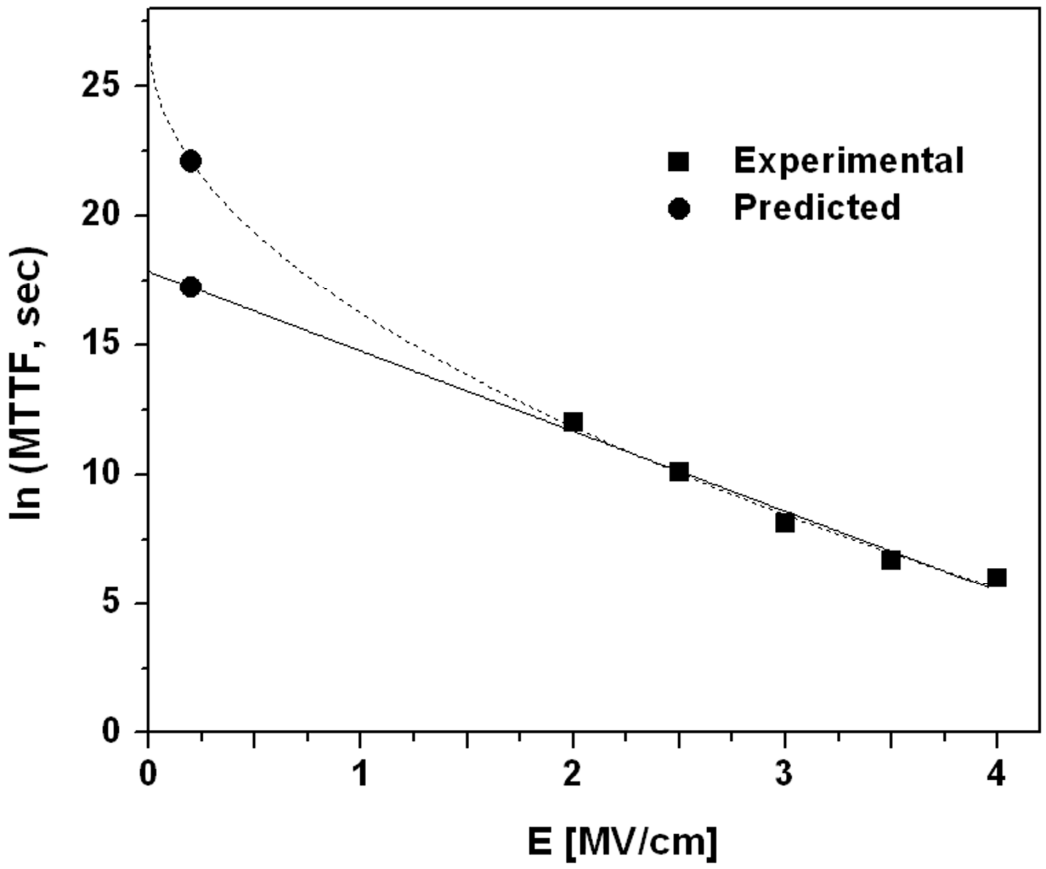

Figure 2.3. TTF for Ru(P) liner structures extrapolated to 0 MV/cm. The $\sqrt{E}$ model prediction (- - - - -) deviates from the linear E model (——) by nearly ten powers of e in the absence of an electric field. TTF predicted with the $\sqrt{E}$ model at 0.2 MV/cm is >100 years, while the E model predicts <1 year.

would operate in future technology generations in order to address resistivity and electromigration concerns. Because the $\sqrt{E}$ model predicts 5 nm Ru(P) is a sufficient barrier at 200 °C, only the E model requires consideration at lower temperatures. To account for temperature adjustments in the E model, the activation energy of structure failure and γ at the temperature of interest are needed. The E model predicts an inverse relationship between γ and temperature, but both Suehle and Chaparala [29] and Shiono and Itsumi [30] found γ to be independent of T for SiO_2 TDDB, and Hwang, *et al.*, report that γ for failure of Cu/SiO_2 is virtually independent of T [31]. Chen, *et al.*, found that γ for SiCOH failure due to Cu diffusion through a Ta-based barrier was weakly temperature dependent [25]. For these reasons, γ is treated as a constant herein.

Activation energy of Cu-diffusion induced failure has been found to be electric field-dependent. The change in E_a from 2.5 MV/cm to 4.0 MV/cm is shown in Fig. 2.4. As the field decreases, the median time to failure increases at each temperature, as does the activation energy. Much like the relationship between τ and E, activation energy can be considered to be related to E or $\sqrt{E}$, depending on which of the several models is selected, and both possibilities are presented in Fig. 2.5. The pure *thermal* activation energy (*i.e.*, zero field) is 2.66 eV and 1.83 eV for $\sqrt{E}$ and E dependence, respectively. At the operating condition of 0.2 MV/cm, the activation energies are 2.47 eV and 1.78 eV, respectively. For a conservative estimate, E_a for the case of the linear relationship as required by the E model evaluated at 0.2 MV/cm is useful, as it is the lowest. Fig. 2.6 shows the lifetime calculated at different temperatures using E_a of 1.78 eV and γ determined at 200 °C. The E model predicts a 5 nm Ru(P) liner is sufficient to meet the ten year lifetime requirement for temperatures up to ~165 °C.

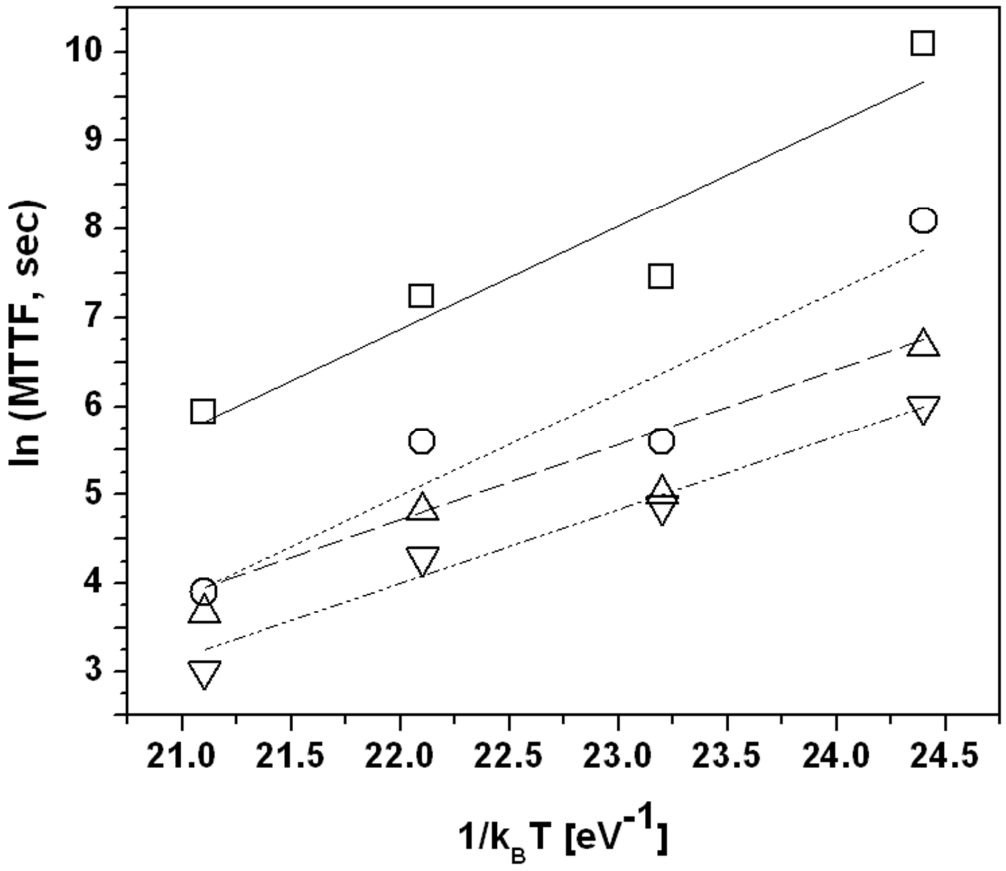

Figure 2.4. Plot of TTF versus $1/k_BT$ for Ru(P) liner structures stressed at 2.5 MV/cm (□), 3.0 MV/cm (○), 3.5 MV/cm (Δ), and 4.0 MV/cm (∇). The activation energy of structure failure is field-dependent.

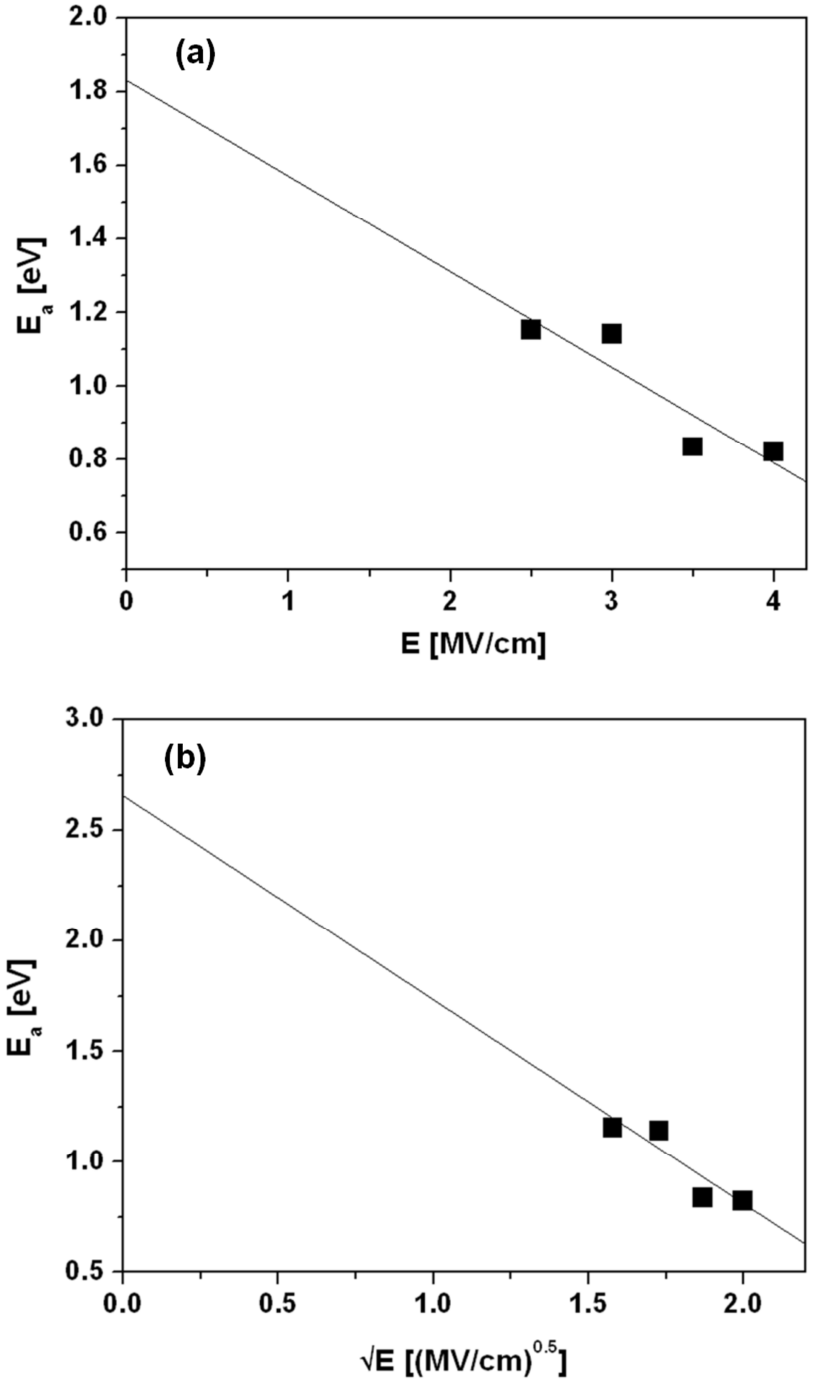

Figure 2.5. Field-dependent activation energy fit to both (a) E and (b) $\sqrt{E}$ dependence.

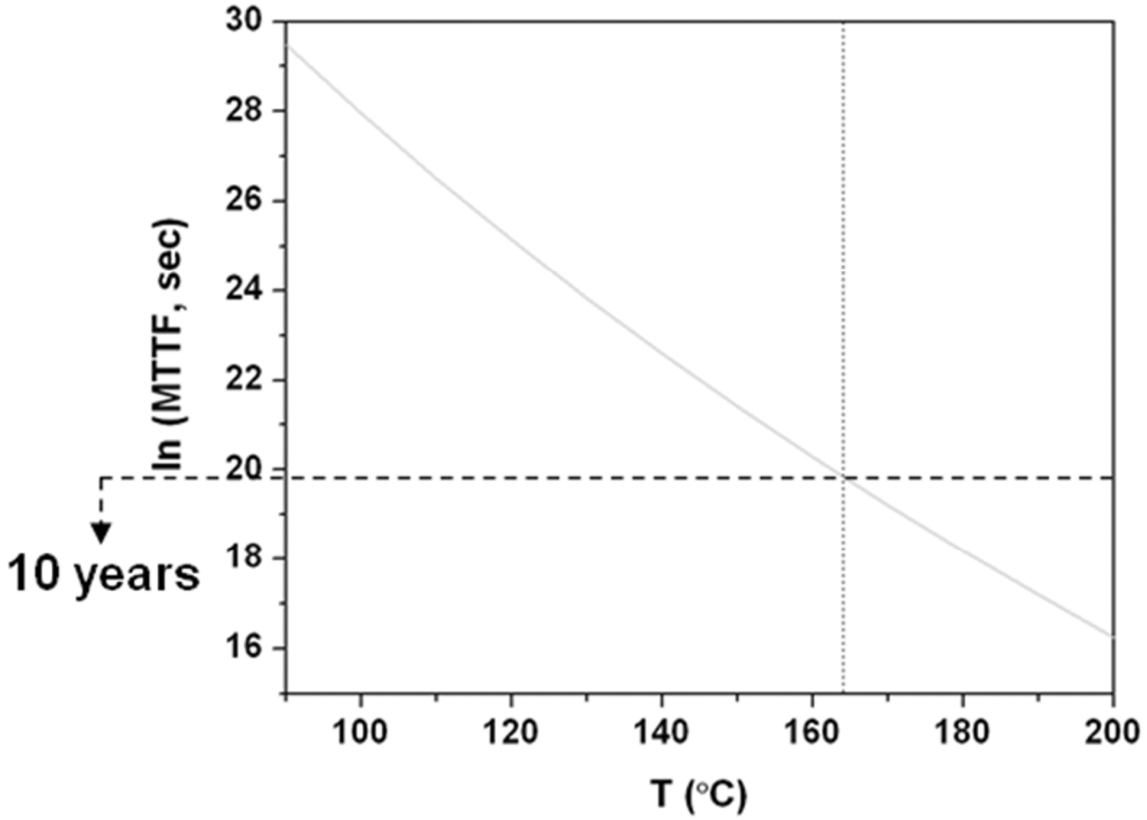

Figure 2.6. Calculated lifetime of 5 nm Ru(P) film at various temperatures using the *E*-model.

2.4. SUMMARY

CVD Ru(P) has been evaluated using bias-temperature stress time-to-failure analysis. A 5 nm film is at least comparable to 5 nm PVD TaN film containing <10% O at 200 ºC in preventing SiO_2 failure due to Cu diffusion. Modeling TTF data at 200 ºC using the Schottky-type $\sqrt{E}$ model indicate that Ru(P) is an acceptable barrier, with a functional lifetime in excess of 100 years. The E model predicts that Ru(P) is insufficient as a barrier at 200 ºC, but evaluation of the activation energy of MIS structure failure allows extrapolation to lower temperatures. Using the field acceleration parameter measured at 200 ºC and the most conservative estimate of MIS structure failure activation energy, the E model indicates that 5 nm Ru(P) is a functional barrier up to ~165 ºC.

2.5. REFERENCES

1. A. A. Istratov, C. Flink, H. Hieslmair, and E. R. Weber, Phys. Rev. Lett., 81, 1243 (1998).
2. J. D. McBrayer, R. M. Swanson, and T. W. Sigmon, J. Electrochem. Soc., 133, 1242 (1986).
3. Y. Shacham-Diamand, A. Dedhia, D. Hoffstetter, and W. G. Oldham, J. Electrochem. Soc., 140, 2427 (1993).
4. F. Lanckmans and K. Maex, Microelectron. Eng., 60, 125 (2002).
5. International Technology Roadmap for Semiconductors, 2007 Edition; http://public.itrs.net
6. A. E. Kaloyeros, E. Eisenbraun, Annu. Rev. Mater. Sci., 30, 363 (2000).

7. D. Josell, D. Wheeler, C. Witt, and T. P. Moffat, Electrochem. Solid-State Lett., 6, C143 (2003).

8. O. Chyan, T. N. Arunagiri, and T. Ponnuswamy, J. Electrochem. Soc., 150, C347 (2003).

9. T. N. Arunagiri, Y. Zhang, O. Chyan, M. J. Kim, and T. Q. Hurd, J. Electrochem. Soc., 152, G808 (2005).

10. M. Damayanti, T. Sritharan, Z. H. Gan, S. G. Mhaisalkar, N. Jiang, and L. Chan, J. Electrochem. Soc., 153, J41 (2006).

11. J.-H. Shin, A. Waheed, K. Agapiou, W. A. Winkenwerder, H.-W. Kim, R. A. Jones, G. S. Hwang, and J. G. Ekerdt, J. Am. Chem. Soc., 128, 16510 (2006).

12. J.-H. Shin, A. Waheed, W. A. Winkenwerder, H.-W. Kim, K. Agapiou, R. A. Jones, G. S. Hwang, and J. G. Ekerdt, Thin Solid Films, 515, 5298 (2007).

13. J.-H. Shin, H.-W. Kim, G. S. Hwang, and J. G. Ekerdt, Surf. Coat. Technol., 201, 9256 (2007).

14. J.-H. Shin, H.-W. Kim, K. Agapiou, R. A. Jones, G. S. Hwang, and J. G. Ekerdt, J. Vac. Sci. Technol. A, 26, 974 (2008).

15. H. Kizil and Ch. Steinbrüchel, Thin Solid Films, 449, 158 (2004).

16. R. Gonella, P. Motte, and J. Torres, Microelectron. Reliab., 40, 1305 (2000).

17. Zs. Tőkei, M. Patz, M. Schmidt, F. Iacopi, S. Demuynck, and K. Maex, Microelectron. Eng., 76, 70 (2004).

18. G. Bai, S. Wittenbrock, V. Ochoa, R. Villasol, C. Chiang, T. Marieb, D. Gardner, C. Mu, D. Fraser, and M. Bohr, Mater. Res. Soc. Symp. Proc., 403, 501, (1996).

19. B. K. Lim, H. S. Park, L. K. Chin, S. W. Woo, A. K. H. See, C.-S. Seet, T.-J. Lee, and N. L. Yakovlev, J. Vac. Sci. Technol. B, 22, 2286 (2004).

20. J. W. McPherson and H.C. Mogul, J. App. Phys., 84, 1513 (1998).

21. J. Lee, I. Chen, and C. Hu, IEEE Trans. Electron Dev., 35, 2268 (1988).

22. K. Schuegraf and C. Hu, Semicond. Sci. Technol., 9, 989 (1994).

23. J. R. Lloyd, E. Liniger, and T. M. Shaw, J. App. Phys., 98, 084109 (2005).

24. N. Suzumura, S. Yamamoto, D. Kodama, K. Makabe, J. Komori, E. Murakami, S. Maegawa, and K. Kubota, Proceedings of the 44th Annual International Reliability Physics Symposium, p.484 (2006).

25. F. Chen, O. Bravo, K. Chanda, P. McLaughlin, T. Sullivan, J. Gill, J. Lloyd, R. Kontra, and J. Aitken, Proceedings of the 44th Annual International Reliability Physics Symposium, p.46 (2006).

26. G. Raghavan, C. Chiang, P. B. Anders, S.-M. Tzeng, R. Villasol, G. Bai, M. Bohr, and D. B. Fraser, Thin Solid Films, 262, 168 (1995).

27. E. R. Engbrecht, Y.-M. Sun, K. H. Junker, J. M. White, and J. G. Ekerdt, J. Vac. Sci. Technol. B, 23, 463 (2005).

28. G. Barbottin and A. Vapaille (Eds.), Instabilities in Silicon Devices: Silicon Passivation and Related Instabilities, Elsevier, Amsterdam, 1986, p. 133.

29. J. S. Suehle and P. Chaparala, Microelectron. J., 27, 657 (1996).

30. N . Shiono and M. Itsumi, Proceedings of the 31st Annual International Reliability Physics Symposium, p. 1 (1993).

31. S.-S. Hwang, S.-Y. Jung, and Y.-C. Joo, J. Appl. Phys., 101, 074501 (2007).

Chapter 3: Chemical vapor deposition of amorphous cobalt-phosphorus films

3.1. INTRODUCTION

Due to its low bulk resistivity (~6 μΩ·cm), strong adhesion to Cu [1], and low solubility in Cu [2], thin Co and Co-based alloy films, such as Co(P), are currently being investigated for use in Cu interconnects (IC). The focus of much of this Co research is primarily motivated by the benefits of replacing the current Si-based dielectric Cu-capping layers with Co-based layers. Use of a Co-based layer increases the electromigration lifetime of Cu interconnects by orders of magnitude by improving upon the weak bonding between Cu and the dielectric capping layer [3-5]. Considering the relatively high dielectric constant (κ) of dielectric capping layers [6], a Co-based capping layer also permits the added benefit of lowering the effective κ value of layers throughout the IC architecture, which results in lower resistive-capacitive delay. Currently, Co-based alloys films such as Co(P) and Co(W,P) can be deposited using electro- and electroless deposition chemistries, which can exhibit highly-selective growth on Cu [7-10]. Aqueous deposition can also produce amorphous films that are metastable and will crystallize at sufficiently high temperatures [7,11]. Because of the lack of crystal grain boundaries, amorphous films should have improved Cu diffusion barrier properties over polycrystalline films [12].

3.2. EXPERIMENTAL DETAILS

Films were grown in a multi-chamber system composed of two load locks, a vacuum sample transfer chamber, physical and chemical vapor deposition chambers, and an analysis chamber equipped with X-ray photoelectron spectroscopy (XPS) (Physical Electronics 3057; Mg Kα) [13]. Amorphous Co(P) films were deposited at 350°C and ~12 Pa in a cold-wall reactor on 400 nm chemically grown (using tetraethylorthosilicate) SiO_2/Si(100) wafers obtained from Sematech. The wafers were cut into 20 mm × 20 mm pieces and heated radiatively from below. A dual source CVD chemistry of dicobaltoctacarbonyl [$Co_2(CO)_8$] (95-99%, stabilized in 1-5% hexane, Alfa Aesar; precursor used without further purification) and trimethylphosphine [PMe_3, (Me = CH_3)] (99%, Sigma-Aldrich) was used for deposition. $Co_2(CO)_8$ was chosen due to its high volatility and its potential for use in CVD over a wide range of substrate temperatures [14]. Additionally, the Co in $Co_2(CO)_8$ is in the zero-valent state, meaning thermal decomposition alone results in high-purity metallic Co films without the need of a co-reactant gas [15]. The room temperature Co precursor was carried to the chamber using ultra-high purity H_2 (99.999%, Matheson Tri-Gas). PMe_3 vapor was dosed through a leak valve. Films were characterized using scanning electron microscopy (SEM), X-ray diffraction (XRD), and XPS. Sheet resistance was measured using a Veeco FPP-5000 automatic four point probe.

Film compositions were measured using *ex situ* high-resolution XPS analysis (Kratos AXIS Ultra DLD; monochromatic Al Kα). Samples were first sputter-cleaned with 4 kV Ar^+ ions for ~40 sec to remove surface C contamination and to remove a thin layer of oxidized Co that developed upon exposure to ambient; the thin oxidized layer

was not observed during *in situ* XPS analysis conducted immediately after film growth. No O was detected in the film bulk during *in situ* or *ex situ* analysis.

3.3. RESULTS AND DISCUSSION

Table 3.1 shows the composition of sample films as measured just below the native oxide layer, as well as film thickness measured in cross-sectional SEM (Zeiss Supra 40 VP) and film resistivities calculated from the measured thickness and sheet resistance. Amorphous Co(P) alloys contained a P:Co ratio as low as 1:9. Representative XPS spectra for the amorphous alloy are shown in Fig. 3.1. In the P 2p spectrum (Fig. 3.1a), the $2p_{3/2}$ peak was located at a binding energy (BE) of 129.6 eV, with a separation between the $2p_{1/2}$ and $2p_{3/2}$ peak of 0.9 eV. The Co 2p spectrum (Fig. 3.1c) shows a doublet with highly asymmetric peaks, with the major $2p_{3/2}$ peak located at 778.3 eV and the $2p_{1/2}$ peak located 793.4 eV. Nemoshkalenko, *et al*. [16], found the BE for the P $2p_{3/2}$ peak for CoP and Co_2P were indistinguishable from each other (~129.4-129.5 eV) and located very near the BE range listed by the National Institute of Standards and Technology (NIST) XPS Database (version 3.5) [17] for elemental P (129.9 eV to 130.35 eV). NIST also lists the BE for the $2p_{3/2}$ peak of elemental Co as 777.8 eV to 778.5 eV, and only one standard for Co in CoP and Co_2P, both of which have BE that fall in the NIST range for elemental Co [16-17]. However, according to Nemoshkalenko, *et al*., the Co $2p_{3/2}$ peak BE increases up to 0.7 eV in the standard CoP and Co_2P when compared to a metallic Co standard [16]. In the current investigation, no difference in 2p peak BE was observed in Co(P), CVD Co, or Co foil (99.95%, ESPI Metals) in XPS, nor

%Co	%P	%C	Thickness (nm)	ρ (μΩ cm)	Microstructure
69.6	7.7	22.7	47	678	Amorphous
60.7	10.3	29.0	32	1077	Amorphous
58.5	12.3	29.1	65	523	Amorphous
72.0	10.8	17.2	38	741	Amorphous
51.0	16.0	33.0	47	1066	Amorphous
74.7	6.5	18.8	136	1496	Polycrystalline
95.0	-	5.0	106	244	Polycrystalline

Table 3.1. Composition (atomic percent) and resistivity of Co(P) films deposited on SiO_2.

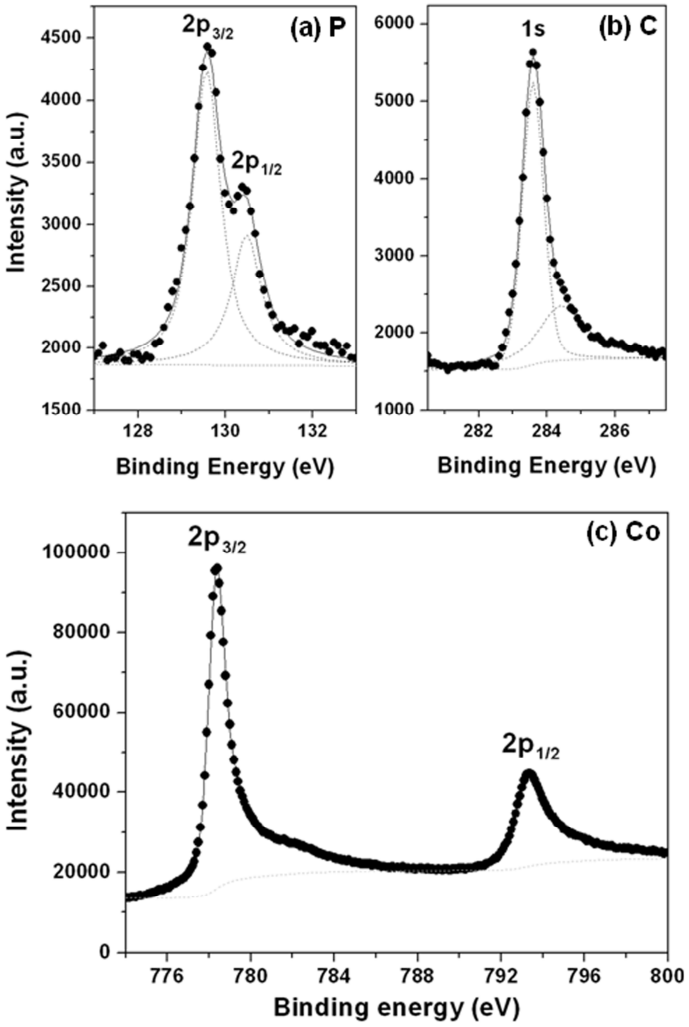

Figure 3.1. High resolution XPS of (a) P 2p, (b) C 1s, and (c) Co 2p spectra.

were there any noticeable difference in peak shapes. The reduction in P BE with no accompanying increase in Co BE has been previously observed elsewhere [18]. Therefore, while there appears to be some extent of electron density transfer to P atoms, the chemical states within the film are differentiated from typical CoP or Co_2P.

XPS depth profiling was used to track the change in P concentration through the film. As shown in Fig. 3.2, as the film was sputtered through, the P:Co atomic ratio decreases from ~0.19 after 10 sec sputtering to ~0.05 after 190 sec sputtering. No change in the chemical state of Co or P was observed through the bulk of the film. This trend is consistent with both electrodeposited Co(P) [19] and amorphous CVD Ru(P) [13]. The film contained some amount of C contamination (~20-30%) in the bulk, but CVD conducted in the absence of PMe_3 resulted in metallic Co, containing only 5% C impurity (see Table 1). The hexane stabilizer and CO ligands from the precursor do not contribute greatly to the C contamination in Co(P) films. C was incorporated in Co(P) in two distinct chemical states. The C 1s spectrum (Fig. 3.1b) contains a large peak at 283.6 eV, indicating C-Co bonding [20], with a small shoulder at 284.5 eV, corresponding to graphitic C-C bonding [17]. All C spectra featured similar peak area ratios between the two bonding states of C. Note that the formation of C-Co bonds is not differentiable from elemental Co in Co 2p XPS due to a negligible BE shift (~0.1 eV) [21]. Although C has low solubility and low residual resistivity in Cu [22], any unnecessary increase in line resistance would be undesirable. Also, the presence of C at the interface substituting for Co would decrease the extent of very strong Co-Cu interaction. Therefore, it would be more preferable to reduce the amount of C in the films, perhaps using PH_3 in place of PMe_3 during CVD.

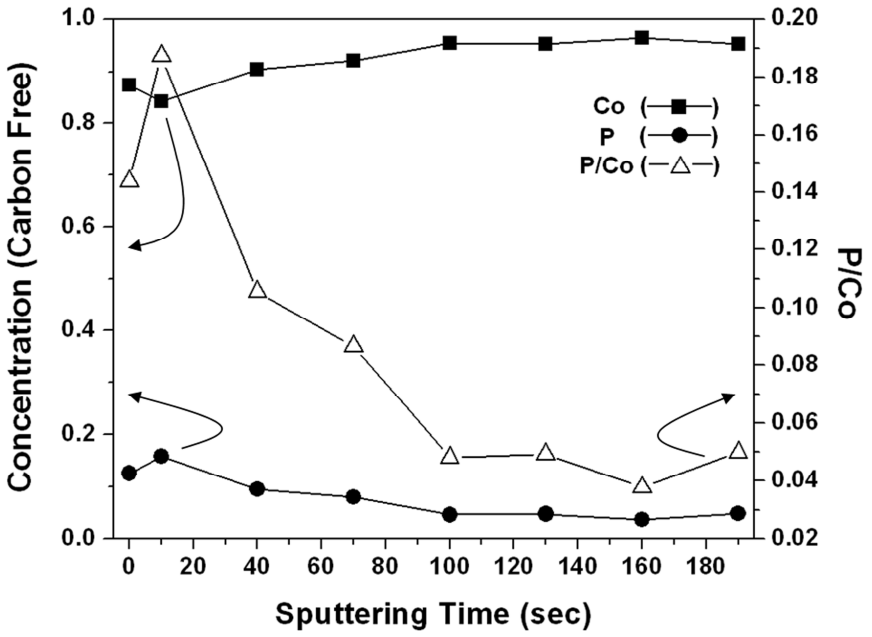

Figure 3.2. XPS depth profiles of amorphous Co(P), excluding surface/bulk C and surface O contamination.

The thermal stability of amorphous CVD Co(P) films was evaluated by furnace annealing and XRD (Bruker-Nonius D8). Fig. 3.3 shows the grazing angle (1°) pattern for CVD Co and Co(P). Co grown without trimethylphosphine (Spectrum 3.3a) shows peaks at 42.34°, 45.12°, and 48.14°, which are assigned to the (100), (002), and (101) planes of hcp Co, respectively [23]. The peaks for Co(P) containing a low level of P (6.5%, including C) incorporation (Spectrum 3.3b) are broader, and the (002) peak is reduced in intensity. However, no peaks exist for as-deposited P-rich Co(P) alloy (7.7% P) within this range of 2θ (Spectrum 3.3c), nor were any other Co or Co_xP peaks observed in extended 2θ scans (20°-120°, not shown), indicating the film is XRD-amorphous. Spectrum 3.3d shows the diffraction pattern for the 7.7% Co(P) film after being annealed for 3 hr at 500 °C in 67 Pa flowing 90% N_2 forming gas. There are no peaks in this or the extended (not shown) 2θ range, and the film remains amorphous under this annealing condition. Electrodeposited Co(P) typically forms crystallites below 500 °C [7,11,24]. The reason for the difference in thermal stability between CVD and aqueous-deposited films is unclear, and may be due to a different film growth mechanism or higher C impurity levels in the CVD films. It is also possible that nanocrystals may have nucleated in the CVD film and were too small to be detected by XRD.

3.4. SUMMARY

Amorphous Co(P) was grown on SiO_2 from $Co_2(CO)_8$ by co-dosing PMe_3 and incorporating P in the film. The binding energy of P was shifted slightly lower than elemental P, however the absence of an accompanying shift to a higher binding energy in the Co 2p spectrum indicates that the film is not composed of typical CoP or Co_2P. Films

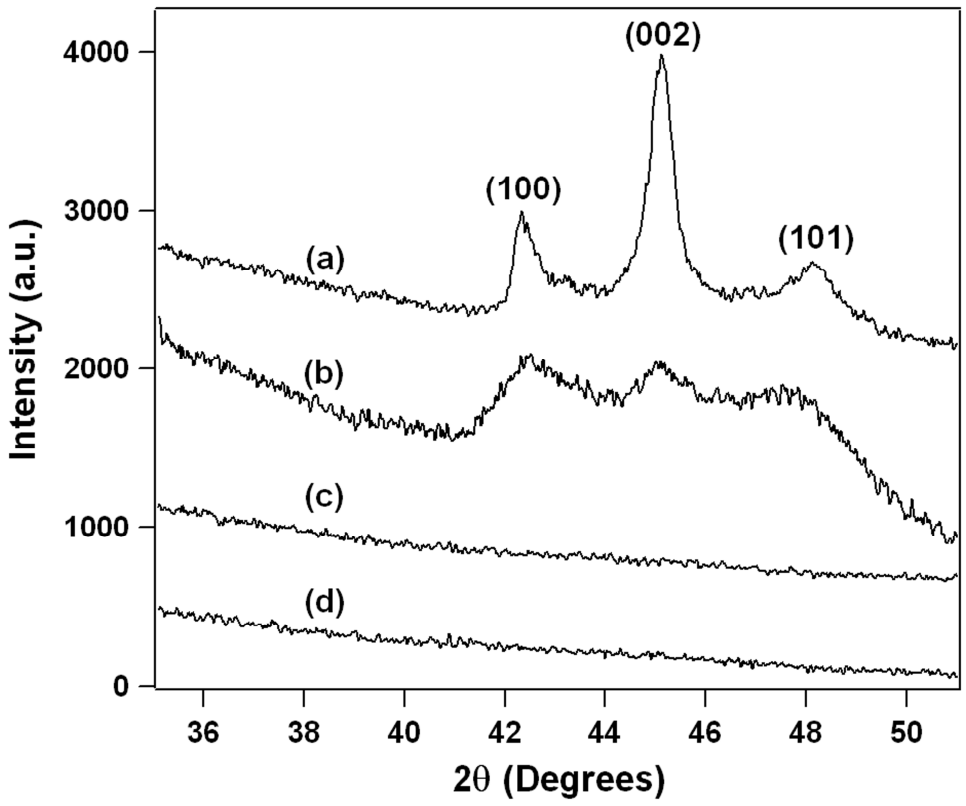

Figure 3.3. Grazing angle XRD of CVD films: (a) Co with 0% P, (b) polycrystalline Co(P) (6.5% P), (c) amorphous Co(P) (7.7% P), (d) amorphous Co(P) (7.7% P) after annealing at 500 °C for 3 hr.

incorporated C impurities, which showed a strong tendency to form Co-C bonds. Unlike aqueous deposited Co(P), the CVD film remains stable in the amorphous phase after undergoing a 500 °C anneal.

3.5. REFERENCES

1. Z. Li, R. G. Gordon, D. B. Farmer, Y. Lin, and J. Vlaasak, Electrochem. Solid-State Lett., 8, G182 (2005).

2. H. Li and B. P. Tonner, Surf. Sci., 237, 141 (1990).

3. E. Zschech, M. A. Meyer, S. G. Mhaisalkar, A. V. Vairagar, A. Krishnamoorthy, H. J. Engelmann, and V. Sukharev, Thin Solid Films 504, 279 (2006).

4. C.-K. Hu, D. Canaperi, S. T. Chen, L. M. Cignac, B. Herbst, S. Kaldor, M. Krishnan, E. Liniger, D. L. Rath, D. Restaino, R. Rosenberg,. J. Rubino, S.-C. Seo, A. Simon, S. Smith, and W.-T. Tseng, IEEE International Reliability Physics Symposium Proceedings, p. 222 (2004).

5. C.-K. Hu, L. Gignac, R. Rosenberg, E. Liniger, J. Rubino, C. Sambucetti, A. Stamper, A. Domenicucci, and X. Chen, Microelectron. Eng., 70, 406 (2003).

6. N. Matsunaga, N. Nakamura, K. Higashi, H. Yamaguchi, T. Watanabe, K. Akiyama, S. Nakao, K. Fujita, H .Miyajima, S .Omoto, A. Sakata, T. Katata, Y. Kagawa, H. Kawashima, Y. Enomoto, T. Hasegawa, and H. Shibata, Proceedings of the IEEE International Interconnect Technology Conference, p. 6 (2005).

7. M.A. Sheikholeslam, M.H. Enayati, and K. Raeissi, Mater. Lett., 62, 3629 (2008).

8. S. M. S. I. Dulal, H. J. Yun, C. B. Shin, and C.-K. Kim, J. Electrochem. Soc., 154, D494 (2007).

9. R. Tarozaitė, M. Kurtinaitienė, A. Džiūvė, and Z. Jusys, Surf. Coat. Technol., 115, 57 (1999).

10. J. Gambino, J. Wynne, J. Gill, S. Mongeon, D. Meatyard, B. Lee, H. Bamnolker, L. Hall, N. Li, M. Hernandez, P. Little, M. Hamed, I. Ivanov, and C. L. Gan, Microelectron. Eng., 83, 2059 (2006).

11. F. Cebollada, J. M. González, and P. Adeva, J. Mater. Res., 8, 105 (1993).

12. L. B. Henderson and J. G. Ekerdt, Thin Solid Films, 517, 1645 (2009).

13. J.-H. Shin, A. Waheed, W. A. Winkenwerder, H.-W. Kim, K. Agapiou, R. A. Jones, G. S. Hwang, and J. G. Ekerdt, Thin Solid Films, 515, 5298 (2007).

14. D.-X. Ye, S. Pimanpang, C. Jezewski, F. Tang, J. J. Senkevich, G.-C. Wang, and T.-M. Lu, Thin Solid Films, 485, 95 (2005).

15. J. Lee, H. J. Yang, J. H. Lee, J. Y. Kim, W. J. Nam, H. J. Shin, Y. K. Ko, J. G. Lee, E. G. Lee, and C. S. Kim, J. Electrochem. Soc., 153, G539 (2006).

16. V. V. Nemoshkalenko, V. V. Didyk, V. P. Krivitskii, and A. I. Senekevich, Zh. Neorg. Khim., 28, 2182 (1983).

17. NIST X-ray Photoelectron Spectroscopy Database, Version 3.5 (National Institute of Standards and Technology, Gaithersburg, 2003); http://srdata.nist.gov/xps/

18. A. W. Burns, A. F. Gaudette, and M. E. Bussell, J. Catal., 260, 262 (2008).

19. R. C. da Silva, M. L. Sartorelli, M. Sardela, and A. A. Pasa, Phys. Status Solidi A, 187, 85 (2001).

20. H. Wang, S. P. Wong, W. Y. Cheung, N. Ke, G. H Wen, X. X. Zhang, and R. W. M. Kwok, J. Appl. Phys., 88, 4919 (2000).

21. F. L. Wang, J. C. Jiang, and E. I. Meletis, J. Appl. Phys., 95, 5069 (2004).

22. K. Barmak, C. Cabral, K. P. Rodbell, and J. M. E. Harper, J. Vac. Sci. Technol. B, 24, 2485 (2006).

23. C. Wisniewski, I. Denicoló, and I. A. Hümmelgen, J. Electrochem. Soc., 142, 3889 (1995).

24. F. Branda, L. Lanotte, A. Costantini, and P. Matteazzi, J. Mater. Sci., 28, 1824 (1993).

Chapter 4: Effect of phosphorus and carbon incorporation in amorphous cobalt films prepared by chemical vapor deposition

4.1. INTRODUCTION

The primary force driving technological advances in the semiconductor industry is the significant cost reduction that accompanies device scaling. This continuous shrinking of dimensions causes conditions within the chip, such as the maximum current density (J_{max}) through the interconnect (IC), to change from generation to generation, which often forces reassessment of materials used in fabrication. Those materials that are expected to be incompatible in future technology generations must be identified and replaced with more functional materials. Currently, once a level of IC Cu metallization is complete, a thin layer of dielectric material is deposited across the wafer surface, including directly on the Cu itself. A Si-based dielectric material such as SiN, SiC, or SiCN is commonly used as the capping layer, but the predicted J_{max} is expected to exceed the acceptable limits for dielectric capping layers as soon as 2013, when it is predicted to increase to 2.11×10^{6} A cm^{-2} for intermediate wiring [1].

In a Cu IC, the time to electromigration (EM) failures is directly related to the interfacial adhesion between Cu and the adjacent material [2], and the poor adhesion between dielectric materials and Cu will become a limiting factor in IC reliability when EM failure times at this weak interface reach unacceptable levels. Non Si-based materials are now under investigation to replace the dielectric capping layer, and include Co and other Co-based alloy films [3-6], which are of great interest due to the strong bonding between Co and Cu [7] many orders of magnitude above Cu/dielectric bonding

[8]. By improving upon the weak bonding, a Co-based layer can increase EM lifetimes by orders of magnitude [9-11]. Additionally, Co has very low bulk resistivity (ρ = 5.7 $\mu\Omega$·cm) and low solubility in Cu [12-13], making it an attractive candidate for Cu IC applications. By removing the high-dielectric constant (κ) Si-based capping layers and replacing them with thin Co-based capping layers, low κ materials could then be more extensively applied throughout the IC architecture, thereby lowering the effective κ value and reducing the resistive-capacitive delay within the chip [8]. This technology pathway requires the substituted Co/dielectric combination to provide sufficient prevention of Cu diffusion, which would rapidly diffuse into Si and cause device failure.

Co itself is a very poor barrier to Cu diffusion at temperatures characteristic of back-end fabrication processes, in large part due to the existence of fast diffusion paths along the crystalline grain boundaries of Co films [14-15]. Grain boundaries provide a direct pathway for rapid Cu diffusion into the surrounding dielectric, which itself would provide poor resistance to Cu diffusion if low-κ materials are utilized [16-19]. The diffusivity of Cu in nanocrystalline Co decreases by a few orders of magnitude by incorporating only low levels ($\leq$10%; all percentages reported herein are overall atomic percentages) of P in films because of grain boundary stuffing [15,20-21]. Slowing the diffusion through grain boundaries can transform a material through which Cu quickly diffuses when polycrystalline, such as Ru [22-26], W [27-28], or Co [14-15], into a potential diffusion barrier if the grain boundaries are stuffed or completely eliminated, as in amorphous films, by adding an alloying element, such as N [29-30] or P [15,20-21,31-33]. Numerous electro- and electroless methods and chemistries for deposition of Co(-based) films have been reported, and often show good selectivity for growth on Cu [6-9].

Electrodeposited Co(P) alloy was reported to exist in a metastable amorphous phase when the P concentration is >12% [34], and the resistivity of amorphous Co(P) is typically ~100-200 μΩ·cm.

Recently, we reported chemical vapor deposition (CVD) of amorphous Co(P) as a way to circumvent aqueous conditions during deposition [35]. Films were grown from a dual-source chemistry of dicobaltoctacarbonyl and trimethylphosphine at 350 °C on SiO_2. The films showed very good thermal stability, maintaining their amorphous nature after a 3 h anneal at 500 °C. Carbon was incorporated as an impurity in both the graphitic and carbidic states. In this study, we report in greater detail the effect of P and C incorporation on the microstructure, resistivity, and thermal phase stability of these films, as well as the role of deposition temperature on the extent of P and C incorporation and resistivity. Measurements and evaluations were conducted using X-ray photoelectron spectroscopy (XPS), scanning electron microscopy (SEM), and four-point probe measurements. Film properties pertaining to the proposed IC applications of Co-based films were studied after annealing at milder temperatures typical of back-end processing.

4.2. EXPERIMENTAL DETAILS

Films were grown in a combined vacuum deposition and analysis system [36], including a load lock, vacuum sample transfer chamber, CVD chamber, and analysis chamber. The CVD chamber (base pressure 4.0×10^{-6} Pa) is a cold-wall, stainless steel reactor, where samples are heated to the deposition temperature radiatively with a bulb from below. The analysis chamber (base pressure $<5.3\times10^{-8}$ Pa) is equipped with X-ray photoelectron spectroscopy (Physical Electronics 3057, Mg Kα) and low-energy ion

scattering spectroscopy. Co(P) films were grown on 20 mm × 20 mm pieces of 400 nm chemically grown (from tetraethylorthosilicate) SiO_2/Si(100) 200 mm wafers provided by Sematech. Wafer pieces were cleaned with He gas immediately prior to loading.

The Co precursor was dicobatoctacarbonyl [$Co_2(CO)_8$] (95-99%, stabilized in 1-5% hexane, Alfa Aesar, and precursor was used without further purification), which is solid at room temperature, as part of a dual-source deposition chemistry. Thermal CVD using the unfiltered precursor has previously been shown to result in high-purity metallic Co films over a large range of temperatures [37-40]. The Co precursor was contained in a glass saturator through which ultra-high purity H_2 (99.999%, Matheson Tri-Gas) carrier gas flowed at 2.0 sccm. Due to its high volatility [41], $Co_2(CO)_8$ maintained at room temperature during growth provided sufficient vapor pressure for transport to the chamber and growth. Trimethylphosphine [PMe_3, Me = CH_3] (99%, Sigma-Aldrich) was co-dosed directly to the reactor through a leak valve to serve as the source of P. Substrate temperatures ranged from 250 °C to 350 °C during deposition, and the substrate was degassed in the chamber at the deposition temperature in flowing H_2 for at least 1 h prior to CVD. The pressure ranged from 0.9 Pa to 1.6 Pa, and pressure changes were mainly dependent on the level of PMe_3 co-dosing. A mechanical pump was fully opened to the chamber during deposition. *In situ* XPS analysis was performed after surface contamination was removed by 2 kV Ar^+ ion sputter cleaning for 120 sec. Based on previous work [42], these sputtering conditions were estimated to also remove ~2 nm of Co(P) film. Films deposited on SiO_2 were relatively thick (~ 25-65 nm) and *ex situ* cross-sectional SEM (Zeiss Supra 40 VP) imaging was used to measure thickness in order to avoid possible errors associated with deconvolution of the Si 2p XP peak (~103

eV in SiO_2) and Co 1s XP peak (~101 eV in metallic Co) from *in situ* measurements affecting an extrapolated thickness [42]. *Ex situ* chemical state analysis was performed with a Kratos AXIS Ultra DLD high-resolution XPS (equipped with monochromatic Al Kα) after sputter cleaning with 4 kV Ar^+ ions. Sensitivity factors used for quantitative chemical compositional analysis are published elsewhere [43]. Film microstructure was established by grazing angle (1°) X-ray diffraction (XRD) (Bruker-Nonius D8). Sheet resistance was measured with a Veeco FPP-5000 automatic four point probe and used in conjunction with SEM-measured thicknesses for resistivity calculation. Annealing was conducted for 3 h at 400 °C in a quartz vacuum tube furnace evacuated by a mechanical pump. The total ramp up time was ~2.5 h, and the time required to cool to room temperature was ~3 h. Ramp up, annealing, and cool down were all performed in 40 Pa flowing H_2.

4.3. RESULTS AND DISCUSSION

The effect of varying the amount of PMe_3 co-dosing on the composition of films grown at 350 °C as measured near the film surface by *ex situ* high-resolution XPS and on the microstructure as measured by grazing angle XRD is shown in Fig. 4.1. There is a clear microstructural change near 7% P incorporation. All films containing ≥8% P are amorphous, and all films containing ≤7% P are polycrystalline. This microstructural change is also exhibited when the concentration of C reaches ~22%. All polycrystalline films have ≤21% C, and all but one film containing ≥23% C are amorphous. A particularly P-rich (11 % P), C-poor (17% C) film remains amorphous. Although C alone can act to amorphize Co under certain conditions, the precise effect of C impurity on the

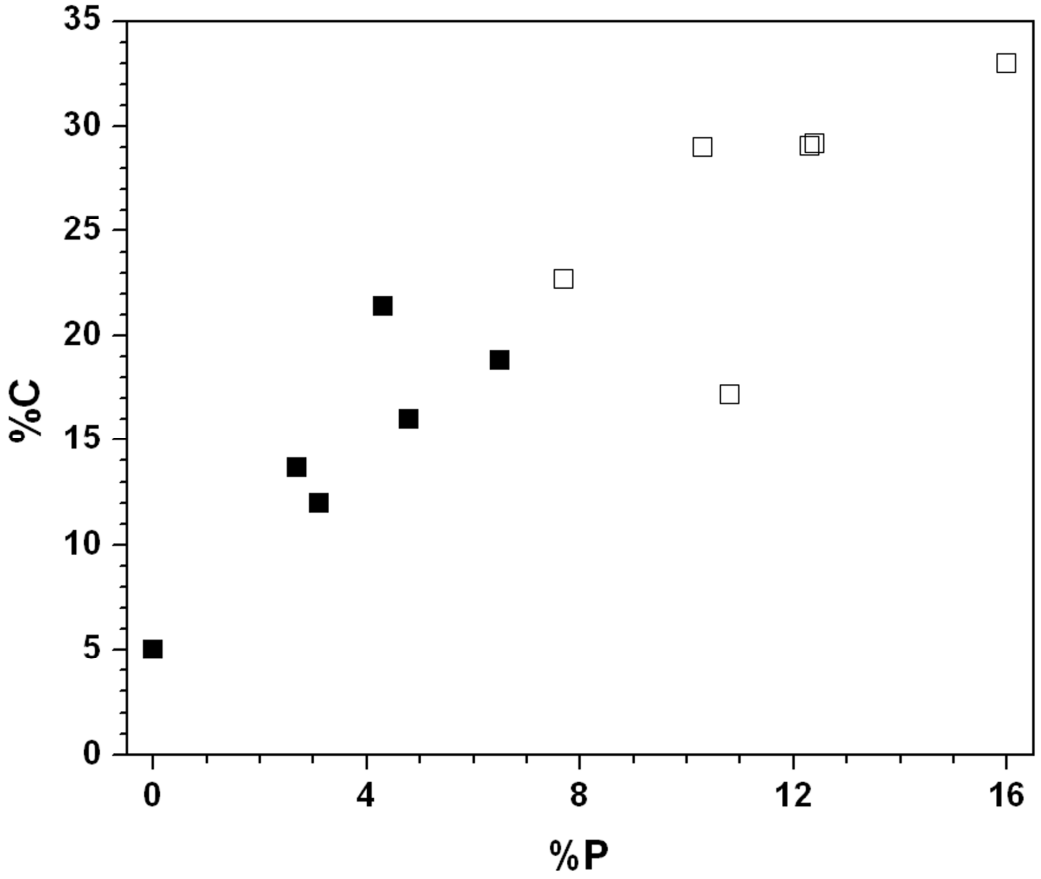

Figure 4.1. The effect of composition on microstructure. All amorphous films (□) incorporate >8%P, all polycrystalline films (■) incorporate <7%P.

microstructure of Co(C) alloy films has been less clearly defined than the effect of P in electrodeposited Co(P), with widely varying amounts of C required to form an amorphous alloy [44-51]. Table 4.1 lists the composition and microstructure of reported Co(C) films. As it shows, the microstructure of Co(C) films is dependent upon other factors, such as deposition method and C chemical state. When compared to the levels of incorporated P in amorphous CVD films, the higher amount of C required to ensure the transition to the glassy state indicates that under these growth conditions it is less efficient at forcing the amorphous phase than P. The minimum concentration of P required to eliminate crystallinity is lower than the minimum amount required to amorphize C-free electrodeposited Co(P) films [34]. It is clear, therefore, in this case that C must contribute to the reduction in the amount of P required to force the microstructural transition. Also shown in Fig. 4.1 is that an increase in the amount of P within a film generally corresponds to an increase in the amount of C. Although some C impurity originates from either the precursor itself or the hexane stabilizer, as indicated by a P-free CVD Co film containing 5% C, the majority of C found in the other films must then originate from the PMe_3 itself. The rate of increase in C composition relative to P is twice as fast in the polycrystalline films (~2.2:1) than in the amorphous films (~1.1:1, excluding the outlying low C-containing film). The average rate of C incorporation over the entire range is slightly less than twice as fast as P incorporation (1.7:1), and the residual C incorporation continuously and smoothly decreases as P incorporation increases.

Similarly, Co(P) resistivity does not exhibit a noticeable change in trend at the polycrystalline-amorphous transition, as shown in Fig. 4.2. Film resistivity more than

%C	Deposition method	Microstructure	ρ (μΩ·cm)	Reference
46	Ion beam sputtering, 200 °C	Amorphous-like	-	45
36	Ion beam sputtering, 200 °C	Poly Co + graphite	-	45
27	Ion beam sputtering, 300 °C	Poly carbides and Co	-	45
≤24	RS, MP, RT	Poly carbides and Co	-	46
≥36	RS, MP, RT	Amorphous	-	46
17-42	RS, MP	Amorphous	-	47
≥10	DC Magnetron Sputtering	Amorphous	-	48
5	DC Magnetron Sputtering	fcc CoC	-	48
≥5.8	RS, MP, 160 °C	Amorphous	-	49
≤2.2	RS, MP, 160 °C	α-Co	-	49
50	300 °C CVD with $CoCp(CO)_2$	Amorphous	>2,000	50
25-40	Pulsed vacuum arc deposition	Amorphous	130-300	51
-	RS, MP, RT	Amorphous	540,000	52
-	RS, MP, 250 °C	Poly Co + graphite	5,000	52

Table 4.1. Microstructure and composition of reported Co(C) films. Resistivity is listed if reported. [RS = reactive sputtering, MP = methane plasma, RT = room temperature, DC = direct current, Cp = C_5H_5]

doubles from ~244 μΩ·cm for the polycrystalline CVD Co (5% C) film to ~678 μΩ·cm for the lowest-resistivity amorphous film. Amorphous films always have higher resistivity than their (poly)crystalline analogs, and the resistivity is also negatively affected in this case due to the addition of non-metallic alloying elements P and C. However, further increases in the concentration of P and C beyond the minimums necessary to force the amorphous phase do not noticeably affect the rate at which resistivity increases. The addition of either P and/or C as alloying elements causes only a roughly linear increase in resistivity regardless of microstructure, providing a direct contrast with our previous report of the compositional effect on resistivity in amorphous CVD C impurity-containing Ru(P), which showed that C had no discernable effect on microstructure but had a large, negative effect on resistivity [30].

In this study the opposite is observed when C is incorporated into Co. Here, C has an effect on Co microstructure, although its influence is less pronounced than that of P. Furthermore, the data also indicate that C incorporation has a less detrimental apparent effect on resistivity than does P; the average residual resistivity per atomic percent (μΩ·cm/at.%) for P incorporation as shown in Fig. 4.2a is 55 μΩ·cm/at.%, but the average for C incorporation in Fig. 4.2b is only 32 μΩ·cm/at.%. However, residual resistivities do not account for the effect of reducing and ultimately eliminating crystalline grains during the transformation to the amorphous phase; for this reason, C impurity may only appear more resistively favorable than P additive because C is incorporated faster than P over the full range of compositions while the change in microstructure is the major cause of the increase in resistivity in this alloy system. Regardless of the exact role of microstructural change in resistivity increases of the

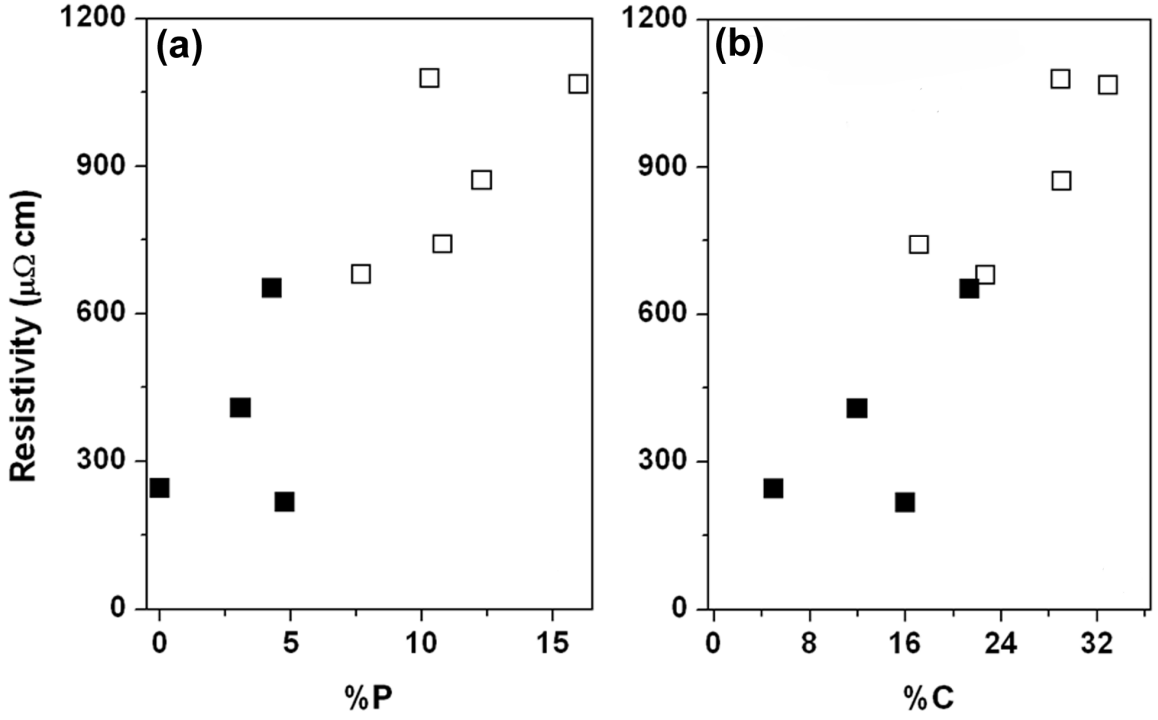

Figure 4.2. Resistivity of amorphous (□) and polycrystalline (■) Co(P) deposited at 350 °C across incorporated concentrations of (a) P and (b) C impurities.

alloys, C incorporation in CVD Co(P) does not negatively impact resistivity to an extent that would necessitate its complete elimination. The difference in the effect of P and/or C addition on the resistivity of Ru and Co is likely due to differences in the incorporation and distribution of C in either film. Both Ru [52] and Co [53] can form compounds with P, such as Ru_2P, RuP, RuP_2, CoP, and Co_2P, but C and Co can also form compounds, such as Co_2C and Co_3C [54], the type of interactions that are not possible at temperatures this low in the Ru-C system [55]. The potential for strong interaction between either Co and C or Co and P means that P and C should be roughly homogeneously dispersed.

The substrate temperature during deposition was reduced to 300 °C and 250 °C to investigate changes in chemical state and additive incorporation for Co(P) optimization. As measured by XRD (not shown), amorphous films could be grown at all three temperatures. All films incorporated some level of C impurity, both as graphitic and carbidic C. Representative XP spectra for O 1s (*in situ*), P 2p, and Co 2p (both *ex situ*) photoelectrons are shown in Fig. 4.3; XPS of C is discussed in detail later. Prior to ambient exposure, no O was detected beneath the surface of films deposited at any temperature (Fig. 4.3a), either as molecularly adsorbed CO (~531.8 eV) [56-57], adsorbed O (~530.2 eV) [58] or CoO_x (~529.4-531.4 eV) [59]. Only a pronounced Co LMM Auger peak at 544 eV is visible near the binding energy (BE) range of O 1s photoelectrons. The BE of the P 2p XP doublet (Fig. 4.3b) indicates either the zero-valent state or a very slight increase in electron density around the atoms, as the P $2p_{3/2}$ peak BE ranged from 129.9 eV to 129.6 eV. However, Co BE comparisons to a pure Co foil (99.95%, ESPI Metals), shown in Fig. 4.3c, show Co 2p XP peak positions in Co(P) film are aligned with metallic Co, and the peak shapes are the same for both types of Co,

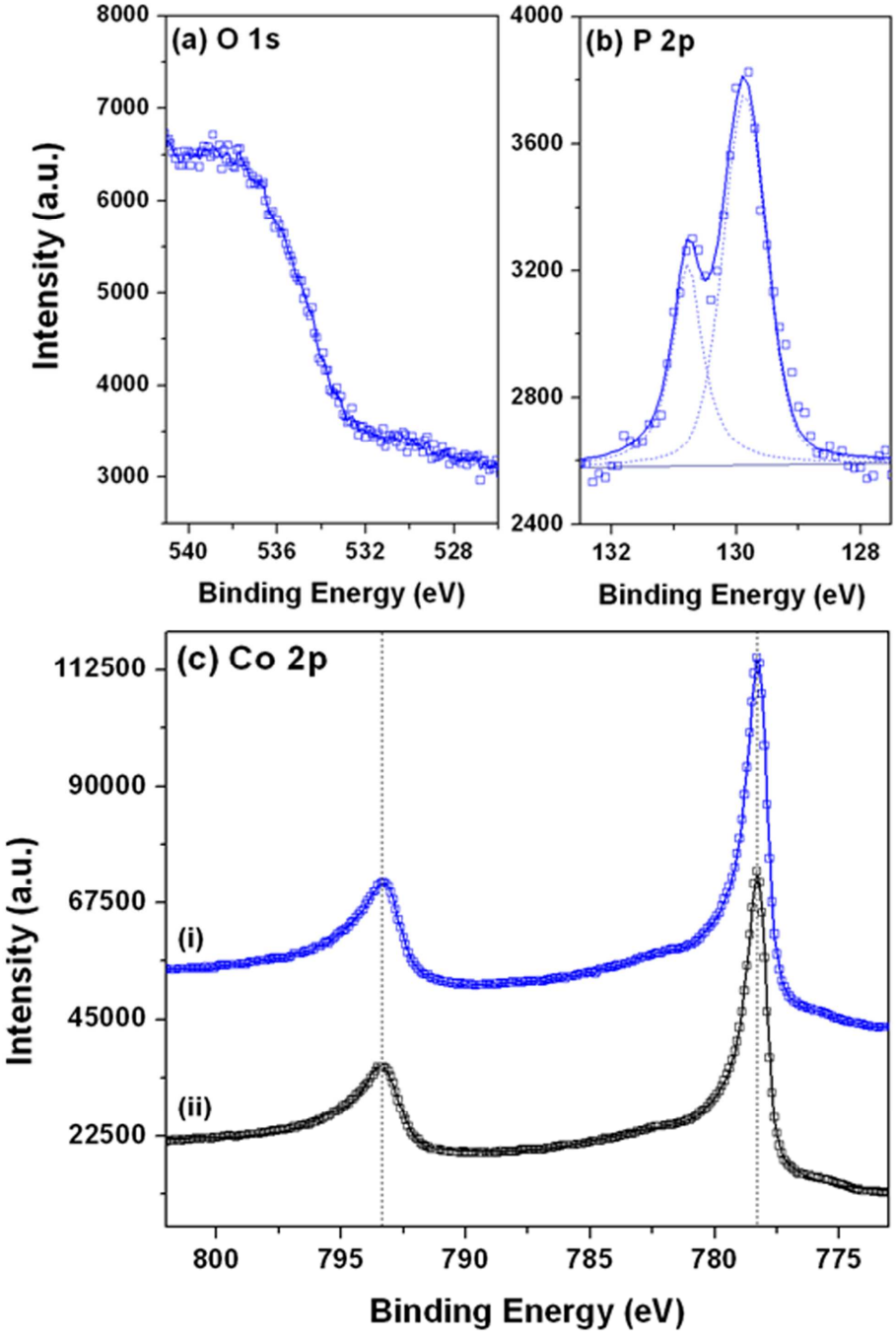

Figure 4.3. (a) O 1s, (b) P 2p, and (c.i) Co 2p XP spectra of a representative Co(P) film deposited at 250 °C; (c.ii) is the Co 2p XP spectrum of a standard Co foil.

indicating that Co in Co(P) is in the zero-valent state for all deposition temperatures. The absence of a corresponding ~0.7 eV shift to higher BE of the Co 2p peaks in Co(P) compared to metallic Co indicates that Co and P did not form phosphide compounds (CoP or Co_2P) at any deposition temperature [60].

The additive compositions in amorphous films as measured by *in situ* XPS are summarized in Fig. 4.4. All films incorporate less C relative to P as the amount of P increases, and no films included more P than C. We did not attempt to differentiate between the binding states of C *in situ*, and the amount described in this figure is the total amount of all C present. Surface studies of PMe_3 on Co surfaces have not been reported, but PMe_3 has been studied on various surfaces of other transition metals. PMe_3 does not decompose on Ag(111) [61], but was reported to decompose through various mechanisms and leave atomic P on Cu(110) [62], Pt(111) [63], and Ru(0001) [64]. Atomic C also remained on Cu and Pt surfaces [62-63], but overlap of the Ru $3d_{3/2}$ and C 1s XP peaks prevented detection of surface C on Ru [64]. Fig. 4.4 implies that PMe_3 can adsorb dissociatively ($C:P \neq 3$) on Co, and some C is able to leave the surface. The ratio of C:P and range of P in Co(P) grown at 300 °C and 350 °C are not clearly differentiable. Lowering the temperature to 250 °C reduces the levels of C incorporation relative to P, but requires a greater amount of PMe_3 co-fed to the reactor to reach a given amount of P relative to CVD at higher temperatures. The amount of P present after Co(P) deposition at 250 °C reached a chamber-specific practical limit near 12-13% incorporation; further increases in the amount of PMe_3 dosing would have quickly exhausted the source, but comparable PMe_3 dosing rates during deposition at 300 °C resulted in >18% P in the film. Both the average amount of total additive (P + C) and the average growth rate of

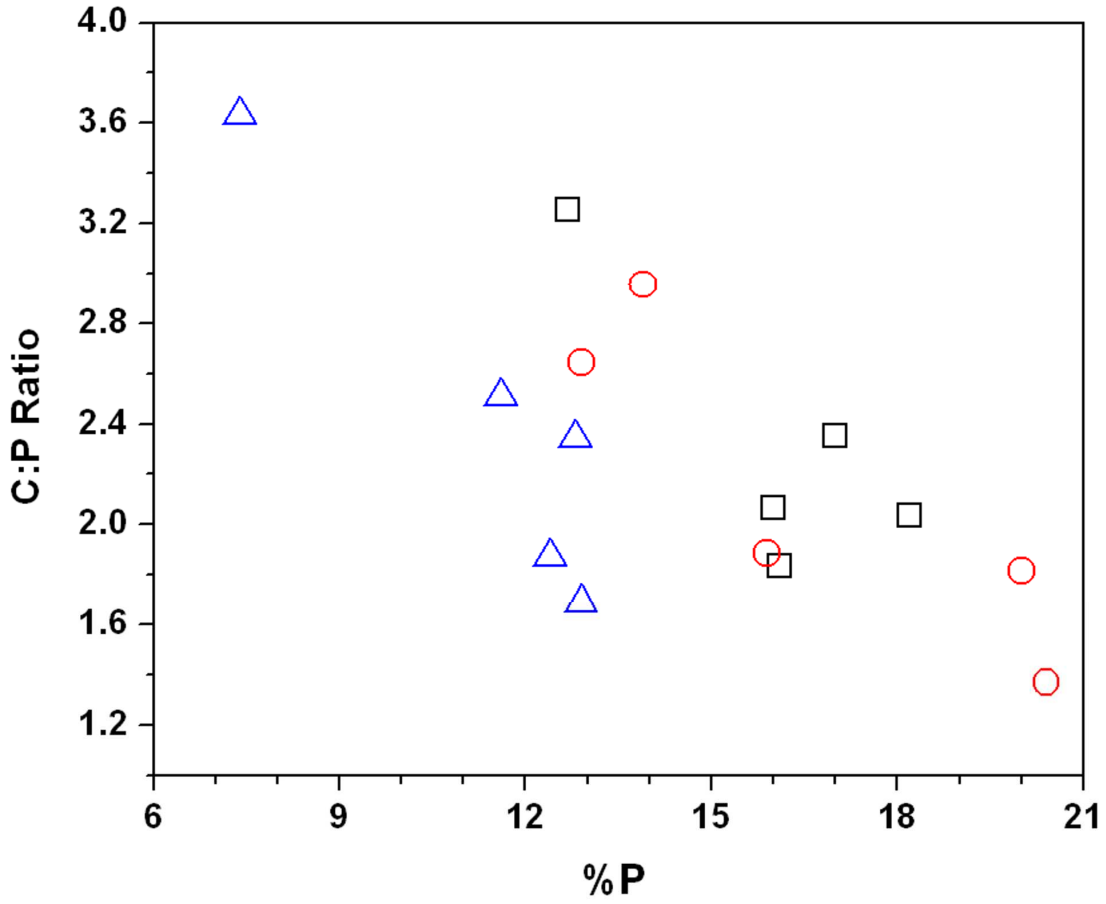

Figure 4.4. Composition of impurities in amorphous Co(P) films deposited at different temperatures: (□) 350 °C, (○) 300 °C, (△) 250 °C.

Co(P) increase with increasing temperature, as shown in Fig. 4.5. Reducing the substrate temperature during deposition is an efficient method to both reduce the growth rate and C contamination. Furthermore, the reduction of overall impurities associated with lower deposition temperatures would mean more Co existing at the Cu interface and a greater extent of Co-Cu interaction, maximizing the interfacial adhesion that acts to reduce EM-related failures.

The effect of deposition temperature on film resistivity is summarized in Fig. 4.6. Despite the lower relative amount of total C impurity, amorphous Co(P) deposited at 250 °C have higher resistivities than those of Co(P) grown at 300 °C. Deposition at 300 °C resulted in amorphous Co(P) with lower resistivities than Co(P) grown at 350 °C, despite comparable rates of C impurity incorporation. Co(P) films deposited at 250 °C or 300 °C were subjected to further testing of thermal stability, undergoing annealing for 3 h at 400 °C, conditions specifically chosen to reflect back-end processing. Films deposited at 350°C were not tested in this manner because the combination of high C incorporation and high resistivity makes these films less attractive for Cu IC applications than films deposited at the lower temperatures. The wafer pieces were cut in half after CVD and prior to annealing. Co(P) microstructure was then reassessed for each film after annealing. XRD spectra of an as-deposited polycrystalline CVD Co (5% C, 0% P) and a representative post-anneal amorphous Co(P) film (29% C, 12% P) are shown in Fig. 4.7. P-free Co exhibits peaks at 2θ of 42.34°, 45.12°, and 48.14°, which are assigned to the (100), (002), and (101) surfaces of hcp Co, respectively. For amorphous films post-anneal, no peaks associated with hcp or fcc Co, CoC_x, CoP_x, or crystalline C were seen, including over broader 2θ ranges extending from 30° to 90° examined for some films

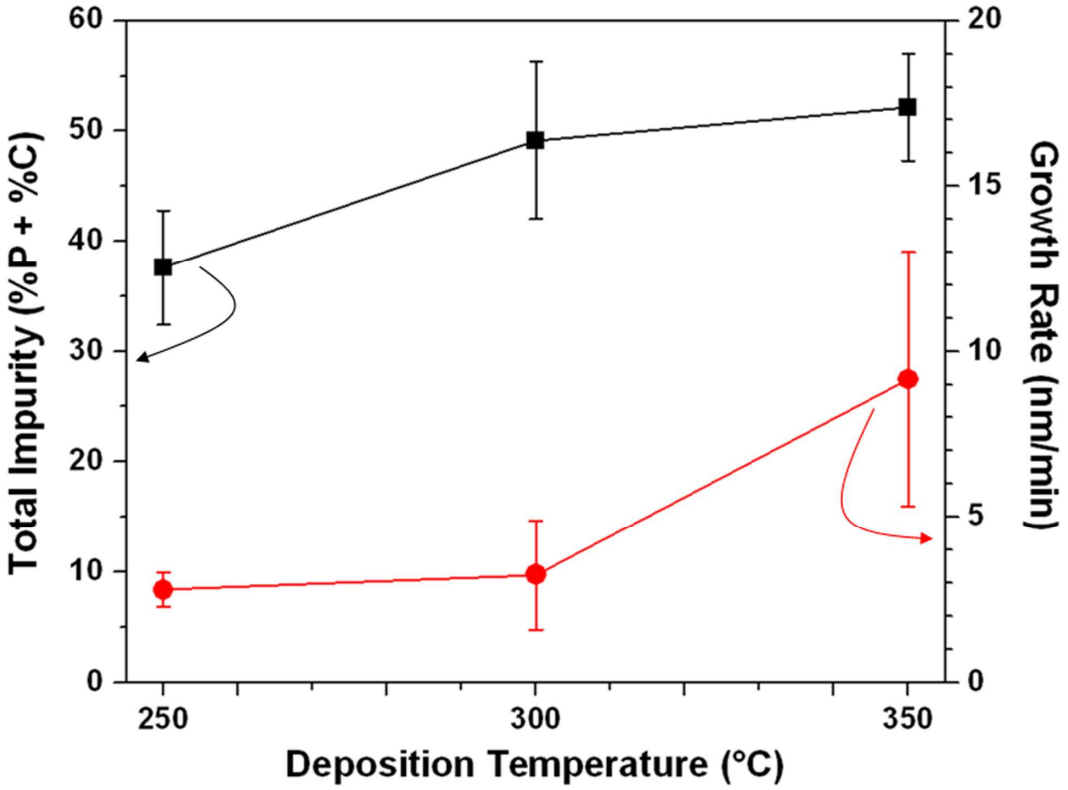

Figure 4.5. Correlation between Co(P) growth rate (●) and total additive incorporation (■). Error bars represent the full experimental range of either metric.

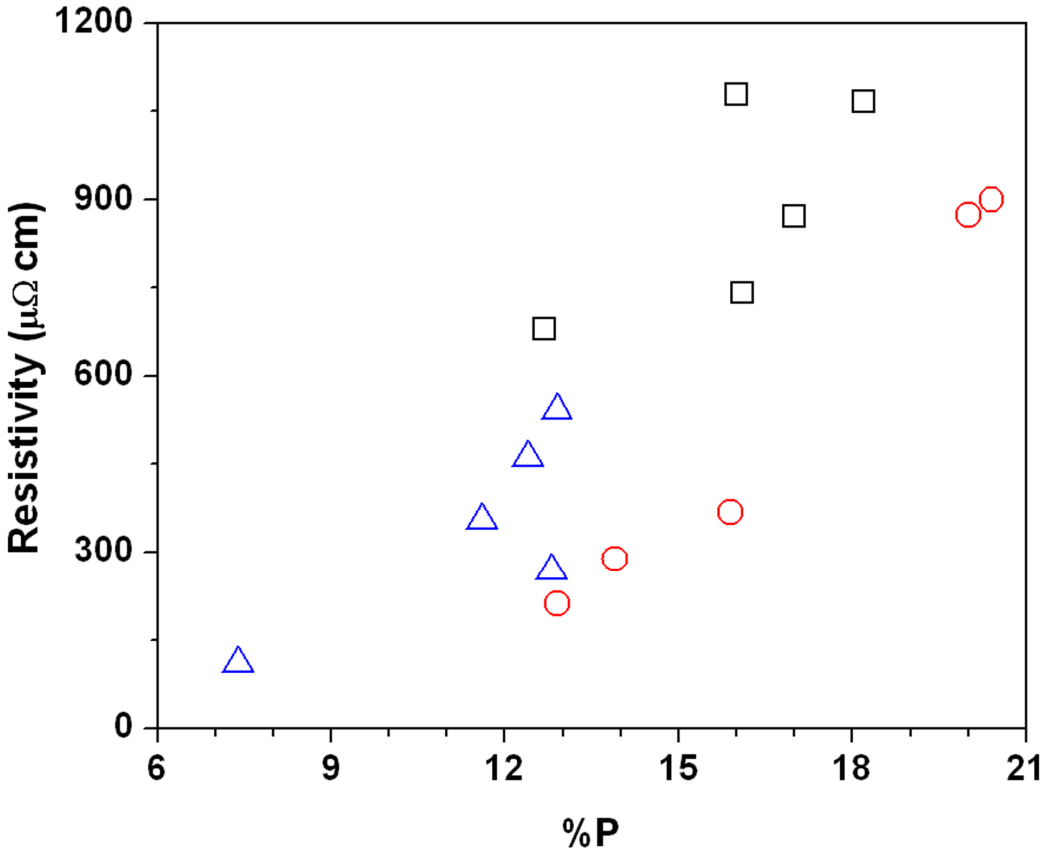

Figure 4.6. Resistivity of as-deposited films: (□) 350 °C, (○) 300 °C, (△) 250 °C.

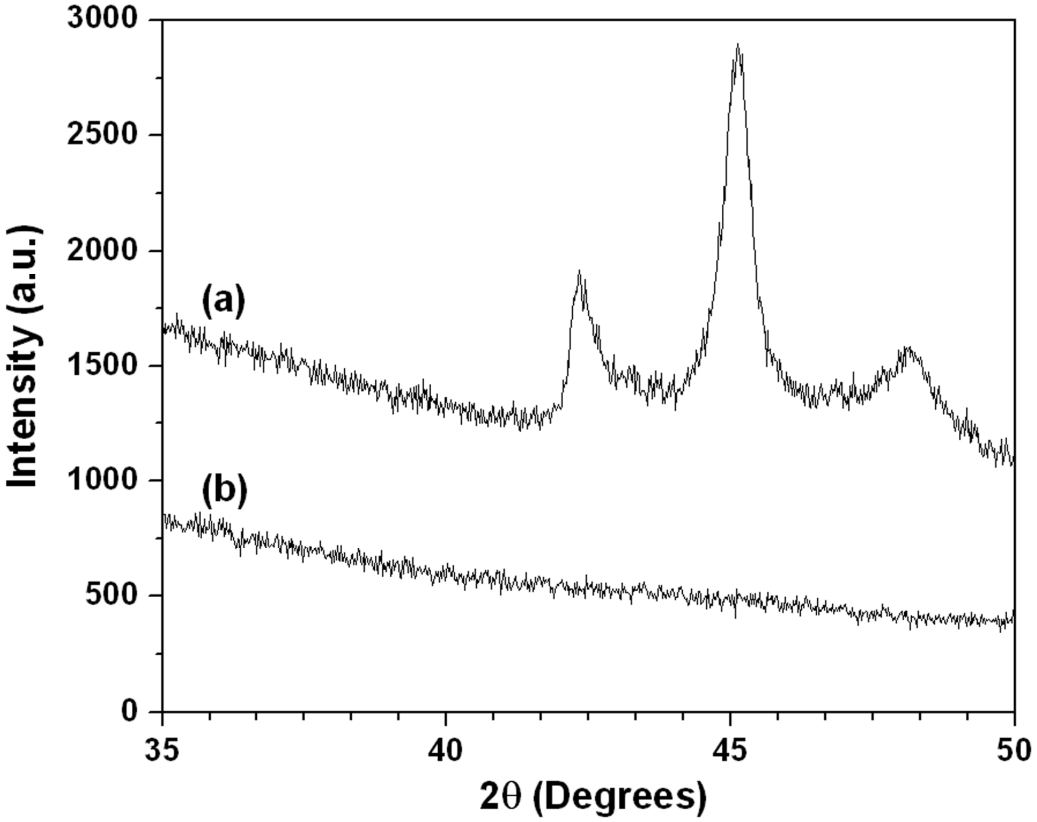

Figure 4.7. X-ray diffraction of (a) P-free CVD Co from $Co_2(CO)_8$ and (b) Co(P) (deposited at 250 °C; 12 %P, 29 %C) after annealing at 400 °C for 3 h.

(not shown), indicating the films remained X-ray amorphous. Increasing the amount of C in amorphous Co(C) [46] or P in amorphous Co(P) [65], increases the crystallization temperature somewhat, but 400 °C is above temperatures at which Co(P) alloys [6,65] and Co(C) alloys [46-47,66-69] typically crystallize. The enhanced thermal stability associated with the addition of C to Co(P) films (or, equally in this case, of adding P to Co(C) films) is similar to that caused by adding a third alloying element with favorable interaction properties to other binary systems, such as W to Co(P) [70] or Ni(P) [71], C to TiN [72] or TaSi [73], or P to Pd_2Si [74].

The change in resistivity after annealing is summarized in Table 4.2, where Co(P) film compositions are those measured *in situ* prior to annealing. While the resistivity was reduced for all Co(P) films, the resistivities remained many times greater than that of bulk Co (~6 μΩ·cm) and were within or above the range expected for amorphous Co(P). Only the lowest P-containing films deposited at either temperature have resistivities lower than 150 μΩ·cm. It is possible these low P-contain films formed nanocrystallites during the annealing step that are below the detection capabilities of XRD. Both the annealed and unannealed halves of one film deposited at both 250 °C and 300 °C were selected for investigation in *ex situ* high-resolution XPS to study the effect of film composition on resistivity changes. Both the annealed and unannealed halves of the wafer piece were sputtered for 120 sec to remove surface C plus a thin native CoO_x layer that formed upon ambient exposure. Sputtering allowed assessment of the chemical states of the component species within the film bulk at the same depth in either film. The XP spectra of Co and P (not shown) of annealed Co(P) featured no shifts in BE or

Deposition T	%P	%C	ρ (as deposited)	ρ (post-anneal)	Drop in ρ
300	16	23	368	279	24%
300	20	28	900	343	62%
300	13	34	212	79	63%
300	14	41	289	162	44%
300	20	36	875	399	54%
250	7	27	111	55	51%
250	12	23	462	306	34%
250	13	22	541	342	37%
250	12	29	355	188	47%
250	13	30	269	154	43%

Table 4.2. Resistivity (in μΩ·cm) of high-quality Co(P) films.

appearance of additional peaks that would indicate changing chemical environments around those atoms. Only the C 1s XP spectrum showed any change, as shown for the 250 °C film in Fig. 4.8. C comprised ~10% of the overall composition at these depths, and it existed in three distinct chemical states. The smallest peak at 286.0 eV is attributed to CO adsorbed on Co, which was not apparent at higher C concentrations closer to the surface of CVD Co(P) deposited at 350 °C [35]. Molecular CO completely desorbs intact from polycrystalline Co at no more than 200 °C [75-76], and because any O that may have been present within Co(P) was below the XPS detection limit *in situ* at all deposition temperatures, the CO XP likely originated from small amounts of CO adsorbed from the XPS analysis chamber background (primarily H_2O, CO, and CO_2; base pressure 2.7×10^{-7} Pa) in the several minutes that passed between sputter cleaning and acquisition of the C 1s XP spectrum. This was confirmed by the presence of a small peak of similar size and shape at 286.2 eV in the C 1s XP spectrum from a sputter cleaned Co foil. The peak at 283.7 eV is assigned to carbidic C bonding with Co [77]. This Co-carbide bonding is not apparent in the Co 2p peak, because the associated peak shift is so small (~0.1 eV) [78] as to prevent resolution between the two states. The other peak centered at 284.5 eV is graphitic C, *i.e.* zero-valent elemental C.

Incorporated C is predominantly carbidic both prior to (Fig. 4.8a) and after (Fig. 4.8b) annealing, but the ratio of carbidic C to graphitic C dropped significantly from 2.9 to 1.8 due to a decrease in carbidic C concentration and a corresponding increase in graphitic C concentration. Unlike Co_xC, for which electrical properties have not been reported, the electrical properties for other, non-Co transition metal carbides, such as TiC_x, TaC_x, ZrC_x, and many others have been the subject of studies for several decades.

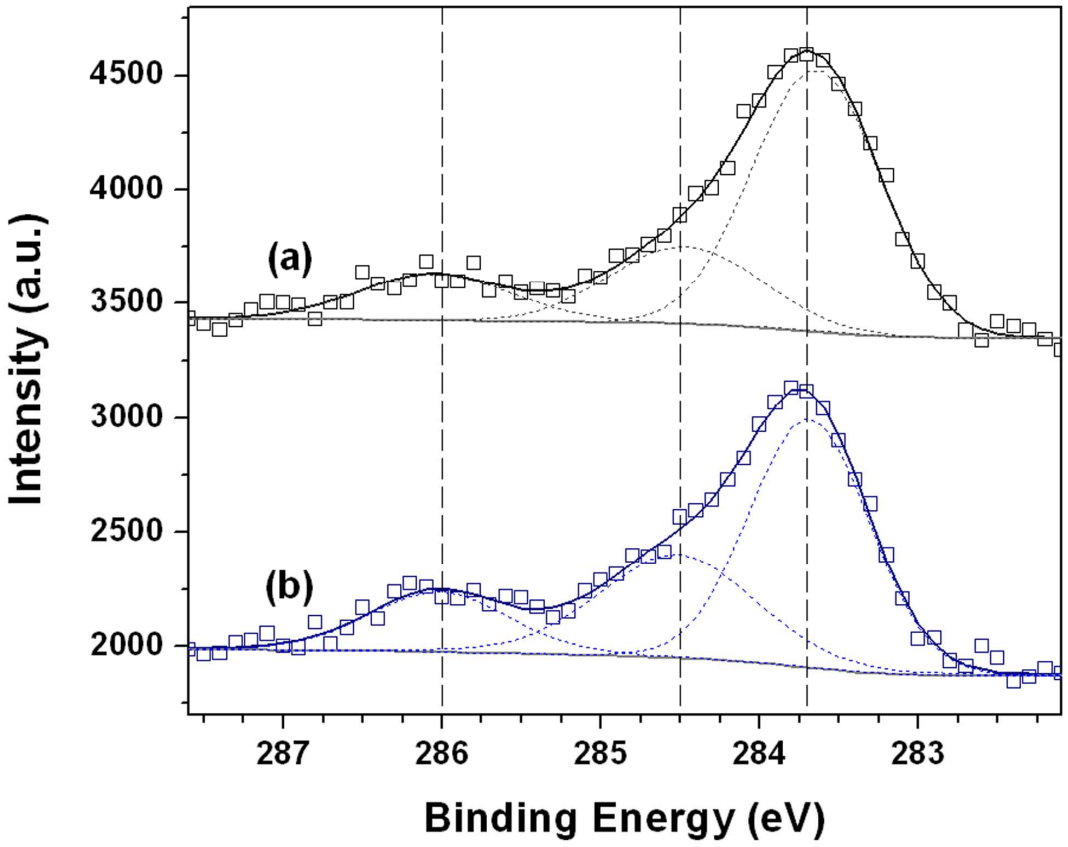

Figure 4.8. High-resolution C 1s XP spectra from Co(P) (a) as deposited at 250 °C and (b) after 3 h anneal at 400 °C.

Generally, these materials have resistivities in the realm of conductors, and are sometimes therefore referred to as "metallic ceramics" [79], but are mostly more resistive, by as many as a few multiples, than their pure metal analogues [79-82]. Co_2C and Co_3C rapidly decompose α-Co and C or to α-Co, β-Co, and C, respectively, at temperatures below 400 °C [45,83]. The breakdown of carbides resulting in the formation of a greater amount of non-carbidic, metallic Co, which remains amorphous due to the additional presence of P, is a contributing reason for the drop in film resistivity. A similar change was observed in Co(P) deposited at 300 °C, which had a lower initial concentration of carbide relative to graphitic C than Co(P) deposited at 250 °C, and the percent drop in carbide concentration was greater than that of Co(P) deposited at 250 °C, explaining both the generally lower initial resistivity and the generally larger drop after annealing observed in the full set of films deposited at 300 °C compared to those deposited at 250 °C.

4.4. SUMMARY

Amorphous Co(P) alloys containing large amounts of C as an impurity were grown on chemical SiO_2 by CVD from a dual-source chemistry of $Co_2(CO)_8$ and PMe_3 at 250 °C, 300 °C, or 350 °C. Phosphorus was determined to be the more efficient amorphizing agent, but C incorporation also contributes to amorphization, primarily by reducing the amount of P required to force the amorphous phase compared to electrodeposited Co(P). With residual resistivities of P or C addition of the same order, neither P nor C alone can be said to affect film resistivity significantly more detrimentally than the other, likely because Co can strongly chemically interact with both P and C, and

distribution of either should be roughly even. XPS analysis showed that cobalt phosphides were not formed, but that cobalt carbides were. Most, but not all, C was in the form of carbide. Reducing the substrate temperature provided a simple method to reduce the relative C contamination, but reduced the efficiency with which P was incorporated into the film and formed Co(P) with resistivities higher than those of films grown at 300 °C. The films showed good thermal stability, remaining in the amorphous phase after a 400 °C anneal, an improvement over pure Co(P) or pure Co(C) alloys. Annealing caused Co(P) resistivities to drop, and high resolution XPS indicated that a decrease in the amount of carbidic C coupled with an increase in graphitic C, which corresponds to an increase in the concentration of metallic Co, is a major factor in this drop.

4.5. REFERENCES

1. International Technology Roadmap for Semiconductors, 2008 Update, http://public.itrs.net

2. M. W. Lane, E. G. Liniger, and J. R. Lloyd, J. Appl. Phys., 93, 1417 (2003).

3. M. A. Sheikholeslam, M. H. Enayati, and K. Raeissi, Mater. Lett., 62, 3629 (2008).

4. S. M. S. I. Dulal, H. J. Yun, C. B. Shin, and C.-K. Kim, J. Electrochem. Soc., 154, D494 (2007).

5. R. Tarozaitė, M. Kurtinaitienė, A.Džiūvė, and Z. Jusys, Surf. Coat. Technol., 115, 57 (1999).

6. J. Gambino, J. Wynne, J. Gill, S. Mongeon, D. Meatyard, B. Lee, H. Bamnolker, L. Hall, N. Li, M. Hernandez, P. Little, M. Hamed, I. Ivanov, and C. L. Gan, Microelectron. Eng., 83, 2059 (2006).

7. Z. Li, R. G. Gordon, D. B. Farmer, Y. Lin, and J. Vlaasak, Electrochem. Solid-State Lett., 8, G182 (2005).

8. P. Singer, Semicond. Int., 28, 44 (2005).

9. E. Zschech, M. A. Meyer, S. G. Mhaisalkar, A. V. Vairagar, A. Krishnamoorthy, H. J. Engelmann, and V. Sukharev, Thin Solid Films, 504, 279 (2006).

10. C.-K. Hu, D. Canaperi, S. T. Chen, L. M. Cignac, B. Herbst, S. Kaldor, M. Krishnan, E. Liniger, D. L. Rath, D. Restaino, R. Rosenberg, J. Rubino, S.-C. Seo, A. Simon, S. Smith, and W.-T. Tseng, IEEE International Reliability Physics Symposium Proceedings, p. 222 (2004).

11. C.-K. Hu, L. Gignac, R. Rosenberg, E. Liniger, J. Rubino, C. Sambucetti, A. Stamper, A. Domenicucci, and X. Chen, Microelectron. Eng., 70, 406 (2003).

12. H. Li and B. P. Tonner, Surf. Sci., 237, 141 (1990).

13. T. Nishizawa and K. Ishida, Bull. Alloy Phase Diagrams, 5, 161, (1984).

14. K. M. Chow, W. Y. Ng, and L. K. Yeung, Surf. Coat. Tech., 99, 161 (1998).

15. M. Paunovic, P. J. Bailey, and R. G. Schad, J. Electrochem. Soc., 141, 1843 (1994).

16. K. C. Aw, N. T. Salim, W. Gao, and K. Prince, Int. J. Mod. Phys. B, 20, 4165 (2006).

17. Y. Shacham-Diamand, A. Dedhia, D. Hoffstetter, W. G. Oldham, J. Electrochem. Soc., 140, 2427 (1993)

18. F. Lanckmans and K. Maex, Microelectron. Eng., 60, 125 (2002)

19. J. R. Lloyd, C. E. Murray, S. Ponoth, S. Cohen, and E. Liniger, Microelectron. Reliab., 46, 1643 (2006).

20. E. J. O'Sullivan, A. G. Schrott, M. Paunovic, C. J. Sambucetti, J. R. Marino. P. J. Bailey, S. Kaja, and K. W. Semkow, IBM J. Res. Dev., 42, 607 (1998).

21. A. Kohn, M. Eizenberg, and Y. Shacham-Diamand, J. Appl. Phys., 94, 3015 (2003).

22. T. N. Arunagiri, Y. Zhang, O. Chyan, M. J. Kim, and T. Q. Hurd, J. Electrochem. Soc., 152, G808 (2005).

23. M. Damayanti, T. Sritharan, Z.H. Gan, S.G.Mhaisalkar, N. Jiang, and L. Chan, J. Electrochem. Soc., 153, J41 (2006).

24. W. Wei, S. L. Parker, Y.-M. Sun, J. M. White, G. Xiong, A. G. Joly, K. M. Beck, and W. P. Hess, Appl. Phys. Lett., 90, 111906 (2007).

25. K.-C. Tsai, W.-F. Wu, J.-C. Chen, T.-J. Pan, and C.-G. Chao, J. Electrochem. Soc., 152, G83 (2005).

26. H. Kim, T. Koseki, T. Ohba, T. Ohta, Y. Kojima, H. Sato, and Y. Shimogaki, J. Electrochem. Soc., 152, G594 (2005).

27. M. Mercier, S. Weber, A. Jacques, H. Hirabayashi, H. Ohkawa, and M. Kinoshita, Diffus. Defect Data, Pt. A, 143, 1285 (1997).

28. B. H. Lee and K. Yong, J. Vac. Sci. Technol. B, 22, 2375 (2004).

29. J. S. Becker and R. G. Gordon, Appl. Phys. Lett., 82, 2239 (2003).

30. H. Kizil and Ch. Steinbrüchel, Thin Solid Films, 449, 158, (2004).

31. L. B. Henderson and J. G. Ekerdt, Thin Solid Films, 517, 1645 (2009).

32. J. Shin, H.-W. Kim, K. Agapiou, R. A. Jones, G. S. Hwang, and J. G. Ekerdt, J. Vac. Sci. Technol. A, 26, 974, (2008).

33. D.-C. Perng, J.-B. Yeh, and K.-C. Hsu, Appl. Surf. Sci., 257, 6059 (2008).

34. K. Hüller, M. Sydow, and G. Dietz, J. Magn. Magn. Mater., 53, 269 (1985).

35. L. B. Henderson and J. G. Ekerdt, Electrochem. Solid-State Lett., 12, D36 (2009).

36. Y.-M. Sun, S. Y. Lee, A. M. Lemonds, E. R. Engbrecht, S. Veldman, J. Lozano, J. M. White, J. G. Ekerdt, I. Emesh, and K. Pfeifer, Thin Solid Films, 397, 109 (2001).

37. Y. K. Ko, D. S. Park, B. S. Seo, H. J. Yang, H. J. Shin, J. Y. Kim, J. H. Lee, W. H. Lee, P. J. Reucroft, and J. G. Lee, Mater. Chem. Phys., 80, 560, (2003).

38. D.-X. Ye, S. Pimanpang, C. Jezewski, F. Tang, J. J. Senkevich, G.-C. Wang, and T.-M. Lu, Thin Solid Films, 485, 95 (2005).

39. E. P. Boyd, D. R. Ketchum, H. Deng, and S. G. Shore, Chem. Mater., 9, 1154, (1997).

40. Q. Zhao, D. W. Greve, and K. Barmak, Appl. Surf. Sci., 219, 136 (2003).

41. M. L. Garner, D. Chandra, and K. H. Lau, J. Phase Equilib., 16, 24 (1995).

42. J. Shin, H.-W. Kim, G. S. Hwang, and J. G. Ekerdt, Surf. Coat. Technol., 201, 9256, (2007).

43. J. F. Moulder, W. F. Stickle, P. E. Sobol, and K. D. Bomben, Handbook of X-Ray Photoelectron Spectroscopy, Physical Electronics, Inc., Eden Prarie, MN, U.S.A., 1992, p. 253.

44. J. J. Delaunay, T. Hayashi, M. Tomita, and S. Hirono, J. Appl. Phys., 82, 2200 (1997).

45. Y. Fukumiya, Y. Haga, and O. Nittono, Mater. Sci. Eng. A, A312, 248 (2001).

46. E. Bauer-Grosse and A. Aouni, J. Non-Cryst. Solids, 353, 3644 (2007).

47. T. J. Konno and R. Sinclair, Acta Metall. Mater., 42, 1231 (1994).

48. K. Oda, T. Yoshio and K. Oda, J. Mater. Sci. Lett., 9, 1319 (1990).

49. H.-B.-R. Lee and H. Kim, Electrochem. Solid-State Lett., 9, G323 (2006).

50. H. Wang, M. F. Chiah, W. Y. Cheung, and S. P. Wong, Phys. Lett. A, 316, 122 (2003).

51. J. Shi, M. Azumi, and O. Nittono, Appl. Phys. A.: Mater. Sci. Process., 73, 215 (2001).

52. V. B. Chernogorenko, V. G. Ivanchenko and L. Ya. Kulik, in: Binary Phase Diagrams, T. B. Massalski, H. Okamoto, P. R. Subramanian, and L. Kacprzak (Eds.), ASM International, Materials Park, OH, U.S.A., 1990, p. 2979.

53. K. Ishida and T. Nishizawa, Bull. Alloy Phase Diagrams, 11, 555 (1990).

54. K. Ishida and T. Nishizawa, J. Phase Equilib., 12, 417 (1991).

55. B. M. Mollakov, M. P. Glazunov, and V. I. Spitsyn, Russ. Chem. Bull., 22, 635 (1973).

56. J. Lahtinen, J. Vaari, A. Talo, A. Vehanen, and P. Hautojärvi, Vacuum, 41, 112 (1990).

57. D. A. Wesner, G. Linden, and H. P. Bonzel, Appl. Surf. Sci., 26, 335 (1986).

58. J. Nakamura and I. Toyoshima, Surf. Sci., 201, 185 (1988).

59. NIST X-ray Photoelectron Spectroscopy Database, Vers. 3.5 (National Institute of Standards and Technology, Gaithersburg, 2003); http://srdata.nist.gov/xps/

60. V. V. Nemoshkalenko, V. V. Didyk, V. P. Krivitskii, and A. I. Senkevich, Zh. Neorg. Khim., 28, 2182 (1983).

61. X.-L. Zhou and J. M. White, Surf. Sci., 221, 534 (1989).

62. Y.-H. Lai, C.-T. Yeh, H.-J. Lin, C.-T. Chen, and W.-H. Hung, J. Phys. Chem. B, 106, 1722 (2002).

63. G. E. Mitchell, M. A. Henderson, and J. M. White, J. Phys. Chem., 91, 3808 (1987).

64. H.-S. Tao, U. Diebold, N. D. Shinn, and T. E. Madey, Surf. Sci., 375, 257 (1997).

65. F. Cebollada, J. M. Gonzalez, and P. Adeva, J. Mater. Res., 8, 105 (1993).

66. W. B. Mi, L. Guo, E. Y. Jiang, Z. Q. Li, P. Wu and H. L. Bai, J. Phys. D: Appl. Phys., 36, 2393 (2003).

67. T. J. Konno and R. Sinclair, Acta Metall. Mater., 43, 471 (1995).

68. T. J. Konno and K. Bandoh, J. Metastable Nanocryst. Mater., 24, 57 (2005).

69. H. Wang, M. F. Chiah, W. Y. Cheung, and S. P. Wong, Phys. Lett. A, 316, 122 (2003).

70. A. Kohn, M. Eizenberg, Y. Shacham-Diamand, and Y. Sverdlov, Mater. Sci. Eng., A302, 18 (2001).

71. S. B. Antonelli, T. L. Allen, D. C. Johnson, and V. M. Dubin, J. Electrochem. Soc., 153, J46 (2006).

72. Y. H. Lu, and Y. G. Shen, J. Mater. Res., 23, 671 (2008).

73. T.-Y. Lin, H.-Y. Cheng, T.-S. Chin, C.-F. Chiu, and J.-S. Fang, Appl. Phys. Lett., 91, 152908 (2007).

74. M. H. Juang, C. I. Ou-Yang, H. C. Cheng, and C. T. Lin, Mat. Res. Soc. Symp. Proc., 648, P11.31.1 (2001).

75. A. L. Cabrera, W. H. Garrido, and U. G. Volkman, Catal. Lett., 25, 115 (1994).

76. B. Viswanathan, R. Gopalakrishnan, and R. Vetrivel, React. Kinet. Catal. Lett., 18, 209 (1981).

77. H. Wang, S. P. Wong, W. Y. Cheung, N. Ke, G. H. Wen, X. X. Zhang, and R. W. M. Kwok, J. Appl. Phys., 88, 4919 (2000).

78. F. L. Wang, J. C. Jiang, and E. I. Meletis, J. Appl. Phys., 95, 5069 (2004).

79. W. S. Williams, Int. J. Refract. Met. Hard Mater., 17, 21 (1999).

80. W. S. Williams, Science, 152, 34 (1966).

81. W. S. Williams, JOM, 49, 38 (1997).

82. S. T. Oyama, in: The Chemistry of Transition Metal Carbides and Nitrides, S. T. Oyama (Ed.), Blackie Academic & Professional, Glasgow, Scotland, 1996, p. 9.

83. L. J. E. Hofer, E. M. Cohn, and W. C. Peebles, J. Phys. Chem., 53, 661 (1949).

Chapter 5: Capping copper with chemical vapor deposited cobalt-phosphorus film

5.1. INTRODUCTION

In the semiconductor industry, significant economic gains are achieved through the constant shrinking of chips and the devices that comprise them. As the on-chip dimensions continually decrease, operating conditions, such as maximum current density (J_{max}) in the interconnect (IC), change and eventually reach levels incompatible with existing materials and interfaces. Such scaling necessitated the replacement of Al with Cu in the IC several generations ago. To enable the switch to Cu, a multi-step process of adhesion/barrier layer deposition, followed by Cu seed deposition, electroplating, and chemical mechanical polishing, completed by capping Cu with a dielectric film was adopted. Cu has higher resistance to electromigration (EM) than Al alloys [1], and the predominant location of EM failure has shifted to the interfaces Cu shares with surrounding materials [2-4]. Interfaces exhibiting weak adhesion experience failure more rapidly than those exhibiting stronger adhesion [5]. Currently, a Ta/TaN bilayer is used as the Cu adhesion/barrier layer, and a Si-based material, such as SiN, SiC, or SiCN serves as a dielectric etch stop and capping layer [6-8]. Ta provides adequate adhesion to Cu, and investigations of potential Ta replacement materials have focused on other metals that show even greater adhesion to Cu, including Ru, Os, and Mo [9]. The dielectric capping layers, by comparison, adhere quite poorly to Cu, and the predicted J_{max} is expected to exceed levels at which the current technology is sufficient by 2013 [10].

To prevent the expected reliability problem, Co and other Co-based ultrathin films, such as Co(P), are being widely investigated [11-14]. Co has a low bulk resistivity (~6 μΩ cm), low solubility in Cu, and the adhesion between Co and Cu is many orders of magnitude above Cu and dielectric materials [15-16], making it an attractive candidate for Cu IC applications. An added benefit of adopting Co would be the potential to completely remove the relatively high-dielectric constant (κ) capping material, if Co alloys alone can withstand conditions during dielectric deposition and resist stripping, and more widely apply low-κ materials throughout the IC architecture reducing the resistive-capacitive delay. However, this would require that the replacement Co/low-κ combination provide sufficient barrier ability against Cu diffusion, a requirement that neither low-κ materials [17-20] nor Co [21-22] meet. By incorporating some P into Co to form nanocrystalline Co, the diffusivity of Cu through Co drops significantly [22-24], and further P addition to form a grain boundary-free Co amorphous alloy would provide an even more robust barrier. Co-based alloys formed by electro- and electroless deposition in plating baths have been widely reported, many showing good selectivity for growth on Cu [11-14], which is vital in maintaining the electrical isolation between wires in a level of metallization. Still, depositing metals in an aqueous environment where metal(s)-containing solutes are present can result in increases in line-to-line leakage [25-26]. A non-aqueous deposition method, such as chemical vapor deposition (CVD), is a way to bypass these aqueous deposition environments.

A method for CVD of amorphous Co(P) containing C as an impurity on SiO_2 has been previously reported [27]. This paper discusses CVD Co(P) on Cu in terms of film properties most relevant to the proposed IC applications of Co-based films, namely

composition, continuity, adhesion, and growth selectivity, studied with X-ray photoelectron spectroscopy (XPS), low-energy ion scattering spectroscopy (LEISS), scanning electron microscopy (SEM), and a scotch tape peeling test.

5.2. EXPERIMENTAL DETAILS

Films were deposited in a combined vacuum deposition and analysis system, consisting of a load lock, vacuum sample transfer chamber, physical vapor deposition (PVD) chamber (AJA International, Inc.), homemade CVD chamber, and analysis chamber. The physical deposition chamber (base pressure 4×10^{-5} Pa) uses three direct-current (DC) magnetron sputtering guns and Ar^+ plasma. The chemical vapor deposition chamber (base pressure 4×10^{-6} Pa) is a cold-wall, stainless steel reactor, where samples are heated to the deposition temperature radiatively from below. The analysis chamber is equipped with XPS (Physical Electronics 3057, Mg Kα) and LEISS. Co(P) films were grown on 20 mm × 20 mm pieces of either 400 nm chemically grown (from tetraethylorthosilicate) SiO_2/Si(100) 200 mm wafers provided by Sematech (Austin, Texas, USA) or 20 nm Cu/Ta/TaN/SiO_2/Si(100) 300 mm wafers provided by Tokyo Electron, Ltd (Albany, New York, USA). For growth selectivity experiments, a ~200 nm Cu/Ru/TaN/SiO_2/Si(100) stack was deposited on one half of a SiO_2/Si(100) wafer piece through a shadow mask. The Ta:N ratio was 5:4, and there was some O impurity in the film. Ru (99.95%, ACI Alloys) and Cu (99.999%, Kurt J. Lesker Co.) films were impurity free. TaN and Ru were sputtered with 50 W DC power, and Cu was sputtered with 100 W DC power. For all TaN, Ru, and Cu, the Ar flow rate was 20 sccm and the chamber pressure was held constant at 1.33 Pa. Both film stacks with Cu surfaces were

heated to 350 °C in the CVD chamber in flowing H_2 for 1.5 h without deposition, then cooled and evaluated in XPS and LEISS to ensure substrate compatibility at the maximum deposition temperature. For both stacks, only Cu (and low levels of O adsorbed from the vacuum system background) was observed in LEISS, and no peaks from underlying layers were observed in XPS, indicating the top Cu layer remained continuous and thicker than several nm. Substrates with Cu surfaces were heated to 250 °C for 1 h in flowing H_2 in the CVD chamber to confirm that preheating at the minimum deposition temperature was sufficient to reduce Cu oxides that formed in ambient conditions. The substrates were cooled under vacuum and then observed in XPS. The Cu 2p XP spectrum indicated that Cu was metallic, with no CuO_x detected. Some O had adsorbed from the chamber background during cooling and/or sample transfer, and some adventitious C remained on the Cu surface. Cu was also sputtered onto pieces of 500 nm $SiCN/SiO_2/Si$ wafer from Freescale Semiconductor (Austin, Texas, USA) for use during adhesion testing.

Co(P) CVD was conducted using a dual-source chemistry of dicobaltoctacarbonyl [$Co_2(CO)_8$] (95-99%, stabilized in 1-5% hexane, Alfa Aesar, and precursor was used without further purification), carried by ultra-high purity H_2 (99.999%, Matheson Tri-Gas) and trimethylphosphine [PMe_3, Me = CH_3] (99%, Sigma-Aldrich) at substrate temperatures of 250-350 °C. Detailed methods for Co(P) deposition are described elsewhere [28]. *In situ* XPS analysis was performed after surface contamination was removed by 2 kV Ar^+ ion sputter cleaning. For ultrathin films (<5 nm) grown on Cu, Co(P) thickness was directly measured *in situ* using XPS Cu $2p_{3/2}$ peak attenuation. Film surface composition and continuity was evaluated *in situ* by LEISS using 1 kV He^+ ions.

The selectivity of deposition on Cu was established by both *in situ* XPS analysis and *ex situ* cross-sectional SEM (Zeiss Supra 40 VP) imaging. Adhesion was assessed using a scotch tape test (ASTM D 3359-08, Method A: X-cut) [29].

5.3. RESULTS AND DISCUSSION

5.3.1. Deposition Characteristics on Cu

Fig. 5.1 shows a XPS depth profile through a ~3 nm thick Co(P) film deposited on Cu at 350 °C. The amount of both P and C relative to Co drops steadily as the film is slowly sputtered through. As the depth profile approaches the interface with Cu, Co(P) becomes very poor in P compared to the surface, as the Co:P ratio has grown from ~2.8:1 to over 10:1. Within the film, P exists primarily in the zero-valent state, and Co and C exist in a combination of zero-valent and carbidic states [27]. Near the interface, XPS can be used to assess changes in the chemical state of the underlying Cu layer, as Cu and P can potentially form phosphide compounds [30]. The change in binding energy between elemental and phosphided 2p doublets of both Cu and P are similar (~0.4 eV) [31], but any chemical change was unresolvable *in situ* in the P 2p spectrum due to the overlap of the $2p_{3/2}$ and $2p_{1/2}$ peaks of the doublet. However, the Cu 2p XP spectrum does not overlap, and was used to assess the chemical nature of the interface. Fig. 5.2 shows the change in the spectra of Cu from the substrate after Co(P) deposition during depth profiling prior to complete removal of the Co(P) overlayer. The BE of the Cu $2p_{3/2}$ and $2p_{1/2}$ peaks in each spectrum are aligned precisely with the peaks of metallic Cu prior to CVD (not shown). Because even the smallest Cu peaks (*i.e.*, Cu nearest the Co(P) interface) have BE corresponding to metallic Cu, and because no shoulders are apparent,

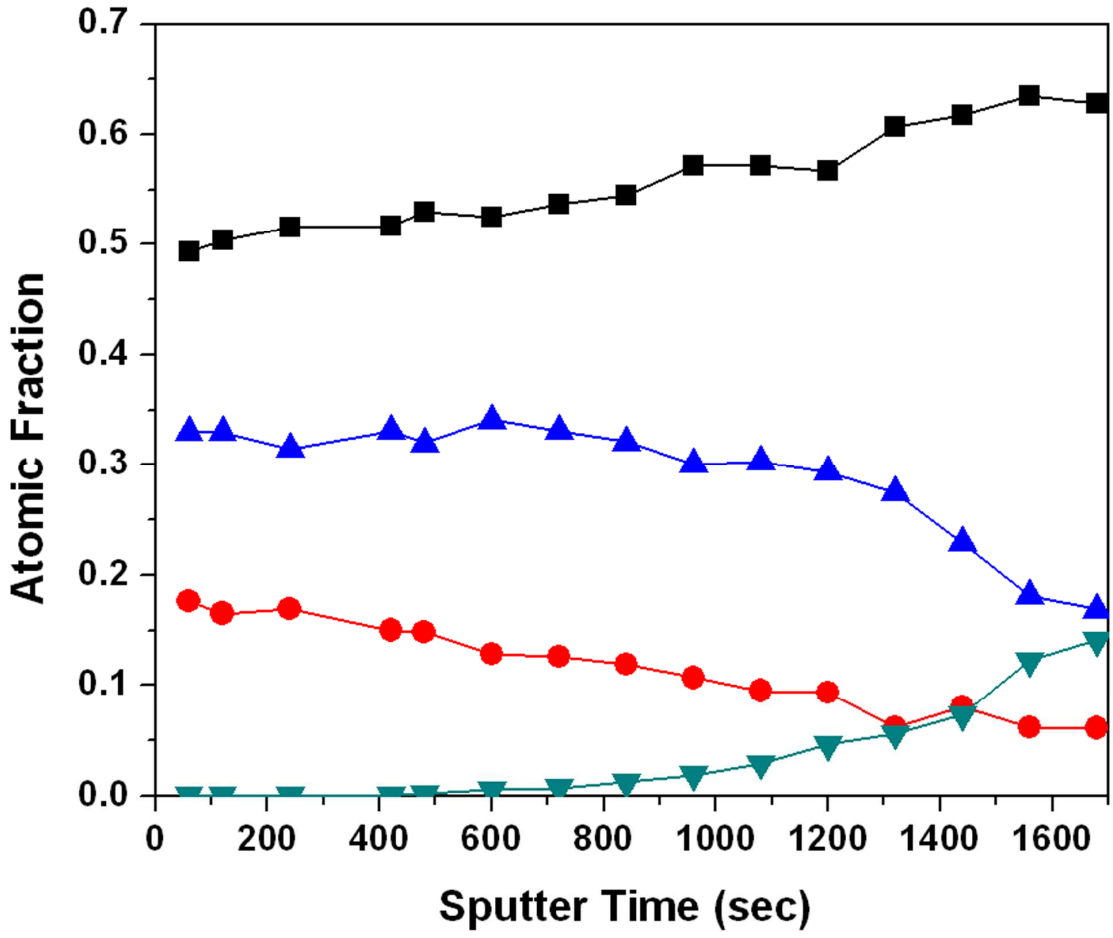

Figure 5.1. XPS depth profiling of Co(P) deposited on Cu showing the overall atomic fraction of Co (■), C (▲), P (●), and Cu (▼); O, from ambient, detectable in the first few scans, has been excluded as there was no O in the film. Cu has not reacted with P to form any measurable amount of phosphide compounds at the interface during deposition.

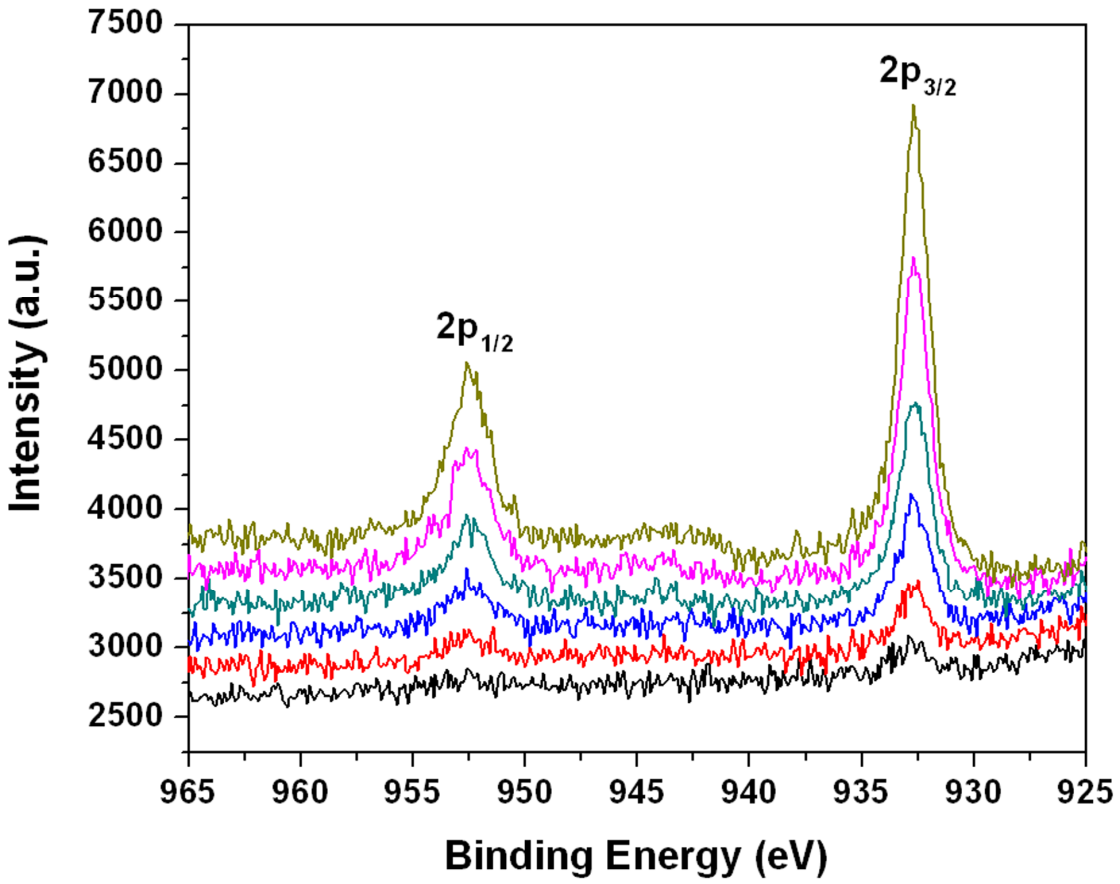

Figure 5.2. Cu 2p XP spectra obtained during depth profiling after CVD of Co(P). The doublet peaks are aligned with metallic PVD Cu peaks and show no shoulders where Cu_xP would be expected. From the bottom spectrum (black) to the top spectrum (yellow), the sputter times begin at 840 sec and increase in increments of 240 sec.

Fig. 5.3 shows LEIS and XP spectra establishing the minimum thickness for continuity of ultrathin Co(P) on Cu. LEIS spectra have been shifted vertically and scaled for ease of comparison, and XP spectra have been shifted vertically and minimally smoothed. Despite the similar atomic weights of Co and Cu, the geometry of the system was sufficient to create significant distance between the energy ratio (E/E_0) peaks to differentiate the two species at the surface [32]. Fig. 5.3a(i) and 5.3b(i) are the LEIS and Cu 2p XP spectra, respectively, for the Cu substrate after being reduced in H_2 in the CVD chamber at 350 °C for 1 h. The LEIS spectrum in Fig. 5.3a(ii), corresponding to the XP spectrum in Fig. 5.3b(ii), and Fig. 5.3a(iii), corresponding to Fig. 5.3b(iii), are spectra obtained from each of two different Co(P) films after performing CVD at 350 °C. Each of these Co(P) films were sputtered for 30 sec with 2 kV Ar^+ ions after CVD to remove surface contamination and maximize the LEISS signal strength. The sputter rate of Co(P) calculated during depth profiling of thicker films on Cu was ~0.1 nm/min, meaning a 30 sec sputter would remove only a negligible amount Co(P) overlayer. The LEIS spectrum in Fig. 5.3a(ii) features two peaks near $E/E_0 = 0.8$ aligned with the values expected for both Co and Cu, indicating the film is discontinuous, plus smaller peaks corresponding to P within the film and on the Cu surface and O adsorbed from the chamber background during sample transfer. In contrast, the Co(P) characterized in Fig. 5.3a(iii) is continuous, as the spectrum shows O, P, and Co peaks, but no Cu peak. The thickness of the continuous Co(P) film calculated using the attenuation in the corresponding Cu 2p XP peak (Fig. 5.3b(iii)) and approximating the electron mean free path through the overlayer as that of Cu 2p photoelectrons through Co (0.48 nm, as calculated using a NIST database [33]) indicates the film is 1.4 nm thick. Using this method and the XP spectrum

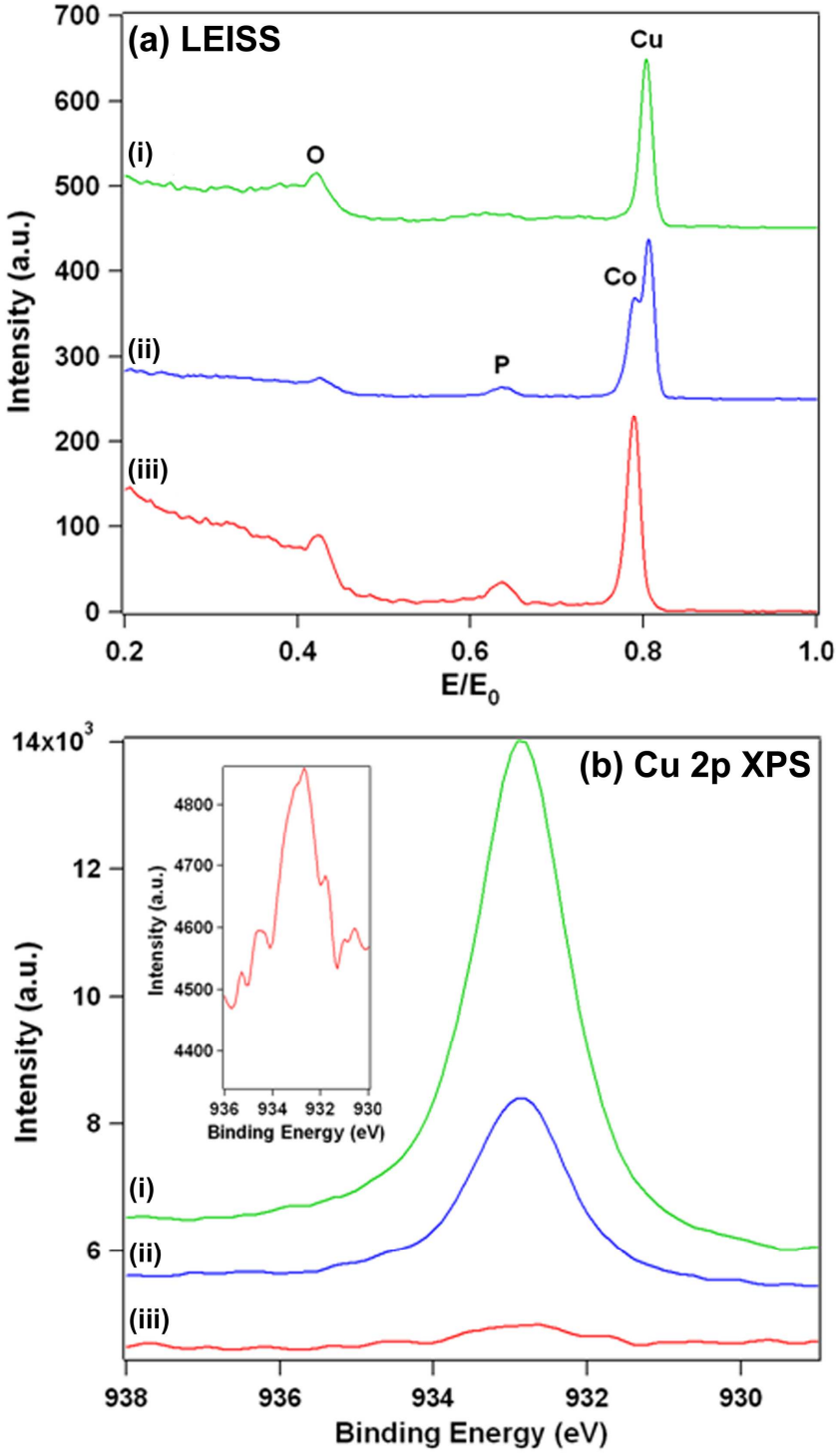

Figure 5.3. (a) LEIS and (b) XP spectra of the (i) Cu substrate prior to CVD, (ii) a discontinuous Co(P) film, and (iii) a fully continuous Co(P) film. The inset in (b) is the curve from b(iii) magnified to show detail.

in Fig. 5.3b(ii), the discontinuous "film" is 0.5 nm thick. Based on the minimal removal of Co(P) during sputter cleaning, Co(P) film becomes continuous on Cu by 1.4 nm.

LEISS results likely represent the true nature of the film surface, and XPS peak attenuation is a valid method of thickness calculation for Co(P) on Cu. The surface of a film that grows in a two-dimensional, layer-by-layer mode would be accurately described by LEISS, but there are possible geometric limitations associated with using this method to confirm continuity. When films grow three-dimensionally, there can be a shadowing effect leading to false impressions that a discontinuous film is continuous if the ion source and detector are not positioned normal to the surface [34]. The surface energy (γ) of Co (2.55 J/m^2) is greater than that of Cu (1.83 J/m^2) [35], so Co should not be expected to grow perfectly two-dimensionally, but the incorporation of P and C will lower the surface energy somewhat. Shin, *et al.* [36], used a similar deposition chemistry to deposit C impurity-containing Ru(P) (γ_{Ru} = 3.05 J/m^2) [35] on thermal SiO_2 (γ = 1.15-2.00 J/m^2) [37] and found that films as thin as 7 nm as measured by XPS were continuous, while Henderson and Ekerdt [38] grew continuous 5 nm Ru(P) on thermal SiO_2, as measured by XPS, and confirmed the film thickness uniformity by transmission electron microscopy (TEM) imaging. Considering the difference in γ in the Ru/SiO_2 system is at least 45% larger than the γ difference in the Co/Cu system, the wetting of Co(P) on Cu should be superior to the wetting of Ru(P) on SiO_2, and XPS and LEISS therefore measure the thickness and surface composition, respectively, of Co(P) on Cu.

5.3.2. Adhesion

The adhesion of Co to Cu is very strong. Because of the incorporation of C and P in the film, the adhesion of this Co(P) alloy to Cu is expected to be reduced due to the loss of favorable Co–Cu interactions at the interface as Co is replaced by P and C. A scotch tape peeling test was used to qualitatively compare adhesion and ensure that, despite the presence of P and C, CVD Co(P) adheres well to Cu. PVD Cu sputtered onto SiCN was tested as a rough approximation to the current method of capping Cu with a dielectric etch-stop layer and to gauge to what extent our peeling test would delaminate films at a known interface of weak adhesion. The entire Cu film below the tape was removed from the SiCN substrate during peeling. Another weakly adhering system, PVD Cu sputtered directly onto SiO_2, was subjected to the peeling test. As expected, the delamination was complete further confirming that our method was sufficient to identify weakly adhering interfaces.

Cu was not sputtered onto Co(P) because Co(P) grown on SiO_2 did not sufficiently adhere to allow Cu-Co(P) adhesion testing in this manner. Co(P) extensively, but not completely, delaminated from SiO_2 during peeling. Because a stack of sputtered PVD Cu/Ru/TaN on a piece of SiO_2/Si wafer showed no delamination, Co(P) was deposited by CVD directly onto Cu of this type. The order of deposition in this case more accurately matches the sequence that would occur in practice during the Cu IC metallization process. Also, considering the depth profile shown in Fig. 5.1, the Co(P)-Cu interface formed by depositing films in the proper order will be relatively P and C poor, increasing the extent of strong Cu–Co bonding. The substrate was metallic and gray after deposition, meaning Co(P) was thick enough to be observed on the tape if it were to delaminate. No Co(P) delaminated from the Cu surface during peeling, nor did

any interface in the stack delaminate during the tape test. XPS showed a strong Co peak and no Cu peak after testing, confirming the adhesion was strong. The relative adhesive strengths as measured with our method based on the extent of delamination are (listed as overlayer-underlayer):

CVD Co(P) – PVD Cu > CVD Co(P) – SiO_2 > PVD Cu – SiCN

It remains unclear whether Co alloy capping layers can be utilized as Cu IC caps without a dielectric capping layer to protect the Co itself from the highly oxidizing environments that would follow in higher level metallization. Regardless of this issue, Co alloys will certainly be capped with a nonmetallic material, either a Si-based etch stop layer or a low-κ material, such as SiO_2-based dielectrics like silica xerogels and aerogels and the family of silsesquioxane-based materials [39-42]. The adhesion between a Co-based alloy and the dielectric overlayer will be highly dependent upon material choice and processing steps, but similar to how the incorporation of N into Ta to form TaN_x increases the adhesion of Ta to SiO_2 as the amount of N increases [43], the relative richness in P and C of the exposed Co(P) surface could serve to enhance the adhesion between the two materials due to favorable interactions between nonmetal atoms located at the interface and should be studied.

5.3.3. Growth Selectivity

The deposition rate of Co(P) on SiO_2 ranges from ~3 nm/min at 250 °C to ~9 nm/min at 350 °C [28]. Growth on SiO_2 featured practically no incubation period, with film thicknesses from 25-65 nm after 5 min CVD. Comparatively, XPS indicated similar conditions for CVD on Cu substrates resulted in films that were <5 nm thick and

occasionally not fully continuous, indicating a very long incubation period. For this reason, it is unlikely that this particular dual-source deposition chemistry could provide selective growth on Cu without deposition on SiO_2. A simple side-by-side comparison was performed to confirm this by performing CVD on a SiO_2 substrate half covered with a Cu-capped stack. Upon removal to ambient after deposition, the wafer sections lacking the Cu cap appeared similar in color to previously observed thick Co(P) films on SiO_2, but the areas capped with Cu did not appear noticeably different in color from typical thick Cu films. Substrates were observed in cross-sectional SEM prior to and after 5 min CVD to check for visible Co(P) deposition on either surface. As expected, after deposition at 250 °C, 300 °C, and 350 °C, thick Co(P) films were clearly visible on the portion of the wafer with bare SiO_2, but no films were seen on the section that had been capped with Cu, meaning this deposition chemistry using the dual source used in this study is not useful for selective Cu capping.

We do not, however, rule out the possibility of using a similar method to selectively deposit Co(P) on Cu. There are some possible explanations for the poor growth selectivity characteristics, which provide direction for future investigations. Lai, *et al.* [44], reported that PMe_3 adsorbed on Cu(110) mostly desorbs intact by 250 °C, but the fraction that remains is fully demethylated by this temperature, leaving surface C and P, which does not diffuse into the bulk and is stable on the surface up to 600 °C. The surface P and C can then block sites for $Co_2(CO)_8$ adsorption and reaction during CVD, slowing the rate of nucleation on Cu while nucleation and film growth on SiO_2 proceeds normally [45]. It is possible that CVD using PEt_3 [Et = CH_2CH_3] or PH_3 instead of PMe_3 could speed the rate of nucleation on Cu, as these molecules result in adsorbed P with

less surface C compared to PMe_3 [44] or no C at all [46], respectively, in the temperature regime studies. This may open additional sites for $Co_2(CO)_8$ reaction, but the persistence of adsorbed P (and minimal C in the case of PEt_3 co-dosing) on Cu would still slow Co nucleation compared to SiO_2. Moreover, $Co_2(CO)_8$ is a highly reactive molecule on a SiO_2 surface. The carbonyl ligands can quickly leave as CO molecules and deposit metallic Co over a wide range of temperatures at high rates with no need for a co-reactant gas [28,47-49]. To overcome this obstacle, a Co precursor that shows less reactivity on SiO_2 and coincident high reactivity on Cu could be used, such as in a pulsed-CVD method where the duration of each pulse is less than the time needed for Co nucleation on SiO_2 [50]. Alternatively, the SiO_2 surface could be made less conducive to $Co_2(CO)_8$ reaction and Co nucleation [51], or a combination of these strategies could be employed.

5.4. SUMMARY

P- and C-containing alloys of Co were grown by CVD from a dual-source chemistry of $Co_2(CO)_8$ and PMe_3 on Cu and SiO_2 to investigate the potential application of a non-aqueous method for capping Cu ICs. P and C were not evenly distributed throughout the depth of the film, with the concentration near the Cu interface being poorer in both than at the surface. Despite the incorporation of P and C, the adhesion between Cu and Co(P) remains strong, and Co(P) adheres slightly better to SiO_2 than does PVD Cu. There is no evidence that Cu_xP formed at the interface during deposition. Co(P) becomes continuous on Cu by 1.4 nm. Because the Co precursor is highly reactive on SiO_2 and surface P and C result in long incubation times for film growth on Cu, the deposition chemistry reported here does not provide acceptable selectivity for use in IC

technology. However, understanding the underlying causes of poor selectivity provides direction for future selective CVD design.

5.5. REFERENCES

1. D. Save, F. Braud, J. Torres, F. Binder, C. Müller, J. O. Weidner, and W. Hasse, Microelectron. Eng., 33, 75 (1997).

2. C.-K. Hu, L. Gignac, and R. Rosenberg, Microelectron. Reliab., 46, 213 (2006).

3. B. Li, T. D. Sullivan, T. C. Lee, and D. Badami, Microelectron. Reliab., 44, 365 (2004).

4. J. R. Lloyd and J. J. Clement, Thin Solid Films, 262, 135 (1995).

5. M. W. Lane, E. G. Liniger, and J. R. Lloyd, J. Appl. Phys., 93, 1417 (2003).

6. M. H. Lin, Y. L. Lin, J. M. Chen, M.-S. Yeh, K. P. Chang, K. C. Su, and T. Wang, IEEE Trans. Electron. Dev., 52, 2602 (2005).

7. S.-M. Yi, C. Shim, H.-C. Lee, J.-W. Han, K.-H. Kim, and Y.-C. Joo, Microelectron. Eng., 85, 621 (2008).

8. N. L. Michael, C.-U. Kim, Q.-T. Jiang, R. A. Augur, and P. Gillespie, J. Electron. Mater., 31, (2002).

9. H. Kim, Y. Naito, T. Koseki, T. Ohba, T. Ohta, Y. Kojima, H. Sato, and Y. Shimogaki, Jap. J. Appl. Phys., 45, 2497 (2006).

10. International Technology Roadmap for Semiconductors, 2008 Update, http://public.itrs.net

11. M. A. Sheikholeslam, M. H. Enayati, and K. Raeissi, Mater. Lett., 62, 3629 (2008).

12. S. M. S. I. Dulal, H. J. Yun, C. B. Shin, and C.-K. Kim, J. Electrochem. Soc., 154, D494 (2007).

13. R. Tarozaitė, M. Kurtinaitienė,A.Džiūvė, and Z. Jusys, Surf. Coat. Technol., 115, 57 (1999).

14. J. Gambino, J. Wynne, J. Gill, S. Mongeon, D. Meatyard, B. Lee, H. Bamnolker, L. Hall, N. Li, M. Hernandez, P. Little, M. Hamed, I. Ivanov, and C. L. Gan, Microelectron. Eng., 83, 2059 (2006).

15. Z. Li, R. G. Gordon, D. B. Farmer, Y. Lin, and J. Vlaasak, Electrochem. Solid-State Lett., 8, G182 (2005).

16. P. Singer, Semicond. Int., 28, 44 (2005).

17. Y. Shacham-Diamand, A. Dedhia, D. Hoffstetter, and W. G. Oldham, J. Electrochem. Soc., 140, 2427 (1993).

18. F. Lanckmans and K. Maex, Microelectron. Eng., 60, 125 (2002).

19. J. R. Lloyd, C. E. Murray, S. Ponoth, S. Cohen, and E. Liniger, Microelectron. Reliab., 46, 1643 (2006).

20. K. C. Aw, N. T. Salim, W. Gao, and K. Prince, Int. J. Mod. Phys. B, 20, 4165 (2006).

21. K. M. Chow, W. Y. Ng, and L. K. Yeung, Surf. Coat. Technol., 99, 161 (1998).

22. M. Paunovic, P. J. Bailey, and R. G. Schad, J. Electrochem. Soc., 141, 1843 (1994).

23. E. J. O'Sullivan, A. G. Schrott, M. Paunovic, C. J. Sambucetti, J. R. Marino. P. J. Bailey, S. Kaja, and K. W. Semkow, IBM J. Res. Dev., 42, 607 (1998).

24. A. Kohn, M. Eizenberg, and Y. Shacham-Diamand, J. Appl. Phys., 94, 3015 (2003).

25. T. Decorps, P. H. Haumesser, S. Olivier, A. Roule, M. Joulaud, O. Pollet, X. Avale, and G. Passemard, Microelectron. Eng., 83, 2082 (2006).

26. S. Y. Chang, C. C. Wan, and Y. Y. Wang, Electrochem. Sol. State Lett., 10, D43 (2007).

27. L. B. Henderson and J. G. Ekerdt, Electrochem. Sol. State Lett., 12, D36 (2009).

28. L. B. Henderson and J. G. Ekerdt, J. Electrochem. Soc., in press.

29. ASTM D 3359-08: Standard Test Methods for Measuring Adhesion by Tape Test, ASTM International, West Conshohocken, PA, U.S.A., (2008).

30. H. Okamoto, Cu-P Phase Diagram, in: ASM Alloy Phase Diagrams Center, P. Villars (Ed.), (ASM International, Materials Park, OH, 2006). http://www.asminternational.org/AsmEnterprise/APD

31. NIST X-ray Photoelectron Spectroscopy Database, Vers. 3.5 (National Institute of Standards and Technology, Gaithersburg, MD, 2003); http://srdata.nist.gov/xps/

32. E. Taglauer and W. Heiland, Appl. Phys., 9, 261 (1976).

33. NIST Electron Effective-Attenuation-Length Database, Vers. 1.0 (National Institute of Standards and Technology, Gaithersburg, MD, 2001).

34. J. Shin, D. Gay, Y.-M. Sun, J. M. White, and J. G. Ekerdt, AIP Conf. Proc., 788, 482 (2005).

35. H. L. Skriver and N. M. Rosengard, Phys. Rev. B, 46, 7157 (1992).

36. J. Shin, H.-W. Kim, G. S. Hwang, and J. G. Ekerdt, Surf. Coat. Technol., 201, 9526 (2007).

37. P. Staszczuk, B. Jańczuk and E. Chibowski, Mater. Chem. Phys., 12, 469 (1985).

38. L. B. Henderson and J. G. Ekerdt, Thin Solid Films, 517, 1645 (2009).

39. K. Maex, M. R. Baklanov, D. Shamiryan, F. Iacopi, S. H. Brongersma, and Z. S. Yanovitskaya, J. Appl. Phys., 93, 8793 (2003).

40. D. Shamiryan, T. Abell, F. Iacopi, and K. Maex, Mater. Today, 7, 34 (2004).

41. H. Treichel, J. Electron. Mater., 30, 290 (2001).

42. B. D. Hatton, K. Landskron, W. J. Hunks, M. R. Bennett, D. Shukaris, D. D. Perovic, and G. A. Ozin, Mater. Today, 9, 22 (2006).

43. M. Lane, R. Dauskardt, N. Krishna, and I. Hashim, Mater. Res. Soc. Symp. Proc., 564, 281 (1999).

44. Y.-H. Lai, C.-T. Yeh, H.-J. Lin, C.-T. Chen, and W.-H. Hung, J. Phys. Chem. B, 106 1722 (2002).

45. J. Shin, H.-W. Kim, K. Agapiou, R. A. Jones, G. S. Hwang, and J. G. Ekerdt, J. Vac. Sci. Technol. A, 26, 974 (2008).

46. L. V. Goncharova, S. K. Clowes, R. R. Fogg, A. V. Ermakov, and B. J. Hinch, Surf. Sci., 515, 553 (2002).

47. M. E. Gross, K. Schnoes Kranz, D. Brasen, and H. Luftman, J. Vac. Sci. Technol. B, 6, 1548 (1988).

48. D.-X. Ye, S. Pimanpang, C. Jezewski, F. Tang, J. J. Senkevich, G.-C. Wang, and T.-M. Lu, Thin Solid Films, 485, 95 (2005).

49. Q. Zhao, D. W. Greve, and K. Barmak, Appl. Surf. Sci., 219, 136 (2003).

50. E. Nakazawa, K. Arita, Y. Tsuchiya, Y. Kakuhara, S. Yokogawa, T. Kurokawa, N. Sasaki, S. Ganguli, H.-C. Ha, W. T. Lee, S.-H. Yu, and M. Sekine, Proceedings of the Advanced Metallization Conference, p. 19 (2008).

51. H. J. Yang, J. Lee, S. Kim, Y. K. Ko, H. J. Shin, J. G. Lee, C. Kim, H. J. Bang, B. S. Cho, Y. H. Bae, J. H. Lee, D. H. Kim, C. O. Jeong, S. Y. Kim, and S. K. Lim, J. Appl. Phys., 100, 113705-1 (2006).

Chapter 6: Nanocrystalline cobalt-based films with high thermal stability from a single molecule

6.1. INTRODUCTION

Co(P) films are of interest due to their multiple potential technological applications. Because of the strong adhesion of Co to Cu [1] and the increased diffusion barrier capability achieved by incorporating a few atomic percent P within a film [2], Co(P) has emerged as a candidate to replace Si-based dielectric films as a capping layer in the Cu interconnect in chips to increase electromigration lifetimes by orders of magnitude [3-4]. Co(P) also is sufficiently hard [5-6] and wear resistant [7] so as to merit investigation as a replacement for Cr coatings, which are commonly deposited from carcinogenic [8-9] hexavalent Cr compounds [10], by processes that create toxic waste. Furthermore, Co begins to exhibit excellent corrosion resistance when alloyed with low-levels of P [11]. Numerous opportunities for use in magnetic random access memory, sensors, recording heads, and multiple other applications are possible due to the magnetic properties of Co(P) varying with changing microstructures [12-13] ranging from hard [14] to soft [15] magnetism.

Furthermore, the addition of P to Co serves to stabilize the microstructure when Co is nanocrystalline (nc), which is essential to retain the typically unique properties of nc materials. In general nc materials are far less thermally stable than their larger-grained analogues because there is a higher driving force towards grain growth due to the comparatively high volume of grain boundaries, which results in an excess of free energy. For any process that requires treatments or applications at even moderate

temperatures, such as microelectronic chip manufacturing, pure nc materials will experience rapid grain growth and potentially lose their desirable properties. Adding low levels of properly selected dopants improves the thermal stability of nc materials [16-18]. High-purity electrodeposited nc Co is only stable up to ~150° C, at which point it begins to exhibit grain growth [19], and has been observed to undergo an allotropic phase transformation from hcp to fcc as low as 300° C [20]. Bulk polycrystalline Co does not undergo this allotropic transformation until ~420° C [21]. P doping levels as low as 1.1 at. % were reported to be sufficient to force the allotropic transformation back to the normal expected range, as well as delaying grain growth to ~440° C at which point the grain boundaries saturate with P, and CoP and Co_2P phosphides begin to precipitate [22-23]. This increased stability makes nc Co(P) an attractive candidate for many high-temperature applications.

The most common methods of deposition for Co(P) films are electro- [24-27] and electroless [28-30] aqueous deposition chemistries, although sputtering [14,31-32] and chemical vapor deposition (CVD) [33] have also been reported. Herein, we report CVD of nc Co(P) films from a single-source precursor, (tetrakis)trimethylphosphine)cobalt(0), $(Me_3P)_4Co$ [Me = CH_3].

6.2. EXPERIMENTAL DETAILS

6.2.1. Synthesis of $(Me_3P)_4Co$

$(Me_3P)_4Co$ was synthesized from $CoCl_2$ (Alfa Aesar, 99.7%) and PMe_3 (Aldrich, 97%) based on the method described in the literature [34-35]. All reactions were performed under a dry, oxygen-free nitrogen atmosphere or under vacuum using standard

Schlenk line and dry box techniques. Solvents were dried prior to use by distillation from benzophenone/sodium. All other reagents were used without further purification. The product was purified by sublimation prior to use.

6.2.2. Film Growth

Films were grown in a multi-chamber system which includes a vacuum sample transfer chamber, a stainless steel cold-wall CVD chamber (base pressure 4.0×10^{-6} Pa), and an analysis chamber (base pressure $<5.3\times10^{-8}$ Pa) equipped with X-ray photoelectron spectroscopy (XPS) (Physical Electronics 3057; Mg Kα). Films were deposited on 20 mm × 20 mm pieces of 400 nm chemically-grown (using tetraethylorthosilicate) SiO_2/Si(100) wafers (obtained from International Sematech), which were heated radiatively from below to 125 °C - 325 °C in 50 °C increments. The temperature range was selected to begin below the temperature of grain growth in pure nc Co and conclude above the temperature of allotropic phase transformation in nc Co [19-20]. The precursor was heated in a Pyrex saturator to ~95 °C to develop sufficient vapor pressure and carried to the chamber using ultra-high purity H_2 (99.999%, Matheson Tri-Gas) flowing at 2 sccm. To prevent condensation of the precursor, the stainless steel gas lines and showerhead leading to the chamber were heated to ~105 °C. The deposition pressure was ~1.2 Pa. No co-reactant gas was used.

6.2.3. Film characterization

XPS was performed both *in situ* (Physical Electronics 3057, Mg Kα) and *ex situ* (Physical Electronics 5500, Al Kα; or Kratos AXIS Ultra DLD, monochromatic Al Kα).

Further film characterization was performed with scanning electron microscopy (SEM) (Zeiss Supra 40 VP), and grazing angle (2° incident) X-ray diffraction (XRD) (Bruker-Nonius D8, Cu Kα). To assess thermal stability, annealing was conducted in a quartz-tube furnace under vacuum of < 0.7 Pa. Grain sizes of nc films were calculated from XRD peak broadening using the Scherrer Equation (Eq. 6.1):

$$D = \frac{K\lambda}{\beta \cos\theta} \tag{6.1}$$

where D is the crystallite size, K is the Scherrer constant (~0.94), λ is the wavelength of the incident X-ray radiation, β is the XRD peak full width at half maximum (FWHM), and θ is the Bragg angle [36]. Note that this method excludes the contribution of strain to peak broadening, and the average grain sizes reported using this equation should only be considered to be estimates. The slight additional peak broadening caused by Cu $K\alpha_2$ radiation (λ = 1.5444 Å) was eliminated leaving only the contribution of Cu $K\alpha_1$ (λ = 1.5406 Å) prior to calculating the approximate grain sizes. Curve fitting software using contributions of both Gaussian and Cauchy-Lorentz distributions was used to establish the FWHM of each peak in the XRD spectra. A Co foil (99.95%, ESPI Metals) was used as a material standard.

6.3. RESULTS AND DISCUSSION

6.3.1. Compositional Analysis

Substrate temperatures ≥ 225 °C resulted in film growth, while continuous films could not be grown at temperatures ≤ 175 °C despite multiple attempts. As shown in XP spectra (*in situ* Physical Electronics 3057; Mg Kα) in Fig. 6.1, Co, C, and P were present

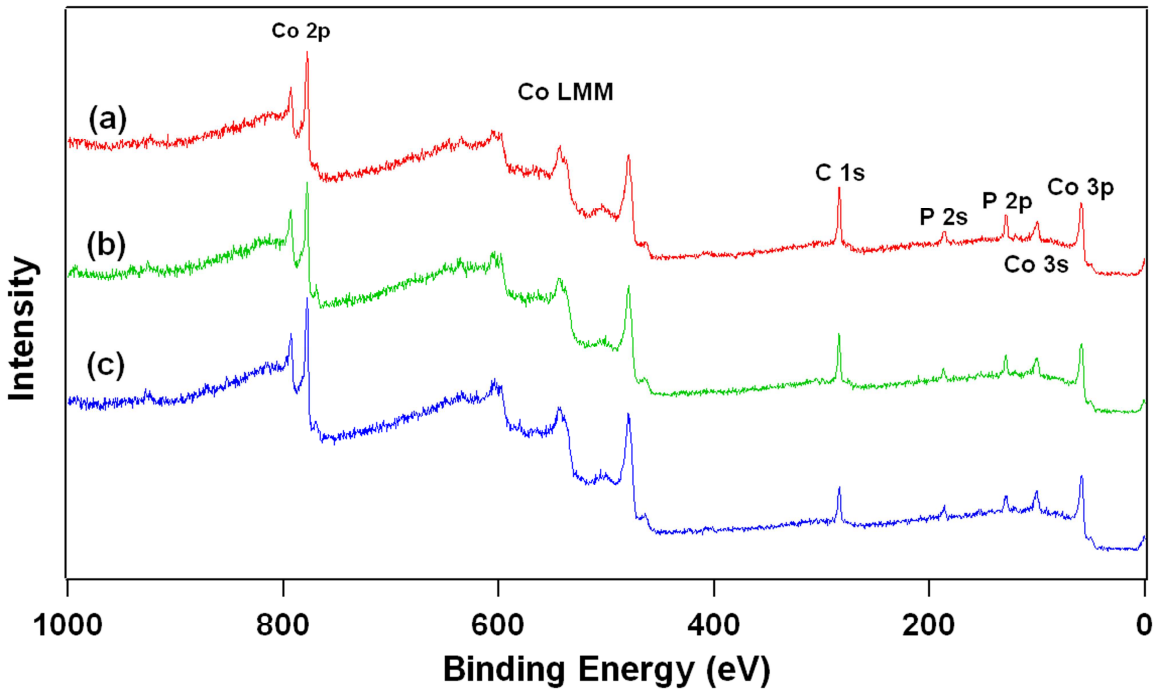

Figure 6.1. Vertically shifted *in situ* XPS survey scans of films deposited at (a) 325 °C, (b) 275° C, and (c) 225 °C showing only peaks associated with Co, C, or P.

in films deposited at all temperatures ≥ 225 °C, and there were no traces of any impurities, such as Cl, from precursor synthesis. *Ex situ* XPS with the monochromatic source was used to more carefully assess the chemical states of Co, C, and P within the films. Co 2p and C 1s XP spectra (not shown) were similar to those reported in amorphous Co(P) grown with a dual-source chemistry [33]. The C 1s peak was always composed of two separate peaks, one centered at a binding energy (BE) of ~285.0 eV, graphitic C, and another at ~283.7 eV, indicating the presence of carbidic C bonded to Co [37]. The shape and BE of the CVD Co 2p doublet was similar to Co foil and did not change among films, indicating Co in the film is almost entirely metallic with a $2p_{3/2}$ BE of ~778.2 eV and no shoulders. Note that Co-C bonding would not be detectable in the Co 2p XP spectrum due to a very small BE change (~0.1 eV) [38].

The chemical state of P was unlike that in amorphous Co(P) [33] and more ambiguous than C or Co. The P 2p maxima were located at ~129.5-129.6 eV, which is slightly below the expected range of zero-valent P and near the value expected for CoP or Co_2P [39]. Others have claimed the P $2p_{3/2}$ BE as low as 129.3 eV in electrodeposited Co-based films is still elemental [40], but these claims are in contrast to the NIST standards [41]. Furthermore, the BE of P reported here is lower than the previously reported amorphous CVD Co(P) grown from a dual-source chemistry, which featured the same Co BE but higher P BE (~129.6 eV to ~129.9 eV) denoting a clear absence of phosphide formation in those films [42]. In this case, the P 2p XP spectrum fit was usually improved by including four peaks, similar to the results reported by Kohn, *et al.* [43]. Using the fitting constraints and values in Ref. [43] as a guideline, our best fitting indicated the majority of P (up to 80%) exists in the zero-valent state, with the rest some

phosphide of Co at all deposition temperatures. An example of the fit obtained with this method in which ~70% of the P is elemental is shown in Fig. 6.2. The BE locations in Fig. 6.2 for the phosphide doublet are at 128.9 eV and 129.8 eV, and at 129.6 eV and 130.4 eV for the elemental doublet.

Depth profiling using XPS (Physical Electronics 5500, Al Kα) revealed that P and C are not evenly distributed throughout the film. An *ex situ* depth profile through a film deposited at 325 °C is shown in Fig. 6.3a. Prior to sputtering, the surface of the film is comprised of more P and C than Co, which is due largely to adsorbed species, and the amount of P and especially C rapidly drops off. The thin oxide layer was completely removed after the first sputtering step (120 s); O was not detected within the film and has not been included in Fig. 6.3a. After initially being as high as 10 at. % after 120 s of sputtering, the amount of P in the film levels off at 3 at. %. Likewise, C incorporated in the film decreases as the film is sputtered through, although the amount of C decreases somewhat more gradually than the amount of P and is always present in concentrations a few times greater than that of P. After 2400 s of sputtering, the Si 2s XP peak became visible indicating the SiO_2 interface had nearly been reached (not shown in the figure), and sputtering was discontinued. Moreover, the ratio of elemental P or C to its phosphidic or carbidic counterpart is not constant. In Fig. 6.3b, a depth profile, obtained separately from Fig. 6.3a but from the same sample while using a monochromatic source (Kratos AXIS Ultra DLD, monochromatic Al Kα), shows a region where the amount of carbidic C relative to graphitic C continually increases, while the ratio of phosphidic P to elemental P rapidly decreases and remains low. C is always found primarily in the carbidic state, but P exists primarily in the elemental state throughout the film. Note that

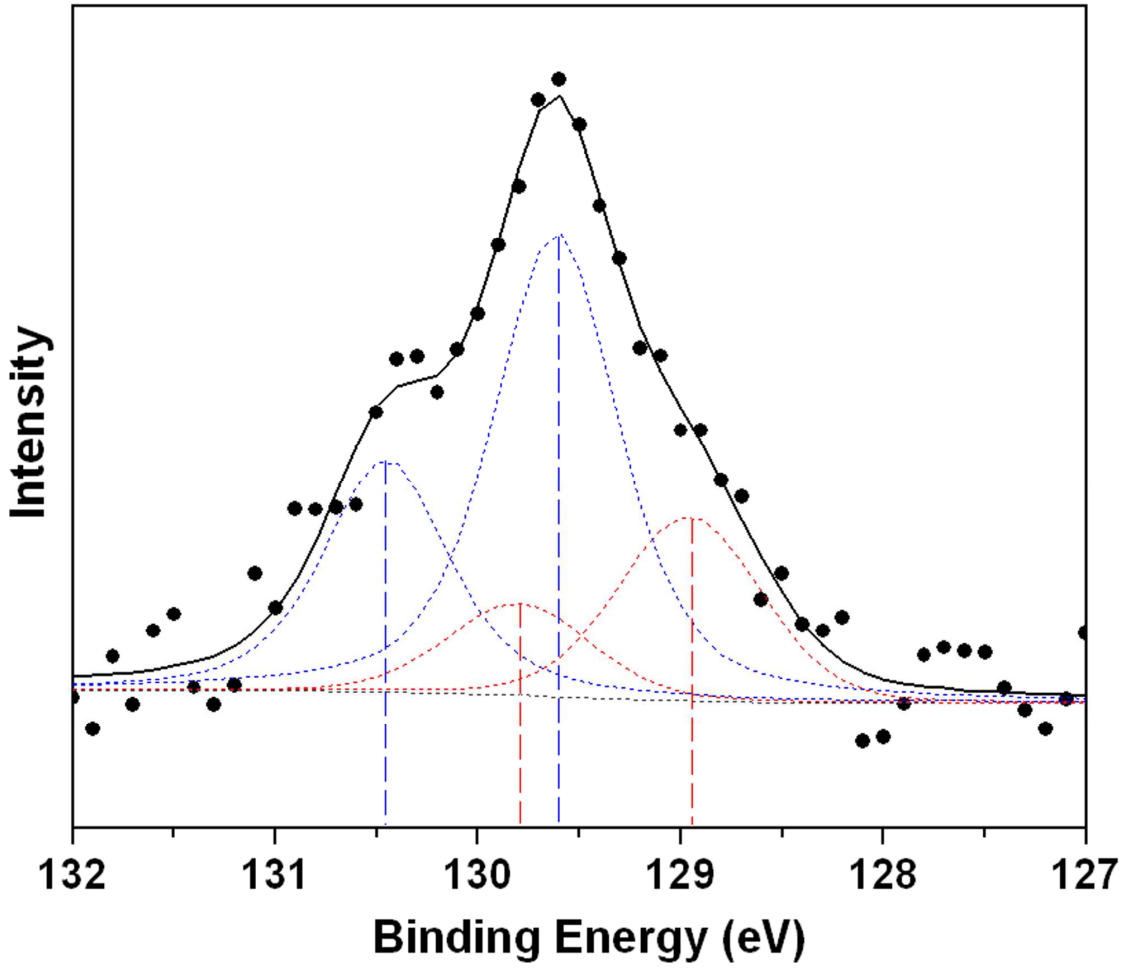

Figure 6.2. P 2p spectrum from a film deposited at 325 °C and fit using the method outlined in Ref. [43] showing both phosphidic and elemental components.

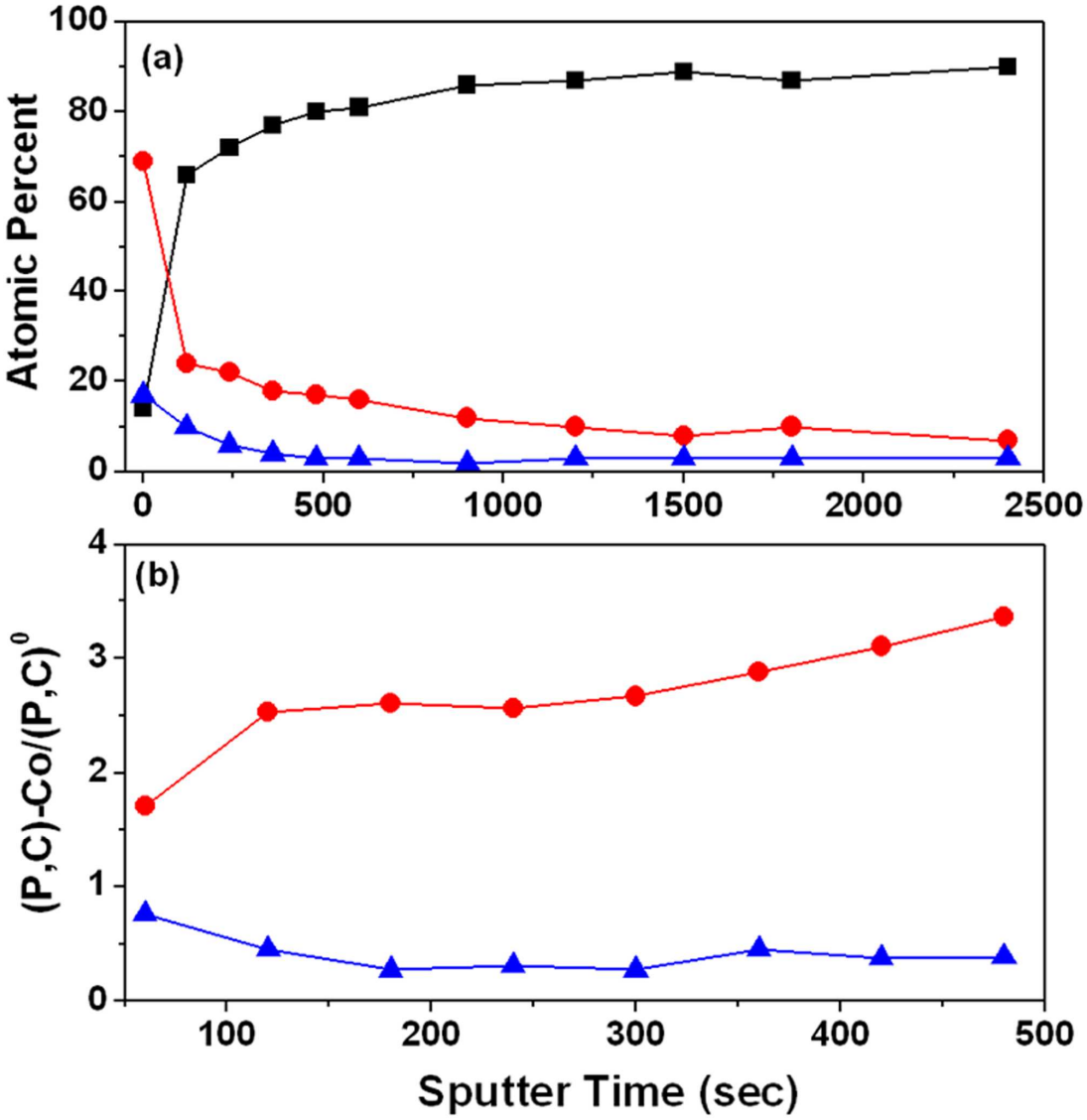

Figure 6.3. (a) XPS depth profile of a film deposited at 325 °C tracking Co (■), C (●), and P (▲) and (b) a separate depth profile tracking the change in the ratio Co-bonded C (●) and P (▲) to elemental C and P.

since the depth profiles in Figs. 6.3a and 6.3b were obtained using separate machines, the time scales are not comparable; the sputter rate is higher in Fig. 6.3b (Kratos AXIS Ultra DLD, monochromatic Al Kα).

6.3.2. Microstructure

The films had a granular surface morphology. SEM images (not shown) revealed film surfaces that appeared rough and composed of small, round grains. Films deposited at all temperatures were nc (*n.b.*: nc is commonly defined as comprised of crystallites < 100 nm in size). Fig. 6.4 shows a typical XRD spectrum from an 80 nm CVD film deposited at 325 °C, which is above the temperature at which nc Co was reported to transform to the fcc phase [20]. The data are plotted with Joint Committee on Powder Diffraction Standards (JCPDS)-catalogued peak locations and relative intensities of hcp Co [JCPDS File 05-0727] and fcc Co [JCPDS File 15-0806]. Although the fcc (111) and the hcp (002) peaks are very near each other in the standard patterns (2θ of 44.2° and 44.6°, respectively) and could be overlapping in the central broad peak, peaks that correspond uniquely to the (100) and (101) orientations of hcp Co are present at 41.6° and ~47.1°, respectively, and a peak that would uniquely correspond to the (200) orientation of fcc Co at 51.6° is absent. Furthermore, peaks that would indicate the presence of Co carbide or Co phosphide crystallites are absent, indicating that these peaks are entirely reflections of hcp Co. Table 6.1 lists peaks of high intensity in JCPDS standards for other possible compounds, the absence of which confirm the hcp Co crystallite structure of the film. The only other peaks observed in the extended range were the (110) and (200) reflections of hcp Co (not shown) at 75.9° and 92.6°,

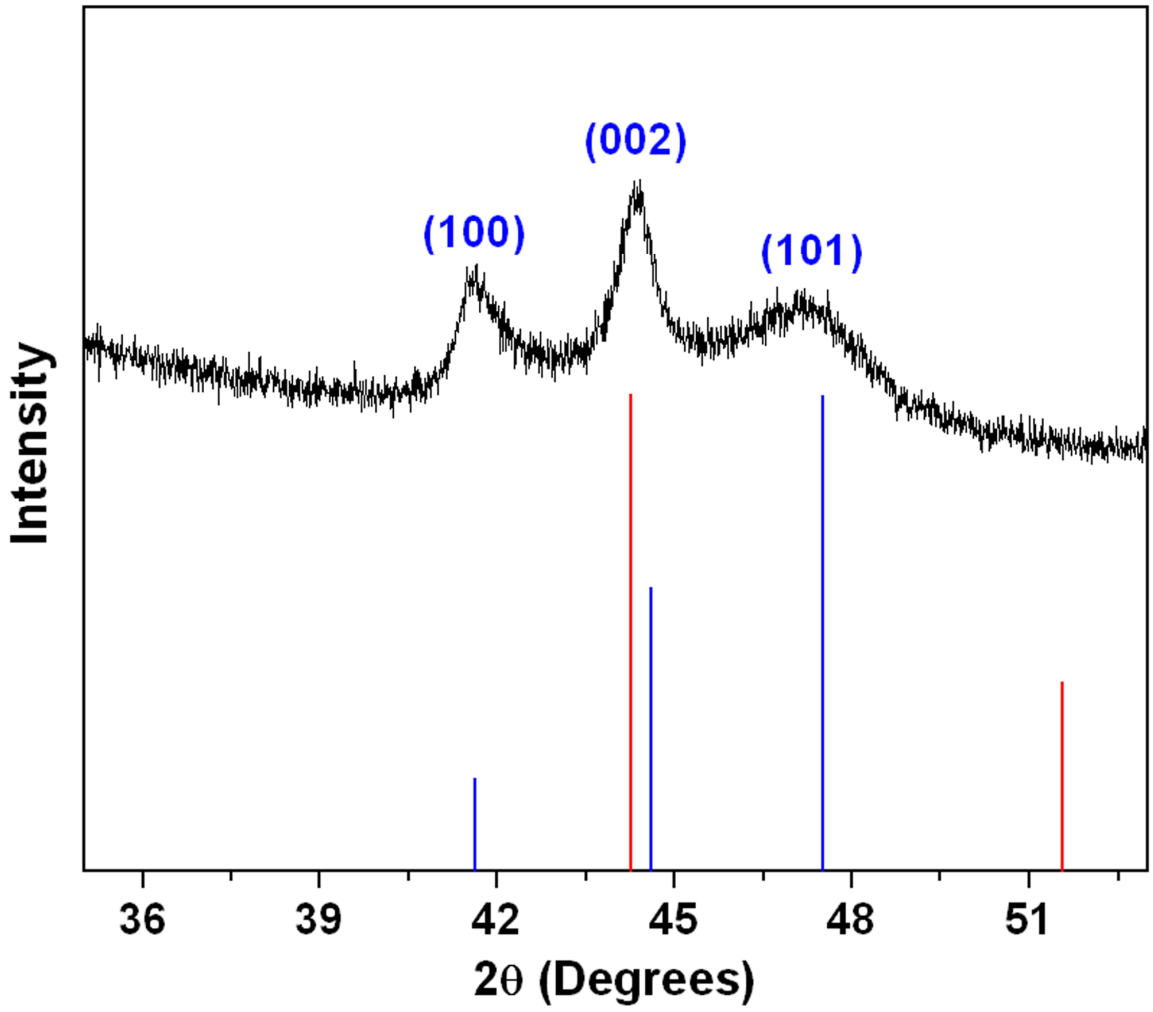

Figure 6.4. Representative XRD pattern of Co(P) film after deposition and JCPDS standard patterns for hcp Co and fcc Co.

Phase	Orientation	Expected 2θ	JCPDS File
fcc Co	(200)	51.6°	15-0806
Co2C	(110)	37.0°	72-1369
Co3C	(122)	49.9°	26-0450
Co2P	(121)	40.7°	32-0306
CoP	(111)	36.3°	29-0497
CoP3	(310)	36.9°	27-1121
CoP4	(310)	36.8°	20-0336

Table 6.1. Peaks of high relative intensity in JCPDS standard patterns that are widely separated from hcp Co peaks and absent from XRD spectra.

respectively, which were extremely weak compared to the peaks in Fig. 6.4 and not always strong enough to be clearly distinguished. Similar XRD spectra were obtained for all films deposited within the examined temperature range.

All films incorporate nc hcp Co oriented in the (101), (002), and (100) orientations, and all exclude any peaks associated with fcc Co or other compounds. Reducing the deposition temperature below 325 °C resulted in peaks that were broader, meaning that a reduction in deposition temperature led to smaller average grain sizes. Furthermore, films showed no strongly preferred orientation. Table 6.2 lists the calculated crystallite size for each of the three primary orientations from films 80 nm to 110 nm thick, as well as the dominant texture as indicated by the largest peak integral area(s) and the average crystallite size weighted by those calculated areas. The nc nature of the films deposited is not unique to the precursor chemistry, however. A dual-source chemistry using $Co_2(CO)_8$ and PMe_3 can result in nc Co-based film deposition [33], or force a fully amorphous microstructure if the amount of PMe_3 added is sufficient [33,42]. The single molecule precursor $(PMe_3)_4Co$ lacks a sufficient number of PMe_3 ligands to force a fully amorphous film, but sufficient to disrupt grain growth during deposition and result in nc films. Amorphous films, however, did not appear to incorporate phosphidic P [33,42] in measurable amounts, and the presence of grain boundaries at which P can saturate may be required for that particular reaction to occur.

Strain ($\Delta d/d$) is evident from shifts in the d-spacing, meaning the unit cells have been deformed to some extent, and the Scherrer equation underestimates grain size. As shown in examples in Fig 6.5, attempts to correct for strain-induced broadening using the method (Eq. 6.2) of Williamson and Hall [44] were unsuccessful.

	Crystallite Size (nm)				
Deposition temperature	(100)	(002)	(101)	Weighted average	Dominant texture
325 °C	19	18	9	15	(002) and (101)
275 °C	15	8	7	9	(101)
225 °C	12	9	7	9	(002)

Table 6.2. Average crystallite size calculated from XRD FWHM data for films between 80 nm and 110 nm.

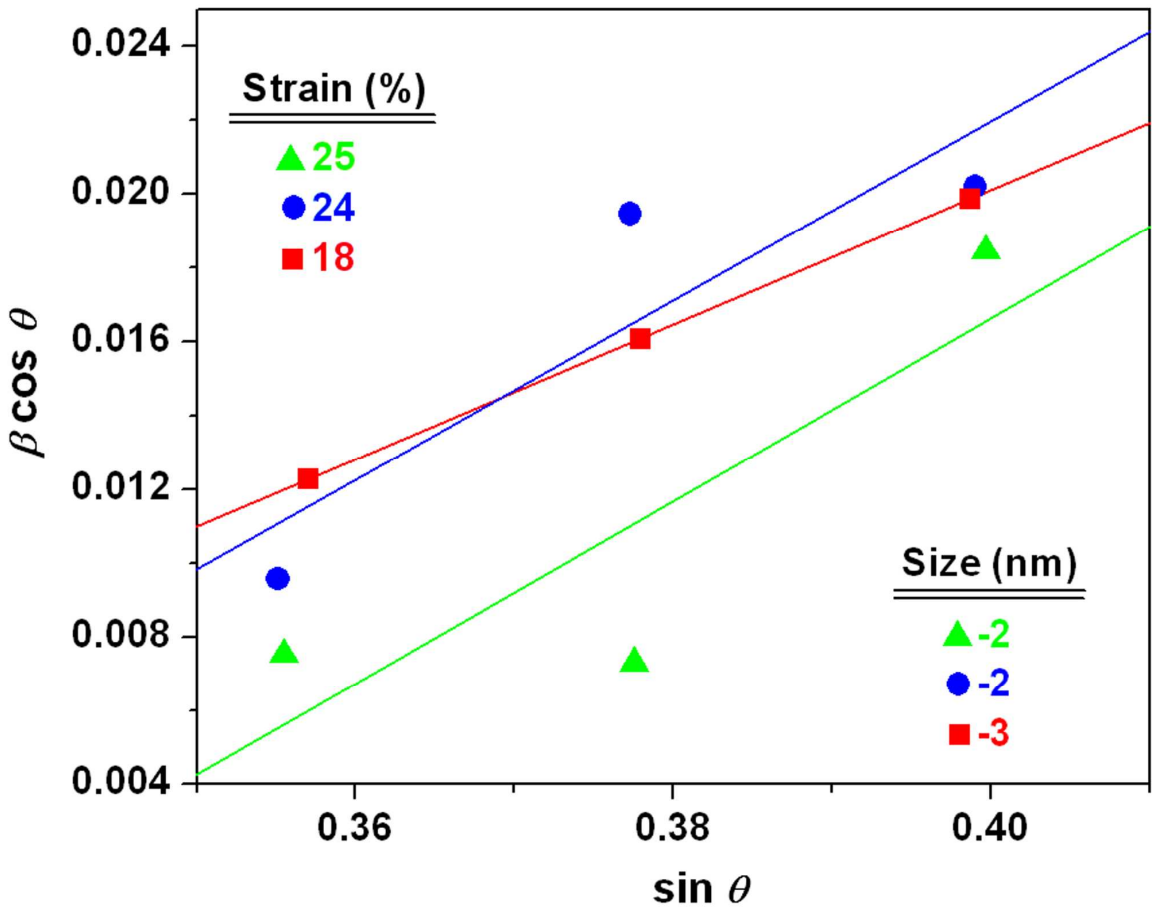

Figure 6.5. Physically unrealizable strain and grain sizes calculated using the Williamson-Hall equation.

$$\beta \cos\theta = \frac{K\lambda}{D} + \varepsilon \sin\theta \qquad (6.2)$$

Here ε is the strain and all other variables are as defined previously in Eq. 6.1. The diffraction data did not always provide a good fit to linear regression and often led to negative grain sizes and physically unrealizable strain (> 20%), a problem that is not uncommon with this method [45-49].

6.3.3. Thermal Stability

Fig. 6.6 shows a representative XRD spectrum after subjecting films to a 3 h anneal at 400 °C. This annealing condition was selected to be above the hcp to fcc transformation in electrodeposited nc Co, but below the phase transformation of bulk Co and electrodeposited nc Co(P). The standard diffraction patterns for hcp Co, fcc Co, and Co_2P [JCPDS File 32-0306] are also shown in Fig. 6.6. The particular spectrum shown in this figure is from the same film shown in Fig. 6.4. Several changes occurred within films subjected to annealing. As in Fig. 6.4, three major peaks are again clear. However, there is also a small peak around 41° and an even smaller bump near 51.6°. The location of the bump is unique to the (200) orientation of fcc Co, and would indicate some minimal extent of the allotropic phase transition having occurred, but the peak itself is small, broad, and not entirely clear. It is possible that because the allotropic transformation is reversible and the cooling rate was low (cooling time to room

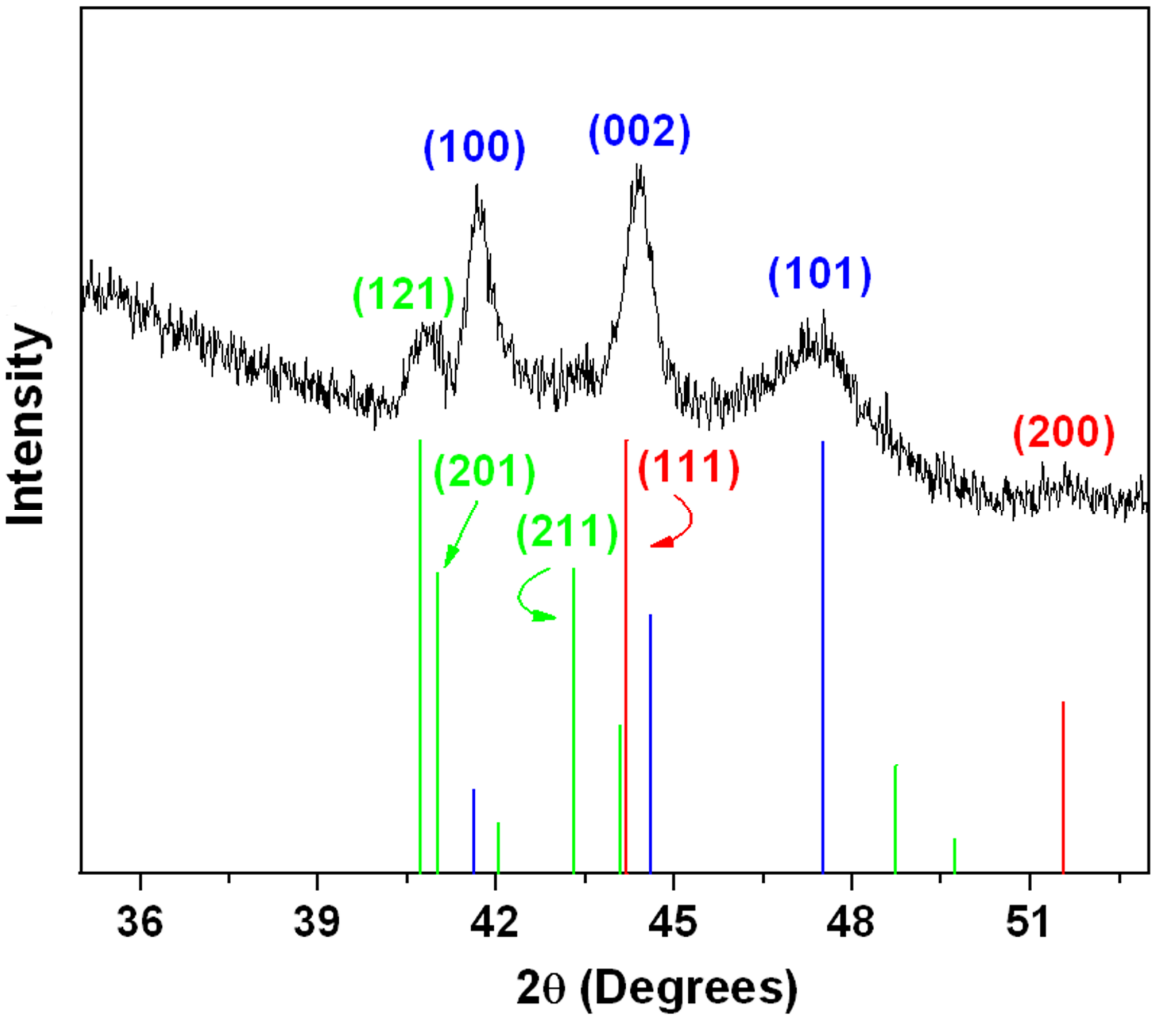

Figure 6.6. Representative XRD pattern of Co(P) film after 3 h anneal at 400 °C and JCPDS standard patterns for hcp Co and fcc Co and Co_2P.

temperature ~3 h) some fcc Co crystallites or regions of fcc Co that formed could have returned to the more stable hcp phase.

To examine this, Co foil, which was composed of hcp and fcc Co as-received, was subjected to the same anneal to see if the extended anneal and slow cooling would reduce the amount of fcc Co present. As shown in Fig. 6.7, the anneal did not reduce the amount of fcc Co relative to hcp Co, meaning fcc Co does not transform back to hcp under the annealing and cooling conditions. Hibbard, *et al.* [19], annealed electrodeposited nc hcp Co film and observed significant hcp to fcc transition after either 30 min at 300 °C or only 5 s at 390 °C, and Kumar and Gupta [50] observed a strong fcc (002) peak after annealing nc Co sputtered onto glass for 1 h at 350 °C. In the contrasting case of the CVD Co(P) film, the addition of P and C to the film was sufficient to prevent extensive transformation to the fcc phase at temperatures significantly below the ~420 °C expected for bulk Co. Therefore, CVD films reported herein show good phase stability compared to pure nc Co.

The slightly larger peak near 41° in Fig. 6.6 is uniquely attributable to the orthorhombic Co-rich monophosphide, *o*-Co_2P (and explicitly no other phosphide or carbide compound of Co), oriented in the (121) and/or (201) directions. Based on the standard relative peak intensities, we expect that this should primarily be (121) *o*-Co_2P, but we have also labeled the 2θ location of the (201) orientation beneath the experimentally obtained spectrum in Fig. 6.6. Other phases and orientations that may be present in small amounts but are not completely discernable in the collected data are also labeled below the obtained spectrum. All CVD films exhibited some extent of Co-rich phosphide-compound crystallization and possible slight transformation to the fcc

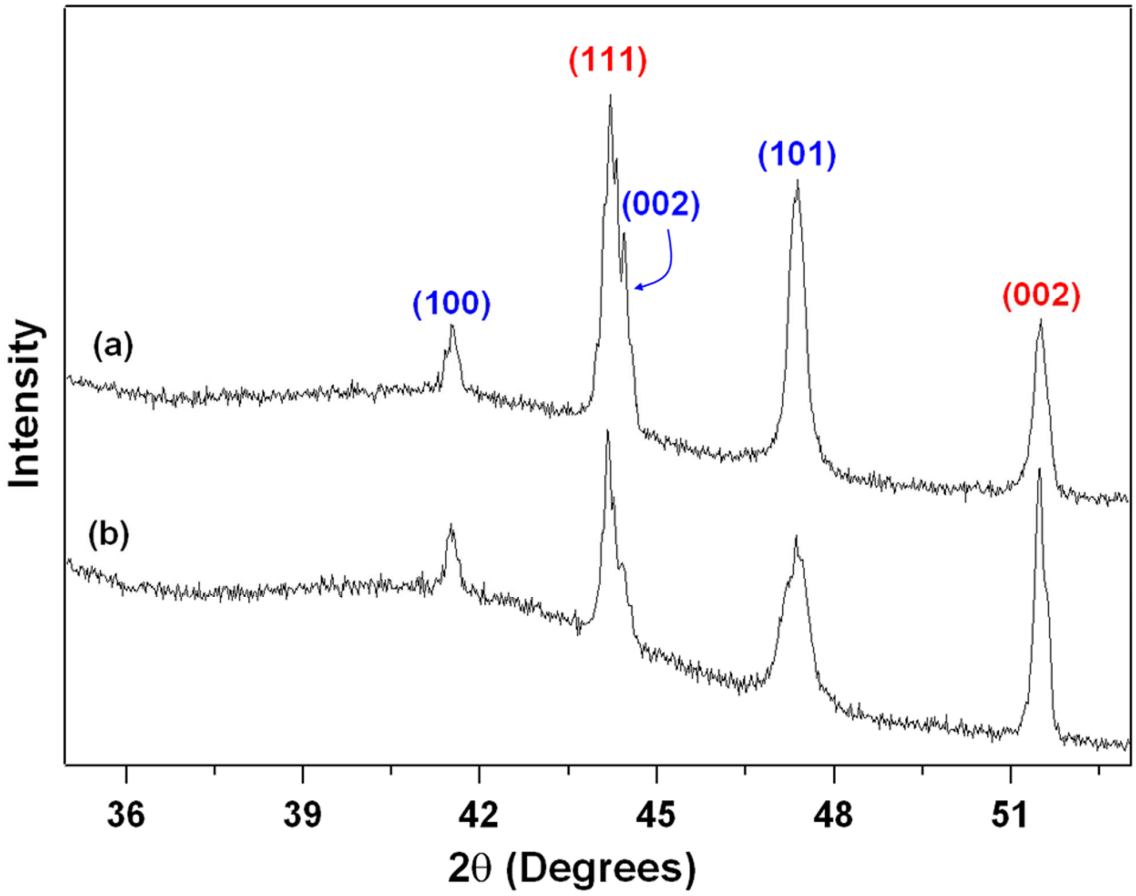

Figure 6.7. XRD pattern of Co foil (a) as received and (b) after 3 h anneal at 400 °C; hcp indices are blue, fcc indices are red, and the patterns have been vertically shifted for comparison.

structure, but hcp Co remained clearly dominant. No peaks for crystalline C or Co_xC compounds were observed. In terms of mechanical strength, the precipitation of Co_2P has been shown to increase the hardness of Co(P) films [6]. Magnetically, however, the effects of P addition in Co(P) films, which are primarily grown via aqueous chemistries, are highly dependent upon deposition and processing conditions [51-58], and upon annealing the *o*-Co_2P that precipitates is itself paramagnetic [60].

Peak narrowing is also evident in Fig. 6.6, indicating grains have grown larger within the film. Table 6.3 presents the average grain sizes calculated using the Scherrer equation for the (100), (002), and (101) hcp peaks, along with the percent change in size due to annealing for the same films listed in Table 6.2. Choi, *et al.* [22], da Silva, *et al.* [23], and Kohn, *et al.* [43], annealed electrodeposited nanocrystalline 1.1 at. %P Co(P), 3.2 at. %P Co(P), and $Co_{0.9}W_{0.02}P_{0.08}$, respectively, for 1 h at 400 °C and reported no fcc Co formation, while Fukumiya, *et al.* [61], annealed Co-C composite films (containing amorphous C, hcp Co particles, and Co carbides) at 400 °C and also observed no transformation to fcc Co. Considering their results, the weak emergence of the fcc (200) bump, and the lack of a clear shoulder feature near the hcp (002) peak for the CVD films, the possible existence of the fcc (111) peak was neglected during grain size calculation of the (002) orientation of hcp Co and the listed sizes are derived from the entire peak FWHM. Only the hcp (100), (002), and (101) peaks were considered. XRD indicates the nc nature of the film was preserved, and only grains in the (100) and (002) directions exhibited significant growth, often doubling or tripling in size. In contrast, the (101) peak remained very broad, and minimal grain growth was calculated. Because the film remains largely hcp Co, it should be magnetically harder (*i.e.* have higher coercivity) than

	Crystallite size (nm)			Size increase (%)		
Deposition temperature	(101)	(002)	(100)	(101)	(002)	(100)
325 °C	37	29	9	95	61	0
275 °C	33	17	8	120	113	14
225 °C	34	29	8	183	222	14

Table 6.3. Increase in crystallite size due to annealing.

fcc Co [62], which is desirable for recording and memory applications. However, the remanent magnetization may not be maximized compared to fcc Co [62]. The minimal grain growth caused by annealing may also further harden the film magnetically [63].

XPS analysis and fitting by the previously explained method showed the P 2p spectra remained predominantly composed of elemental P (not shown) despite the precipitation of Co_2P crystallites, and the Co 2p spectra did not exhibit noticeable changes (not shown), meaning Co still remained primarily metallic. There was a measureable drop in the amount of carbidic C relative to graphitic C upon annealing. Fig. 6.8 shows the ratio of C incorporated as carbidic to graphitic in depth profiling conducted both prior to and after annealing. While the total amount of C within the film still drops during depth profiling, the relative amount of carbidic C increases in both films as the films are sputtered through. Because Co_2C and Co_3C decompose to α-Co and C or to α-Co, β-Co, and C, respectively, at temperatures < 400 °C [61,64], the relative amount that carbidic C drops throughout the film is between 25%-35% after annealing. The graphitic/carbidic C incorporation in the film and the loss of carbidic C upon annealing will also affect the mechanical [61] and magnetic properties of the film [61,65-68].

6.4. SUMMARY

Co-based films containing P and C were deposited on SiO_2 using the single molecule $(Me_3P)_4Co$ from 225 °C to 325 °C. Co was primarily metallic, but P and C existed both in the elemental state (primary state of P) and bonded to Co (primary state of C). Films could not be deposited at ≤ 175 °C. Peak widths measured by XRD indicated

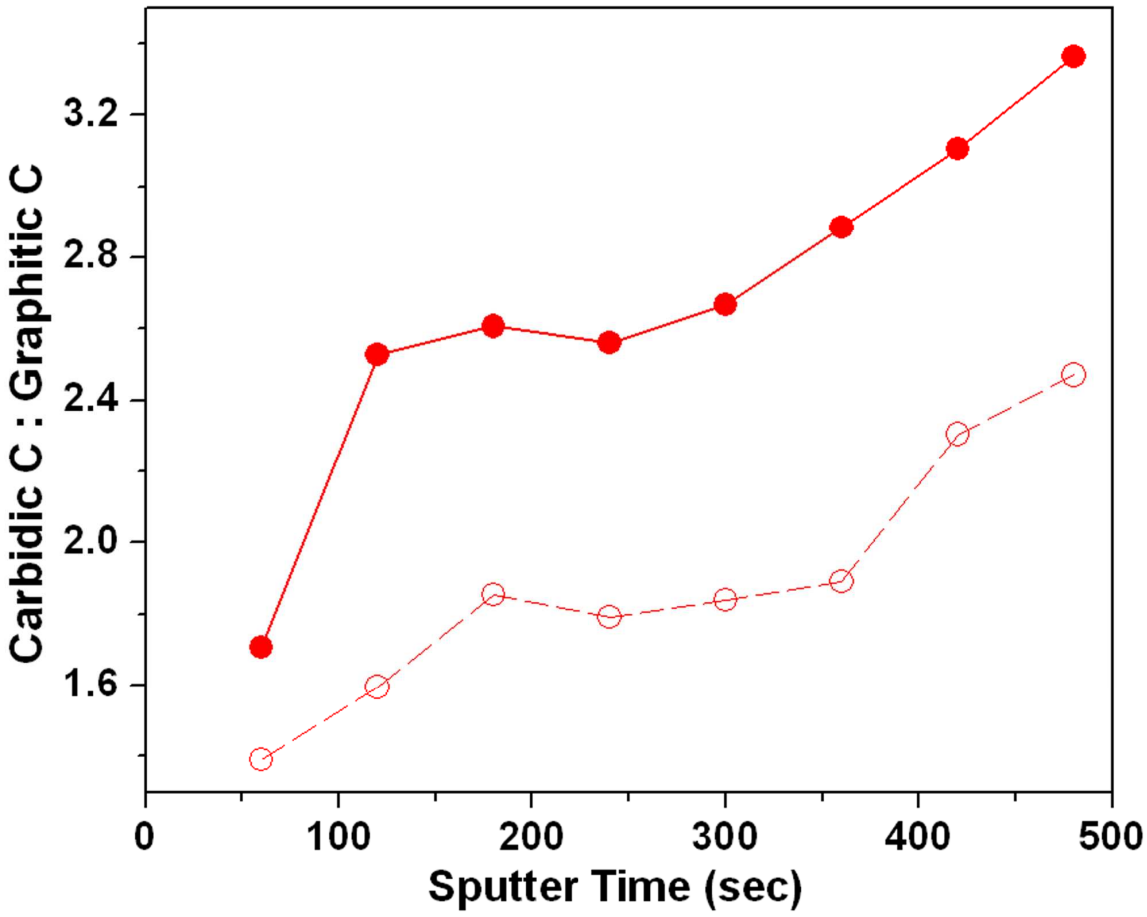

Figure 6.8. XPS depth profile showing the ratio of carbidic C to graphitic C before (—●—) and after (- -○- -) annealing.

that the deposited films were nc and comprised only of hcp Co crystallite sizes several times smaller than the film thickness. Annealing to 400 °C for 3 h caused *o*-Co_2P crystallites to precipitate while the incorporated P remained predominantly zero-valent, as indicated by the BE of the P 2p XP spectra. Annealing also caused the relative amount of carbidic C to drop compared to graphitic C as Co carbides thermally decomposed. However, the allotropic phase transformation to the fcc structure expected in nc Co was almost entirely mitigated by the incorporation of C and P, as the films remained primarily hcp Co. Although grain growth was apparent from XRD analysis, the nc nature of the film was preserved.

6.5. REFERENCES

1. Z. Li, G. Gordon, D. B. Farmer, Y. Lin, and J. Vlasaak, Electrochem. Solid-State Lett. 8, G182 (2005).

2. E. J. O'Sullivan, A. G. Schrott, M. Paunovic, C. J. Sambucetti, J. R. Marino, P. J. Bailey, S. Kaja, and K. W. Semkow, IBM J. Res. Dev. 42, 607 (1998).

3. E. Zschech, M. A. Meyer, S. G. Mhaisalkar, A. V. Vairagar, A. Krishnamoorthy, H. J. Engelmann, and V. Sukharev, Thin Solid Films 504, 279 (2006).

4. C.-K. Hu, L. Gignac, R. Rosenberg, E. Liniger, J. Rubino, C. Sambucetti, A. Stamper, A. Domenicucci, and X. Chen, Microelectron. Eng. 70, 406 (2003).

5. E. W. Brooman, Met. Finish. 102, 42 (2004).

6. M. A. Sheikholeslam, M. H. Enayati, and K. Raeissi, Mater. Lett. 62, 3629 (2008).

7. J.L. McCrea, G. Palumbo, F. Gonzalez, A. Robertson, K. Panagiotopoulos, and U. Erb, AESF SUR/FIN Annual International Technical Conference, p.138 (2001).

8. W. S. Beckett, N. Engl. J. Med. 342, 406 (2000).

9. S. S. Wise, A. L. Holmes, and J. P. Wise, Mutat. Res., Genet. Toxicol. Environ. Mutagen. 610, 2 (2006).

10. A. Aledresse and A. Alfantazi, J. Mater. Sci. 39, 1523 (2004).

11. H. Jung and A. Alfantazi, Corrosion (Houston, TX, U. S.) 63, 159 (2007).

12. B. Bozzini, P. L. Cavallotti, and M. Ivanov, IEEE Trans. Magn. 26, 45 (1990).

13. M. Mirzamaani, L. Romankiw, C. McGrath, and J. Karasinski, J. Electrochem. Soc. 135, 2813 (1988).

14. O. Kohmoto and T. Yamamoto, J. Magn. Magn. Mater. 71, 33 (1987).

15. K. Hüller and M. Sydow, J. Magn. Magn. Mater. 53, 269 (1985).

16. C. C. Koch, R. O. Scattergood, K. A. Darling, and J. E. Semones, J. Mater. Sci. 43, 7264 (2008).

17. P. C. Millett, R. P. Selvam, and A. Saxena, Acta Mater. 55, 2329 (2007).

18.R. K. Rajgarhia, S. W. Koh, D. Spearot, and A. Saxena, Mol. Simul. 34, 35 (2008).

19. G. D. Hibbard, G. Palumbo, K. T. Aust, and U. Erb, Philos. Mag. 86, 125 (2006).

20. G. Hibbard, K. T. Aust, G. Palumbo, and U. Erb, Scr. Mater. 3, 513 (2001).

21. A. E. Ray, S. R. Smith, and J. D. Scofield, J. Phase Equilib. 12, 644 (1991).

22. P. Choi, M. da Silva, U. Klement, T. Al-Kassab, and R. Kirchheim, Acta Mater. 53, 4473 (2005).

23. M. da Silva, C. Wille, U. Klement, P. Choi, and T. Al-Kassab, Mater. Sci. Eng., A 445-446, 31 (2007).

24. R. C. da Silva, M. L. Sartorelli, M. Sardela, and A. A. Pasa, Phys. Status Solidi A 187, 85 (2001).

25. X. Xu and G. Zangari, J. Electrochem. Soc. 155, D742 (2008).

26. J. H. Kim, M. Raja, S. Thanikaikarasan, Y. D. Kim, S. R. Srikuman, and T. Mahalingam, Appl. Surf. Sci. 255, 6540 (2009).

27. N. Fukumuro, J. Nishiyama, K. Shigeta, Y. Morimoto, H. Takagami, S. Yae, and H. Matsuda, Electrochem. Commun. 9, 1185 (2007).

28. N. Petrov, Y. Sverdlov, and Y. Shacham-Diamand, J. Electrochem. Soc. 149, C187 (2002).

29. E. Rudnik and J. Gorgosz, Surf. Coat. Technol. 201, 6953 (2007).

30. K-S. Eom, K-W. Cho, and H-S. Kwon, J. Power Sources 180, 484 (2008).

31. B. R. Natarajan and E. S. Murdock, IEEE Trans. Magn. 24, 2724 (1988).

32. G. J. Tarnopolsky, H. N. Bertram, and L. T. Tran, J. Appl. Phys. 69, 4730 (1991).

33. L. B. Henderson and J. G. Ekerdt, Electrochem. Solid-State Lett. 12, D36 (2009).

34. H.-F. Klein and H. H. Karsch, Chem. Ber. 108, 944 (1975).

35. H.-F. Klein, Angew. Chem., Int. Ed. 10, 343 (1971).

36. B. E. Warren, X-Ray Diffraction, Dover Publications, Inc., Mineola, NY, U.S.A., 1990, p. 253.

37. H. Wang, S. P. Wong, W. Y. Cheung, N. Ke, G. H. Wen, X. X. Zhang, and R. W. M. Kwok, J. Appl. Phys. 88, 4919 (2000).

38. F. L. Wang, J. C. Jiang, and E. I. Meletis, J. Appl. Phys. 95, 5069 (2004).

39. V. V. Nemoshkalenko, V. V. Didyk, V. P. Krivitskii, and A. I. Senkevich, Zh. Neorg. Khim. 28, 2182 (1983).

40. S. M. S. I. Dulal, T. H. Kim, C. B. Shin, and C.-K. Kim, J. Alloys Compd. 461, 382 (2008).

41. NIST X-ray Photoelectron Spectroscopy Database, Vers. 3.5 (National Institute of Standards and Technology, Gaithersburg, 2003); http://srdata.nist.gov/xps/

42. L. B. Henderson and J. G. Ekerdt, J. Electrochem. Soc. in press.

43. A. Kohn, M. Eizenberg, and Y. Shacham-Diamand, J. Appl. Phys. 94, 3810 (2003).

44. G. K. Williamson and W. H. Hall, Acta Metall. 1, 22 (1953).

45. Y. Zhao and J. Zhang, J. Appl. Crystallogr. 41, 1095 (2008).

46. J. D. Hahn, F. Wu, and P. Bellon, Metall. Mater. Trans A 35A, 1105 (2004).

47. J.-D. Kamminga, Th. H. de Keijser, R. Delhez, and E. J. Mittemeijer, J. Appl. Phys. 88, 6332 (2000).

48. B. H. Hwang and S. Y. Chiou, Thin Solid Films 304, 286 (1997).

49. O. O. Mykhaylyk and M. P. Gadzira, Acta Cryst. B55, 297 (1999).

50. D. Kumar and A. Gupta, J. Magn. Magn. Mater. 308, 318 (2007).

51. Y. Moradzadeh, J. Electrochem. Soc. 112, 891 (1965).

52. A. García-Arribas, M. L. Fdez-Gubieda, and J. M. Barandiarán, Phys. Rev. B 61, 6238 (2000).

53. I. Lucas, L. Perez, C. Aroca, P. Sánchez, E. López, and M. C. Sánchez, J. Magn. Magn. Mater. 290-291, 1513 (2005).

54. T. Chen, D. A. Rogowski, and R. M. White, J. Appl. Phys. 49, 1816 (1978).

55. E. L. Nicholson and M. R. Khan, J. Electrochem. Soc. 133, 2342 (1986).

56. M. Mirzamaani, L. Romankiw, C. McGrath, and J. Karasinski, J. Electrochem. Soc. 135, 2813 (1988).

57. F. Cebollada, J. M. González, and J. González, J. Appl. Phys. 73, 5372 (1993).

58. R. C. da Silva, E. M. dos Santos, M. L. Sartorelli, J. P. Sinnecker, A. Gündel, R. L. Sommer, and A. A. Pasa, J. Magn. Magn. Mater. 272-276, 1460 (2004).

59. R. Tarozaitė, M. Kurtinaitienė, A. Džiūvė, and Z. Jusys, Surf. Coat. Technol. 115, 57 (1999).

60. S. Fujii, S. Ishida, and S. Asano, J. Phys. F: Met. Phys. 18, 971 (1988).

61. Y. Fukumiya, Y. Haga, and O. Nittono, Mater. Sci. Eng., A A312, 248 (2001).

62. M. S. Bhuiyan, B. J. Taylor, M. Paranthaman, J. R. Thompson, and J. W. Sinclair, J. Mater. Sci. 43, 1644 (2008).

63. B. Presa, R. Matarranz, M. C. Contreras, J. F. Calleja, L. E. Fernandez-Outon, and K. O'Grady, IEEE Trans. Magn. 44, 2788 (2008).

64. L. J. E. Hofer, E. M. Cohn, and W. C. Peebles, J. Phys. Chem. 53, 661 (1949).

65. S. Tajima and S.-I. Hirano, J. Mater. Sci. Lett. 11, 22 (1992).

66. H. Wang, S. P. Wong, W. Y. Cheung, N. Ke, W. F. Lau, M. F. Chiah, and X. X. Zhang, Mater. Sci. Eng., C 16, 147 (2001).

67. M. Yu, Y. Liu, and D. J. Sellmyer, J. Appl. Phys. 85, 4319 (1999).

68. J. Shi, M. Azumi, and O. Nittono, Appl. Phys. A: Mater. Sci. Process. 73, 215 (2001).

Chapter 7: Research Summary

7.1. CONCLUSION

Two alloy film systems were investigated for their potential application in future Cu IC applications. CVD amorphous Ru(P), which may be useful for Cu IC liner applications, was evaluated as a potential diffusion barrier, while CVD of Co(P) films from either single- or dual-source chemistries was developed and investigated. CVD of amorphous Co(P) films from a dual-source chemistry were studied in terms of their ability to cap Cu.

MOS capacitor structures formed using 5 nm amorphous CVD Ru(P) as a Cu diffusion barrier were subjected to bias-temperature stressing to evaluate the structure time-to-failure and were compared to 5 nm amorphous PVD TaN. The Ru(P) barrier outperformed TaN at every condition tested, and the √E-model indicates that Ru(P) of this thickness performs acceptably as a barrier in excess of 200 °C. The more conservative E-model predicts Ru(P) failure at this temperature, but extraction of the activation energy of failure (1.83 eV in the absence of an electric field) and use in the E-model predicts Ru(P) liners act as Cu diffusion barriers up to 165 °C and are worthy of further investigation as single-material liners.

Chemical methods to deposit Co(P) films are also described. A dual source chemistry of $Co_2(CO)_8$ and PMe_3 was developed to allow independent control of P and Co within deposited films. When the P in the film was in excess of 8 at. %, all inspected films were amorphous. However, C was always incorporated in the films, generally

increasing in concentration with increasing amounts of P. The C in Co(P) films exists in two chemical states, and also affects the film microstructure, likely due to the favorable interactions possible between C and Co. The primary cause of resistivity increases in the film cannot be definitively assigned to P incorporation, C incorporation, or loss of crystallinity and remains an open question. C can be minimized by dropping the deposition temperature to 250 °C, but the film resistivity is minimized at 300 °C. Annealing at 400 °C for 3 h is not sufficient to initiate crystallization, but does begin to decompose Co carbides in the film, which contributes to drops in resistivity. While the dual-source chemistry described herein results in films that still adhere well to Cu despite the existence of C and P at the Co-Cu interface, it will not be useful for capping Cu interconnects, because the selectivity of growth on Cu compared to SiO_2 is poor, and alternative techniques must be used to selectively deposit Co(P) on Cu from the vapor phase.

A single molecule precursor, $(PMe_3)_4Co$, also deposits Co(P) films containing C without the need for a co-reactant gas, however the amount of P and C combined is insufficient to force the amorphous microstructure. Because the films are nanocrystalline as-deposited, P in the film is found in the phosphidic state in addition to the elemental state. There is, however, sufficient P and C within the films to enhance the thermal stability of the films beyond that of typical nanocrystalline Co. There is only minimal grain growth and almost no noticeable transformation to fcc Co after a 400 °C anneal for 3 h, conditions above those required to initiate significant grain growth and fcc transformation in nanocrystalline Co that lacks P incorporation.

7.2. RECOMMENDATIONS FOR FUTURE WORK

The intention of this research was to investigate alternative materials for Cu IC applications, and to develop different methods by which to deposit them. First, since amorphous Ru(P) has now been shown to behave as a Cu diffusion barrier, the next relevant step should be to investigate Cu electrodeposition directly on this material. Previous work by Shin and co-workers indicated that the resistivity of the films was very high due to C incorporation, and it is a very real possibility that the amount of C in the films must be reduced significantly to enable even Cu plating. For this reason, investigating CVD of Ru(P) using PH_3 in place of PMe_3 is recommended, and there may be alternative Ru precursors available that could help to minimize C incorporation and further improve step coverage.

Similarly, using PH_3 during Co(P) CVD is also recommended for future investigation, in part because this can be expected to minimize the C contained in the Co(P) films, but also in light of the poor growth selectivity described in Chapter 5, PH_3 may lead to faster Co(P) nucleation on Cu. The suggestions of using a Co precursor other than $Co_2(CO)_8$ and/or modifying the dielectric surface to improve selectivity as described in Chapter 5 are reiterated. Additional investigations using amorphous and nanocrystalline Co(P) films including magnetic properties, hardness, wear resistance, and corrosion protection are also suggested, as Co(P) films are expected to have numerous uses outside of Cu IC cap applications.

First principle calculations suggest that B is more effective in amorphizing Ru than P, because less B is required. Considering that B is a safer material than P and a high purity B PVD target is available, PVD Ru(B) films should be able to be formed

without much difficulty. Since PVD films have low C impurity levels and B content can be easily controlled in the PVD process, it can offer valuable information on the formation mechanism of amorphous Ru-based alloys and on the first principles calculations themselves. If these initial PVD experiments prove promising, growing CVD Ru(B) alloys using separate Ru and B sources (*i.e.* $Ru_3(CO)_{12}$ and B_2H_6) should be pursued. Additionally, there is much that could be learned by growing amorphous Co(B) by sputtering and/or CVD Co(B) (*i.e.* from $Co_2(CO)_8$, or another precursor which provides better selectivity on Cu, and B_2H_6), if possible.

Appendix

Magnetic properties of Co(P) films grown from tetrakis(trimethylphosphine)cobalt

Nanocrystalline (nc) Co(P) films containing some C impurity grown by thermal CVD of tetrakis(trimethylphosphine)cobalt(0) on 400 nm PECVD SiO_2 (from TEOS) were analyzed by SQUID (superconducting quantum interface device) magnetometry (Quantum Design MPMS SQUID VSM) to measure the magnetic properties of the films and investigate potential technological uses, such as magnetic random access memory or sensors. Small wafer pieces were cut from larger samples after deposition and then measured at 300 K after being subjected to one of three thermal treatments: 1) No annealing (sample measured as-deposited); 2) 400 °C 3 h anneal in H_2; or 3) 500 °C 1 h anneal in H_2. Explicitly, sample pieces were subjected to only one treatment prior to magnetometry, and the same sample piece was not re-measured after receiving a second (or third) thermal treatment, although several sample pieces were cut from the same larger wafer piece in order to measure the effect of different treatments on the same film. There was no external magnetic field applied during annealing. Film thicknesses were measured in cross-sectional scanning electron microscopy (SEM) (Zeiss Supra 40VP). Measurement of a large wafer piece indicated that its contribution to the measured moment was negligible.

This research is incomplete, but the results (coercivity [H_c], squareness [M_r/M_s], and thickness) that have been obtained are summarized below in Table A1. The saturation and remanent total magnetic moments have not been calculated due to the lack of accurately measured size and Co(P) film thickness for each tested sample, and

Sample	Deposition T (°C)	Treatment	H_c (Oe)	M_r/M_s	Thickness (nm)
1	225	As-deposited	57	82	157
2	225	As-deposited	46	86	109
		3 h 400 °C	152	86	-
3	225	As-deposited	45	48	-
4	225	As-deposited	5	-	178
5	225	As-deposited	15	-	41
6	325	As-deposited	231	72	85
	325	3 h 400 °C	365	77	-
	325	1 h 500 °C	370	78	-
7	325	As-deposited	250	69	-

Table A.1. SQUID data collected for several nc Co(P) film samples.

therefore one should not conclude that films with lower squareness values necessarily have lower remanent magnetization. None of the films can be characterized as "soft" magnets (*i.e.* $H_c < 1$ Oe), but some do exceed the minimum required to be considered "hard" magnets (*i.e.* $H_c > 125$ Oe). Films grown at 250 °C and measured as-deposited have lower coercivities than those deposited at 350 °C, two of which are very low compared to the others (5 and 15 Oe). The hysteresis curves near the origin for Sample 2 are shown in Fig. A1(a) and those for Sample 6 are shown in Fig. A1(b). Sample 2 reached its saturation magnetization before the applied field reached 5 kOe, and Sample 6 was saturated near the same applied field. The coercivity of Sample 2 after annealing to 400 °C is lower than the as-deposited (350 °C) coercivities of Samples 6 and 7. Furthermore, the coercivity of Sample 6 is much larger than that of Sample 2 after receiving the same annealing treatment, indicating that increasing the deposition temperature of the films increases the coercivity. Annealing to 400 °C for 3 h serves to further magnetically harden films regardless of deposition temperature, although those with higher H_c initially exhibit higher H_c after annealing. It does not appear that annealing to 500 °C instead of 400 °C greatly affects H_c or M_r/M_s.

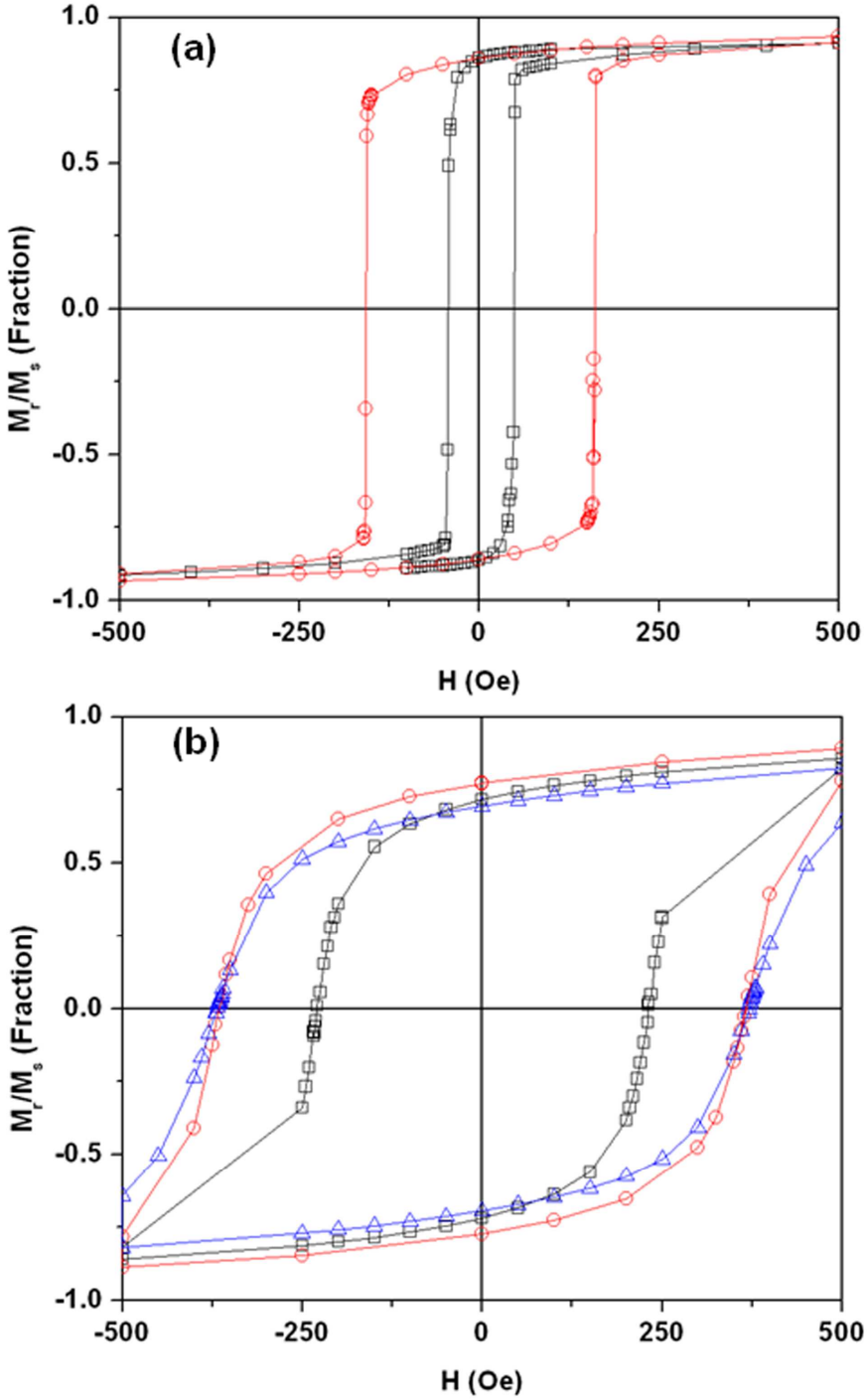

Figure A.1. Hysteresis loops for Co(P) films deposited at (a) 250 °C and (b) 350 °C. The films were given one of three thermal treatments, then measured (□) as-deposited, (○) 3 h 400 °C anneal, or (△) 1 h 500 °C anneal. The loops are presented on the same scale for comparison.

Bibliography

A. Aledresse and A. Alfantazi, J. Mater. Sci. 39, 1523 (2004).

S. B. Antonelli, T. L. Allen, D. C. Johnson, and V. M. Dubin, J. Electrochem. Soc., 153, J46 (2006).

T. N. Arunagiri, Y. Zhang, O. Chyan, M. J. Kim, and T. Q. Hurd, J. Electrochem. Soc., 152, G808 (2005).

ASTM D 3359-08: Standard Test Methods for Measuring Adhesion by Tape Test, ASTM International, West Conshohocken, PA, U.S.A., (2008).

K. C. Aw, N. T. Salim, W. Gao, and K. Prince, Int. J. Mod. Phys. B, 20, 4165 (2006).

G. Bai, S. Wittenbrock, V. Ochoa, R. Villasol, C. Chiang, T. Marieb, D. Gardner, C. Mu, D. Fraser, and M. Bohr, Mater. Res. Soc. Symp. Proc., 403, 501, (1996).

G. Barbottin and A. Vapaille (Eds.), Instabilities in Silicon Devices: Silicon Passivation and Related Instabilities, Elsevier, Amsterdam, 1986, p. 133.

K. Barmak, C. Cabral, K. P. Rodbell, and J. M. E. Harper, J. Vac. Sci. Technol. B, 24, 2485 (2006).

E. Bauer-Grosse and A. Aouni, J. Non-Cryst. Solids, 353, 3644 (2007).

J. S. Becker and R. G. Gordon, Appl. Phys. Lett., 82, 2239 (2003).

W. S. Beckett, N. Engl. J. Med. 342, 406 (2000).

M. S. Bhuiyan, B. J. Taylor, M. Paranthaman, J. R. Thompson, and J. W. Sinclair, J. Mater. Sci. 43, 1644 (2008).

E. P. Boyd, D. R. Ketchum, H. Deng, and S. G. Shore, Chem. Mater., 9, 1154, (1997).

B. Bozzini, P. L. Cavallotti, and M. Ivanov, IEEE Trans. Magn. 26, 45 (1990).

F. Branda, L. Lanotte, A. Costantini, and P. Matteazzi, J. Mater. Sci., 28, 1824 (1993).

E. W. Brooman, Met. Finish. 102, 42 (2004).

A. W. Burns, A. F. Gaudette, and M. E. Bussell, J. Catal., 260, 262 (2008).

A. L. Cabrera, W. H. Garrido, and U. G. Volkman, Catal. Lett., 25, 115 (1994).

F. Cebollada, J. M. Gonzalez, and P. Adeva, J. Mater. Res., 8, 105 (1993).

F. Cebollada, J. M. González, and J. González, J. Appl. Phys. 73, 5372 (1993).

S. Y. Chang, C. C. Wan, and Y. Y. Wang, Electrochem. Sol. State Lett., 10, D43 (2007).

F. Chen, O. Bravo, K. Chanda, P. McLaughlin, T. Sullivan, J. Gill, J. Lloyd, R. Kontra, and J. Aitken, Proceedings of the 44th Annual International Reliability Physics Symposium, p.46 (2006).

T. Chen, D. A. Rogowski, and R. M. White, J. Appl. Phys. 49, 1816 (1978).

V. B. Chernogorenko, V. G. Ivanchenko and L. Ya. Kulik, in: Binary Phase Diagrams, T. B. Massalski, H. Okamoto, P. R. Subramanian, and L. Kacprzak (Eds.), ASM International, Materials Park, OH, U.S.A., 1990, p. 2979.

P. Choi, M. da Silva, U. Klement, T. Al-Kassab, and R. Kirchheim, Acta Mater. 53, 4473 (2005).

K. M. Chow, W. Y. Ng, and L. K. Yeung, Surf. Coat. Technol., 99, 161 (1998).

O. Chyan, T. N. Arunagiri, and T. Ponnuswamy, J. Electrochem. Soc., 150, C347 (2003).

M. da Silva, C. Wille, U. Klement, P. Choi, and T. Al-Kassab, Mater. Sci. Eng., A 445-446, 31 (2007).

R. C. da Silva, E. M. dos Santos, M. L. Sartorelli, J. P. Sinnecker, A. Gündel, R. L. Sommer, and A. A. Pasa, J. Magn. Magn. Mater. 272-276, 1460 (2004).

R. C. da Silva, M. L. Sartorelli, M. Sardela, and A. A. Pasa, Phys. Status Solidi A, 187, 85 (2001).

M. Damayanti, T. Sritharan, Z.H. Gan, S. G.Mhaisalkar, N. Jiang, and L. Chan, J. Electrochem. Soc., 153, J41 (2006).

T. Decorps, P. H. Haumesser, S. Olivier, A. Roule, M. Joulaud, O. Pollet, X. Avale, and G. Passemard, Microelectron. Eng., 83, 2082 (2006).

J. J. Delaunay, T. Hayashi, M. Tomita, and S. Hirono, J. Appl. Phys., 82, 2200 (1997).

S. M. S. I. Dulal, T. H. Kim, C. B. Shin, and C.-K. Kim, J. Alloys Compd. 461, 382 (2008).

S. M. S. I. Dulal, H. J. Yun, C. B. Shin, and C.-K. Kim, J. Electrochem. Soc., 154, D494 (2007).

E. R. Engbrecht, Y.-M. Sun, K. H. Junker, J. M. White, and J. G. Ekerdt, J. Vac. Sci. Technol. B, 23, 463 (2005).

K-S. Eom, K-W. Cho, and H-S. Kwon, J. Power Sources 180, 484 (2008).

S. Fujii, S. Ishida, and S. Asano, J. Phys. F: Met. Phys. 18, 971 (1988).

Y. Fukumiya, Y. Haga, and O. Nittono, Mater. Sci. Eng., A A312, 248 (2001).

N. Fukumuro, J. Nishiyama, K. Shigeta, Y. Morimoto, H. Takagami, S. Yae, and H. Matsuda, Electrochem. Commun. 9, 1185 (2007).

J. Gambino, J. Wynne, J. Gill, S. Mongeon, D. Meatyard, B. Lee, H. Bamnolker, L. Hall, N. Li, M. Hernandez, P. Little, M. Hamed, I. Ivanov, and C. L. Gan, Microelectron. Eng., 83, 2059 (2006).

A. García-Arribas, M. L. Fdez-Gubieda, and J. M. Barandiarán, Phys. Rev. B 61, 6238 (2000).

M. L. Garner, D. Chandra, and K. H. Lau, J. Phase Equilib., 16, 24 (1995).

L. V. Goncharova, S. K. Clowes, R. R. Fogg, A. V. Ermakov, and B. J. Hinch, Surf. Sci., 515, 553 (2002).

R. Gonella, P. Motte, and J. Torres, Microelectron. Reliab., 40, 1305 (2000).

M. E. Gross, K. Schnoes Kranz, D. Brasen, and H. Luftman, J. Vac. Sci. Technol. B, 6, 1548 (1988).

J. D. Hahn, F. Wu, and P. Bellon, Metall. Mater. Trans A 35A, 1105 (2004).

B. D. Hatton, K. Landskron, W. J. Hunks, M. R. Bennett, D. Shukaris, D. D. Perovic, and G. A. Ozin, Mater. Today, 9, 22 (2006).

L. B. Henderson and J. G. Ekerdt, Electrochem. Sol. State Lett., 12, D36 (2009).

L. B. Henderson and J. G. Ekerdt, J. Electrochem. Soc., in press.

L. B. Henderson and J. G. Ekerdt, Thin Solid Films, 517, 1645 (2009).

G. Hibbard, K. T. Aust, G. Palumbo, and U. Erb, Scr. Mater. 3, 513 (2001).

G. D. Hibbard, G. Palumbo, K. T. Aust, and U. Erb, Philos. Mag. 86, 125 (2006).

L. J. E. Hofer, E. M. Cohn, and W. C. Peebles, J. Phys. Chem. 53, 661 (1949).

C.-K. Hu, D. Canaperi, S. T. Chen, L. M. Cignac, B. Herbst, S. Kaldor, M. Krishnan, E. Liniger, D. L. Rath, D. Restaino, R. Rosenberg, J. Rubino, S.-C. Seo, A. Simon, S. Smith, and W.-T. Tseng, IEEE International Reliability Physics Symposium Proceedings, p. 222 (2004).

C.-K. Hu, L. Gignac, and R. Rosenberg, Microelectron. Reliab., 46, 213 (2006).

C.-K. Hu, L. Gignac, R. Rosenberg, E. Liniger, J. Rubino, C. Sambucetti, A. Stamper, A. Domenicucci, and X. Chen, Microelectron. Eng. 70, 406 (2003).

K. Hüller, M. Sydow, and G. Dietz, J. Magn. Magn. Mater., 53, 269 (1985).

B. H. Hwang and S. Y. Chiou, Thin Solid Films 304, 286 (1997).

S.-S. Hwang, S.-Y. Jung, and Y.-C. Joo, J. Appl. Phys., 101, 074501 (2007).

International Technology Roadmap for Semiconductors, 2008 Update, http://public.itrs.net

International Technology Roadmap for Semiconductors, 2007 Edition; http://public.itrs.net

K. Ishida and T. Nishizawa, Bull. Alloy Phase Diagrams, 11, 555 (1990).

K. Ishida and T. Nishizawa, J. Phase Equilib., 12, 417 (1991).

A. A. Istratov, C. Flink, H. Hieslmair, and E. R. Weber, Phys. Rev. Lett., 81, 1243 (1998).

D. Josell, D. Wheeler, C. Witt, and T. P. Moffat, Electrochem. Solid-State Lett., 6, C143 (2003).

M. H. Juang, C. I. Ou-Yang, H. C. Cheng, and C. T. Lin, Mat. Res. Soc. Symp. Proc., 648, P11.31.1 (2001).

H. Jung and A. Alfantazi, Corrosion (Houston, TX, U. S.) 63, 159 (2007).

A. E. Kaloyeros, E. Eisenbraun, Annu. Rev. Mater. Sci., 30, 363 (2000).

J.-D. Kamminga, Th. H. de Keijser, R. Delhez, and E. J. Mittemeijer, J. Appl. Phys. 88, 6332 (2000).

H. Kim, T. Koseki, T. Ohba, T. Ohta, Y. Kojima, H. Sato, and Y. Shimogaki, J. Electrochem. Soc., 152, G594 (2005).

H. Kim, Y. Naito, T. Koseki, T. Ohba, T. Ohta, Y. Kojima, H. Sato, and Y. Shimogaki, Jap. J. Appl. Phys., 45, 2497 (2006).

J. H. Kim, M. Raja, S. Thanikaikarasan, Y. D. Kim, S. R. Srikuman, and T. Mahalingam, Appl. Surf. Sci. 255, 6540 (2009).

H. Kizil and Ch. Steinbrüchel, Thin Solid Films, 449, 158, (2004).

H.-F. Klein, Angew. Chem., Int. Ed. 10, 343 (1971).

H.-F. Klein and H. H. Karsch, Chem. Ber. 108, 944 (1975).

Y. K. Ko, D. S. Park, B. S. Seo, H. J. Yang, H. J. Shin, J. Y. Kim, J. H. Lee, W. H. Lee, P. J. Reucroft, and J. G. Lee, Mater. Chem. Phys., 80, 560, (2003).

C. C. Koch, R. O. Scattergood, K. A. Darling, and J. E. Semones, J. Mater. Sci. 43, 7264 (2008).

O. Kohmoto and T. Yamamoto, J. Magn. Magn. Mater. 71, 33 (1987).

A. Kohn, M. Eizenberg, and Y. Shacham-Diamand, J. Appl. Phys., 94, 3015 (2003).

A. Kohn, M. Eizenberg, Y. Shacham-Diamand, and Y. Sverdlov, Mater. Sci. Eng., A302, 18 (2001).

T. J. Konno and K. Bandoh, J. Metastable Nanocryst. Mater., 24, 57 (2005).

T. J. Konno and R. Sinclair, Acta Metall. Mater., 43, 471 (1995).

D. Kumar and A. Gupta, J. Magn. Magn. Mater. 308, 318 (2007).

J. Lahtinen, J. Vaari, A. Talo, A. Vehanen, and P. Hautojärvi, Vacuum, 41, 112 (1990).

Y.-H. Lai, C.-T. Yeh, H.-J. Lin, C.-T. Chen, and W.-H. Hung, J. Phys. Chem. B, 106 1722 (2002).

F. Lanckmans and K. Maex, Microelectron. Eng., 60, 125 (2002).

M. Lane, R. Dauskardt, N. Krishna, and I. Hashim, Mater. Res. Soc. Symp. Proc., 564, 281 (1999).

M. W. Lane, E. G. Liniger, and J. R. Lloyd, J. Appl. Phys., 93, 1417 (2003).

B. H. Lee and K. Yong, J. Vac. Sci. Technol. B, 22, 2375 (2004).

H.-B.-R. Lee and H. Kim, Electrochem. Solid-State Lett., 9, G323 (2006).

J. Lee, I. Chen, and C. Hu, IEEE Trans. Electron Dev., 35, 2268 (1988).

J. Lee, H. J. Yang, J. H. Lee, J. Y. Kim, W. J. Nam, H. J. Shin, Y. K. Ko, J. G. Lee, E. G. Lee, and C. S. Kim, J. Electrochem. Soc., 153, G539 (2006).

B. Li, T. D. Sullivan, T. C. Lee, and D. Badami, Microelectron. Reliab., 44, 365 (2004).

H. Li and B. P. Tonner, Surf. Sci., 237, 141 (1990).

Z. Li, R. G. Gordon, D. B. Farmer, Y. Lin, and J. Vlaasak, Electrochem. Solid-State Lett., 8, G182 (2005).

B. K. Lim, H. S. Park, L. K. Chin, S. W. Woo, A. K. H. See, C.-S. Seet, T.-J. Lee, and N. L. Yakovlev, J. Vac. Sci. Technol. B, 22, 2286 (2004).

M. H. Lin, Y. L. Lin, J. M. Chen, M.-S. Yeh, K. P. Chang, K. C. Su, and T. Wang, IEEE Trans. Electron. Dev., 52, 2602 (2005).

T.-Y. Lin, H.-Y. Cheng, T.-S. Chin, C.-F. Chiu, and J.-S. Fang, Appl. Phys. Lett., 91, 152908 (2007).

J. R. Lloyd and J. J. Clement, Thin Solid Films, 262, 135 (1995).

J. R. Lloyd, E. Liniger, and T. M. Shaw, J. App. Phys., 98, 084109 (2005).

J. R. Lloyd, C. E. Murray, S. Ponoth, S. Cohen, and E. Liniger, Microelectron. Reliab., 46, 1643 (2006).

Y. H. Lu, and Y. G. Shen, J. Mater. Res., 23, 671 (2008).

I. Lucas, L. Perez, C. Aroca, P. Sánchez, E. López, and M. C. Sánchez, J. Magn. Magn. Mater. 290-291, 1513 (2005).

K. Maex, M. R. Baklanov, D. Shamiryan, F. Iacopi, S. H. Brongersma, and Z. S. Yanovitskaya, J. Appl. Phys., 93, 8793 (2003).

N. Matsunaga, N. Nakamura, K. Higashi, H. Yamaguchi, T. Watanabe, K. Akiyama, S. Nakao, K. Fujita, H .Miyajima, S .Omoto, A. Sakata, T. Katata, Y. Kagawa, H. Kawashima, Y. Enomoto, T. Hasegawa, and H. Shibata, Proceedings of the IEEE International Interconnect Technology Conference, p. 6 (2005).

J. D. McBrayer, R. M. Swanson, and T. W. Sigmon, J. Electrochem. Soc., 133, 1242 (1986).

J. L. McCrea, G. Palumbo, F. Gonzalez, A. Robertson, K. Panagiotopoulos, and U. Erb, AESF SUR/FIN Annual International Technical Conference, p.138 (2001).

J. W. McPherson and H.C. Mogul, J. App. Phys., 84, 1513 (1998).

M. Mercier, S. Weber, A. Jacques, H. Hirabayashi, H. Ohkawa, and M. Kinoshita, Diffus. Defect Data, Pt. A, 143, 1285 (1997).

W. B. Mi, L. Guo, E. Y. Jiang, Z. Q. Li, P. Wu and H. L. Bai, J. Phys. D: Appl. Phys., 36, 2393 (2003).

N. L. Michael, C.-U. Kim, Q.-T. Jiang, R. A. Augur, and P. Gillespie, J. Electron. Mater., 31, (2002).

P. C. Millett, R. P. Selvam, and A. Saxena, Acta Mater. 55, 2329 (2007).

M. Mirzamaani, L. Romankiw, C. McGrath, and J. Karasinski, J. Electrochem. Soc. 135, 2813 (1988).

G. E. Mitchell, M. A. Henderson, and J. M. White, J. Phys. Chem., 91, 3808 (1987).

B. M. Mollakov, M. P. Glazunov, and V. I. Spitsyn, Russ. Chem. Bull., 22, 635 (1973).

Y. Moradzadeh, J. Electrochem. Soc. 112, 891 (1965).

J. F. Moulder, W. F. Stickle, P. E. Sobol, and K. D. Bomben, Handbook of X-Ray Photoelectron Spectroscopy, Physical Electronics, Inc., Eden Prarie, MN, U.S.A., 1992, p. 253.

O. O. Mykhaylyk and M. P. Gadzira, Acta Cryst. B55, 297 (1999).

J. Nakamura and I. Toyoshima, Surf. Sci., 201, 185 (1988).

E. Nakazawa, K. Arita, Y. Tsuchiya, Y. Kakuhara, S. Yokogawa, T. Kurokawa, N. Sasaki, S. Ganguli, H.-C. Ha, W. T. Lee, S.-H. Yu, and M. Sekine, Proceedings of the Advanced Metallization Conference, p. 19 (2008).

B. R. Natarajan and E. S. Murdock, IEEE Trans. Magn. 24, 2724 (1988).

V. V. Nemoshkalenko, V. V. Didyk, V. P. Krivitskii, and A. I. Senkevich, Zh. Neorg. Khim. 28, 2182 (1983).

E. L. Nicholson and M. R. Khan, J. Electrochem. Soc. 133, 2342 (1986).

T. Nishizawa and K. Ishida, Bull. Alloy Phase Diagrams, 5, 161, (1984).

NIST Electron Effective-Attenuation-Length Database, Vers. 1.0 (National Institute of Standards and Technology, Gaithersburg, MD, 2001).

NIST X-ray Photoelectron Spectroscopy Database, Vers. 3.5 (National Institute of Standards and Technology, Gaithersburg, MD, 2003); http://srdata.nist.gov/xps/

E. J. O'Sullivan, A. G. Schrott, M. Paunovic, C. J. Sambucetti, J. R. Marino. P. J. Bailey, S. Kaja, and K. W. Semkow, IBM J. Res. Dev., 42, 607 (1998).

K. Oda, T. Yoshio and K. Oda, J. Mater. Sci. Lett., 9, 1319 (1990).

H. Okamoto, Cu-P Phase Diagram, in: ASM Alloy Phase Diagrams Center, P. Villars (Ed.), (ASM International, Materials Park, OH, 2006). http://www.asminternational.org/AsmEnterprise/APD

S. T. Oyama, in: The Chemistry of Transition Metal Carbides and Nitrides, S. T. Oyama (Ed.), Blackie Academic & Professional, Glasgow, Scotland, 1996, p. 9.

M. Paunovic, P. J. Bailey, and R. G. Schad, J. Electrochem. Soc., 141, 1843 (1994).

D.-C. Perng, J.-B. Yeh, and K.-C. Hsu, Appl. Surf. Sci., 257, 6059 (2008).

N. Petrov, Y. Sverdlov, and Y. Shacham-Diamand, J. Electrochem. Soc. 149, C187 (2002).

B. Presa, R. Matarranz, M. C. Contreras, J. F. Calleja, L. E. Fernandez-Outon, and K. O'Grady, IEEE Trans. Magn. 44, 2788 (2008).

G. Raghavan, C. Chiang, P. B. Anders, S.-M. Tzeng, R. Villasol, G. Bai, M. Bohr, and D. B. Fraser, Thin Solid Films, 262, 168 (1995).

R. K. Rajgarhia, S. W. Koh, D. Spearot, and A. Saxena, Mol. Simul. 34, 35 (2008).

A. E. Ray, S. R. Smith, and J. D. Scofield, J. Phase Equilib. 12, 644 (1991).

E. Rudnik and J. Gorgosz, Surf. Coat. Technol. 201, 6953 (2007).

D. Save, F. Braud, J. Torres, F. Binder, C. Müller, J. O. Weidner, and W. Hasse, Microelectron. Eng., 33, 75 (1997).

Y. Shacham-Diamand, A. Dedhia, D. Hoffstetter, and W. G. Oldham, J. Electrochem. Soc., 140, 2427 (1993).

D. Shamiryan, T. Abell, F. Iacopi, and K. Maex, Mater. Today, 7, 34 (2004).

M. A. Sheikholeslam, M. H. Enayati, and K. Raeissi, Mater. Lett., 62, 3629 (2008).

J. Shi, M. Azumi, and O. Nittono, Appl. Phys. A: Mater. Sci. Process. 73, 215 (2001).

J. Shin, Ph.D. Dissertation, "Growth and Characterization of CVD Ru and Amorphous Ru-P Alloy Films for Liner Application in Cu Interconnect," p. 8 (2007)

J. Shin, D. Gay, Y.-M. Sun, J. M. White, and J. G. Ekerdt, AIP Conf. Proc., 788, 482 (2005).

J. Shin, H.-W. Kim, K. Agapiou, R. A. Jones, G. S. Hwang, and J. G. Ekerdt, J. Vac. Sci. Technol. A, 26, 974 (2008).

J. Shin, H.-W. Kim, G. S. Hwang, and J. G. Ekerdt, Surf. Coat. Technol., 201, 9526 (2007).

J. Shin, A. Waheed, K. Agapiou, W. A. Winkenwerder, H.-W. Kim, R. A. Jones, G. S. Hwang, and J. G. Ekerdt, J. Am. Chem. Soc., 128, 16510 (2006).

J. Shin, A. Waheed, W. A. Winkenwerder, H.-W. Kim, K. Agapiou, R. A. Jones, G. S. Hwang, and J. G. Ekerdt, Thin Solid Films, 515, 5298 (2007).

N. Shiono and M. Itsumi, Proceedings of the 31st Annual International Reliability Physics Symposium, p. 1 (1993).

K. Schuegraf and C. Hu, Semicond. Sci. Technol., 9, 989 (1994).

P. Singer, Semicond. Int., 28, 44 (2005).

H. L. Skriver and N. M. Rosengard, Phys. Rev. B, 46, 7157 (1992).

P. Staszczuk, B. Jańczuk and E. Chibowski, Mater. Chem. Phys., 12, 469 (1985).

J. S. Suehle and P. Chaparala, Microelectron. J., 27, 657 (1996).

Y.-M. Sun, S. Y. Lee, A. M. Lemonds, E. R. Engbrecht, S. Veldman, J. Lozano, J. M. White, J. G. Ekerdt, I. Emesh, and K. Pfeifer, Thin Solid Films, 397, 109 (2001).

N. Suzumura, S. Yamamoto, D. Kodama, K. Makabe, J. Komori, E. Murakami, S. Maegawa, and K. Kubota, Proceedings of the 44th Annual International Reliability Physics Symposium, p.484 (2006).

E. Taglauer and W. Heiland, Appl. Phys., 9, 261 (1976).

S. Tajima and S.-I. Hirano, J. Mater. Sci. Lett. 11, 22 (1992).

H.-S. Tao, U. Diebold, N. D. Shinn, and T. E. Madey, Surf. Sci., 375, 257 (1997).

G. J. Tarnopolsky, H. N. Bertram, and L. T. Tran, J. Appl. Phys. 69, 4730 (1991).

R. Tarozaitė, M. Kurtinaitienė, A.Džiūvė, and Z. Jusys, Surf. Coat. Technol., 115, 57 (1999).

Zs. Tőkei, M. Patz, M. Schmidt, F. Iacopi, S. Demuynck, and K. Maex, Microelectron. Eng., 76, 70 (2004).

H. Treichel, J. Electron. Mater., 30, 290 (2001).

K.-C. Tsai, W.-F. Wu, J.-C. Chen, T.-J. Pan, and C.-G. Chao, J. Electrochem. Soc., 152, G83 (2005).

B. Viswanathan, R. Gopalakrishnan, and R. Vetrivel, React. Kinet. Catal. Lett., 18, 209 (1981).

F. L. Wang, J. C. Jiang, and E. I. Meletis, J. Appl. Phys. 95, 5069 (2004).

H. Wang, M. F. Chiah, W. Y. Cheung, and S. P. Wong, Phys. Lett. A, 316, 122 (2003).

H. Wang, S. P. Wong, W. Y. Cheung, N. Ke, W. F. Lau, M. F. Chiah, and X. X. Zhang, Mater. Sci. Eng., C 16, 147 (2001).

H. Wang, S. P. Wong, W. Y. Cheung, N. Ke, G. H. Wen, X. X. Zhang, and R. W. M. Kwok, J. Appl. Phys. 88, 4919 (2000).

Y. H. Wang, M. R. Moitreyee, R. Kumar, L. Shen, K. Y. Zeng, J. W. Chai, and J. S. Pan, Thin Solid Films, 460, 211 (2004).

B. E. Warren, X-Ray Diffraction, Dover Publications, Inc., Mineola, NY, U.S.A., 1990, p. 253.

W. Wei, S. L. Parker, Y.-M. Sun, J. M. White, G. Xiong, A. G. Joly, K. M. Beck, and W. P. Hess, Appl. Phys. Lett., 90, 111906 (2007).

D. A. Wesner, G. Linden, and H. P. Bonzel, Appl. Surf. Sci., 26, 335 (1986).

W. S. Williams, Int. J. Refract. Met. Hard Mater., 17, 21 (1999).

W. S. Williams, JOM, 49, 38 (1997).

W. S. Williams, Science, 152, 34 (1966).

G. K. Williamson and W. H. Hall, Acta Metall. 1, 22 (1953).

S. S. Wise, A. L. Holmes, and J. P. Wise, Mutat. Res., Genet. Toxicol. Environ. Mutagen. 610, 2 (2006).

C. Wisniewski, I. Denicoló, and I. A. Hümmelgen, J. Electrochem. Soc., 142, 3889 (1995).

X. Xu and G. Zangari, J. Electrochem. Soc. 155, D742 (2008).

H. J. Yang, J. Lee, S. Kim, Y. K. Ko, H. J. Shin, J. G. Lee, C. Kim, H. J. Bang, B. S. Cho, Y. H. Bae, J. H. Lee, D. H. Kim, C. O. Jeong, S. Y. Kim, and S. K. Lim, J. Appl. Phys., 100, 113705-1 (2006).

D.-X. Ye, S. Pimanpang, C. Jezewski, F. Tang, J. J. Senkevich, G.-C. Wang, and T.-M. Lu, Thin Solid Films, 485, 95 (2005).

S.-M. Yi, C. Shim, H.-C. Lee, J.-W. Han, K.-H. Kim, and Y.-C. Joo, Microelectron. Eng., 85, 621 (2008).

M. Yu, Y. Liu, and D. J. Sellmyer, J. Appl. Phys. 85, 4319 (1999).

Q. Zhao, D. W. Greve, and K. Barmak, Appl. Surf. Sci., 219, 136 (2003).

Y. Zhao and J. Zhang, J. Appl. Crystallogr. 41, 1095 (2008).

X.-L. Zhou and J. M. White, Surf. Sci., 221, 534 (1989).

E. Zschech, M. A. Meyer, S. G. Mhaisalkar, A. V. Vairagar, A. Krishnamoorthy, H. J. Engelmann, and V. Sukharev, Thin Solid Films 504, 279 (2006).

Vita

Lucas Benjamin Henderson was born on May 2, 1982, in Baton Rouge, Louisiana. In 2000, he graduated from Parkway South High School in Manchester, Missouri, and enrolled later that year at the University of Missouri - Columbia. After a few years of dominating trivia contests, Luke graduated *cum laude* with a Bachelor of Science degree in chemical engineering from the University in May, 2004. In September, Luke began his graduate studies in chemical engineering at the University of Texas at Austin as a member of Prof. John Ekerdt's research group. His initial research centered on the development of ruthenium atomic layer deposition chemistries using reducing gases, and transitioned to chemical vapor deposition of ruthenium-phosphorus alloys and properties of the films, significantly focusing on the barrier properties of ultra-thin alloy films. Upon moving his entire lab from Welch Hall to the Chemical and Petroleum Engineering Building in 2008, Luke began investigating chemical vapor deposition of cobalt-based films as potential capping layers for copper interconnect applications. This research was funded by the National Science Foundation and the Semiconductor Research Corporation.

Luke authored or co-authored six publications submitted to refereed journals. Research results obtained during doctoral studies were presented to SRC-GRC NYCAIST Annual Review Meetings in Albany, NY, in October of both 2007 and 2008 and at the Advanced Metallization Conference in Del Mar, CA, in September 2008.

Permanent Address: 3456 North Hills Dr. #202, Austin, TX 78731

This dissertation was typed by the author.